JSC-11633

NASA TECHNICAL MEMORANDUM

NASA TM X-58198
January 1977

PROCEEDINGS OF THE SPACE SHUTTLE ENVIRONMENTAL ASSESSMENT WORKSHOP ON STRATOSPHERIC EFFECTS

NATIONAL AERONAUTICS AND SPACE ADMINISTRATION

LYNDON B. JOHNSON SPACE CENTER

HOUSTON, TEXAS 77058

PROCEEDINGS OF THE SPACE SHUTTLE ENVIRONMENTAL ASSESSMENT WORKSHOP ON STRATOSPHERIC EFFECTS

Andrew E. Potter

Lyndon B. Johnson Space Center
Houston, Texas

January 1977

1. Report No.	2. Government Accession No.	3. Recipient's Catalog No.
NASA TM X-58198		

4. Title and Subtitle	5. Report Date
PROCEEDINGS OF THE SPACE SHUTTLE ENVIRONMENTAL ASSESSMENT WORKSHOP ON STRATOSPHERIC EFFECTS	January 1977
	6. Performing Organization Code: JSC-11633
7. Author(s): Andrew E. Potter, Compiler	8. Performing Organization Report No.
	10. Work Unit No.: 383-85-00-00-72
9. Performing Organization Name and Address: Lyndon B. Johnson Space Center, Houston, Texas 77058	11. Contract or Grant No.
	13. Type of Report and Period Covered: Technical Memorandum
12. Sponsoring Agency Name and Address: National Aeronautics and Space Administration, Washington, D.C. 20546	14. Sponsoring Agency Code

15. Supplementary Notes

16. Abstract

The Space Shuttle Environmental Assessment Workshop on Stratospheric Effects of Space Shuttle exhaust was held at the NASA Lyndon B. Johnson Space Center, Houston, Texas, on March 24 to 25, 1976. Representatives of NASA centers and NASA support contractors presented working papers on various aspects of the potential environmental impact of Space Shuttle exhaust. Workshop papers focused mainly on assessment of two potential threats: (1) Increased ultraviolet radiation levels in the biosphere due to destruction of atmospheric ozone and (2) Climatic changes due to aerosol particles affecting the planetary albedo. Papers also dealt with Space Shuttle propellants (including alternate formulations) and measurement of Space Shuttle exhaust products. The working papers were reviewed and discussed by the group. Results of these reviews and discussions, as well as the working papers, are included in this report.

17. Key Words (Suggested by Author(s))	18. Distribution Statement
Man/environment interactions Exhaust gases Global air pollution Greenhouse effect Earth albedo Ozonosphere Ultraviolet radiation	STAR Subject Category: 45 (Environment Pollution)

19. Security Classif. (of this report)	20. Security Classif. (of this page)
Unclassified	Unclassified

*For sale by the National Technical Information Service, Springfield, Virginia 22151

NASA — JSC

JSC Form 1424 (Rev Jul 74)

NASA TM X-58198

PROCEEDINGS OF THE SPACE SHUTTLE ENVIRONMENTAL ASSESSMENT WORKSHOP ON STRATOSPHERIC EFFECTS

Andrew E. Potter, Compiler
Lyndon B. Johnson Space Center
Houston, Texas 77058

Page
Intentionally
Left Blank

"Page missing from available version"

IV

CONTENTS

pgs. iii + iv blank

PROCEEDINGS OF THE SPACE SHUTTLE ENVIRONMENTAL ASSESSMENT WORKSHOP ON STRATOSPHERIC EFFECTS

By Andrew E. Potter,[a] Compiler

1. SUMMARY

Representatives of the various National Aeronautics and Space Administration centers and supporting contractors presented working papers assessing the impact of Space Shuttle exhaust on the environment. Participants in the workshop reviewed and discussed the working papers and made the following conclusions.

Two physical effects on the stratospheric environment might result from Space Shuttle exhaust products.

1. Aluminum oxide dust particles might alter the radiation balance of the stratosphere and modify weather.

2. The gaseous hydrogen chloride and nitric oxide and the aluminum oxide dust might increase the rate of ozone destruction and lead to a reduction of ozone. The average levels of ultraviolet radiation at the surface of the Earth would then increase, with possible adverse biological consequences.

A preliminary evaluation indicated that the only significant effect would probably be ozone depletion by hydrogen chloride. Consequently, the major emphasis was on a more detailed investigation of hydrogen chloride and its effect on the ozone layer. A parallel investigation of low-chlorine propellant combinations based on ammonium nitrate as possible substitutes for the baseline propellant was pursued, should it be necessary to reduce the chlorine content of Space Shuttle exhaust.

A review of ozone-reduction predictions from the various stratospheric models indicated that a reasonable estimate of the ozone reduction from Space Shuttle operation was 0.2 percent (hemispherically averaged). The biological consequences of this reduction were estimated to be too small to be realistically predicted with the current state of knowledge.

---

[a]NASA Lyndon B. Johnson Space Center.

2. INTRODUCTION

The Space Shuttle Environmental Assessment Workshop was held at the NASA Lyndon B. Johnson Space Center (JSC) to assess the impact of Space Shuttle exhaust on the environment. Working papers were presented on the following topics: propellant characteristics, ozone (O_3) depletion, particulates, plume afterburning, and medical/biological effects. These papers are included in their entirety in appendixes A to H. The attendees (listed in table 2-I) reviewed and discussed these topics; the results of their reviews are summarized in this section.

As an aid to the reader, where necessary the original units of measure have been converted to the equivalent value in the Système International d'Unités (SI). The SI units are written first, and the original units are written parenthetically thereafter.

PROPELLANT CHARACTERISTICS

The propellant formulation currently planned for use by the Space Shuttle solid rocket booster is an aluminum/ammonium perchlorate (Al/AP) combination that releases aluminum oxide (Al_2O_3) particles and gaseous hydrogen chloride (HCl) into the stratosphere during launch burn. "Frozen" chemical equilibrium in the rocket nozzle and afterburning with ambient air entrained in the exhaust plume lead to the production of nitric oxide (NO).

OZONE DEPLETION BY HCl

Stratospheric models were used to predict the effects of HCl on O_3 depletion. The simplest models are one dimensional; that is, they consider only vertical mass transport. Transport by horizontal winds is important, since Space Shuttle exhaust products will be introduced into the stratosphere at only two launch points, NASA John F. Kennedy Space Center, Florida; and Vandenberg Air Force Base, California. Latitudinal winds will then spread the products in a band around the globe after only a few days. However, north/south transport is considerably slower. Most stratospheric O_3 depletion predictions have employed one-dimensional models in which the slowness of transequatorial transport was approximated by using chlorine (Cl) concentrations averaged over the Northern Hemisphere. The Space Shuttle O_3 depletion effects predicted by five different one-dimensional models were compared in detail. Predictions agreed within a factor of 3.

A consensus was reached that the substantial differences in predictions from various models could be explained by systematic differences in assumed input parameters. Two types of uncertainties should be considered for the

input parameters. One is systematic; it involves factors such as incorrect initial assumptions on transport coefficients, errors in the laboratory-measured coefficients, or the failure to include important reactions. This type of uncertainty cannot be evaluated by statistical methods but rather must be determined by stratospheric measurements that compare model predictions with observation. These measurements have not yet been made for the Cl chemistry associated with the Space Shuttle exhaust. Therefore, the systematic errors in the model predictions cannot be fully evaluated at this time. Some indication of the possible range of systematic errors might be gained from comparison of results from different stratospheric models. These errors range over a factor of 3. Random errors, such as standard deviation associated with rate-constant determinations, are susceptible to statistical analysis; for one model, these random errors lead to a factor of 3 at a 50-percent confidence level.

The range of reasonable Space Shuttle O_3 depletion predictions is from 0.1 to 0.3 percent for 60 launches per year averaged over the Northern Hemisphere. This range represents a lower limit to the uncertainty in the perturbation. An additional probability distribution of a factor of 3 on either side can be attached to any chosen centerline value. For planning purposes, the JSC Environmental Effects Project Office chose a centerline value of 0.2 percent. This value fits within the random-error bounds of all model predictions considered and represents a reasonable compromise on the systematic errors associated with the choice of assumed input parameters.

Preliminary calculations using multidimensional models have provided an approximate picture of the north/south distributions of total chloride and its depletion effects. Approximately 30 percent of the Cl eventually reaches the Southern Hemisphere in the steady state (rather than 0 percent as assumed for the one-dimensional models). Preliminary calculations also show a seasonally changing "corridor" effect, such that the O_3 depletion near latitude 30° N is 2 times the Northern Hemisphere average during the summer and 1.5 times the average during the spring and fall.

The O_3 reduction effects estimated for the various Space Shuttle exhaust products (one-dimensional models, hemispherically averaged products) are as follows.

Propellant	Depletion by HCl, percent	Depletion by oxides of nitrogen, percent	Depletion by Al_2O_3 particles, percent
Baseline (21 percent HCl)	0.2	<0.001	<0.001
High-Cl alternate (5.8 percent HCl)	.08	<0.001	<0.001
Low-Cl alternate (3 percent HCl)	.04	<0.001	<0.001

EFFECTS OF PARTICULATE EXHAUST EMISSIONS

The Al_2O_3 particles in the exhaust plume could function as catalytic agents for O_3 decomposition or they could alter the radiation balance of the Earth by reflecting sunlight. Both of these effects have been analyzed and found to be negligible. The Al_2O_3 particles could also function as nucleation centers for sulfuric acid (H_2SO_4) aerosols which occur naturally in the stratosphere. Any change in the natural H_2SO_4 aerosols could be climatologically significant. (This problem is currently being studied.)

PLUME AFTERBURNING EFFECTS

"Frozen" chemical equilibrium in the nozzle and an afterburning of the exhaust plume produces NO, which could cause additional O_3 depletion. Conclusions on this subject were as follows.

1. The oxides of nitrogen (NO_x) production rate for the baseline propellant in the stratosphere is two orders of magnitude lower than the HCl production rate.

2. The alternate propellant "A" NO_x production rate in the stratosphere is as much as 10 times greater relative to HCl than for the baseline propellant.

In any case, whether the baseline or alternate propellants are used, the O_3 depletion effect of afterburning will be at least an order of magnitude less than that caused by the HCl content. It is consequently considered to be negligible and will not be further considered.

MEDICAL/BIOLOGICAL EFFECTS OF ESTIMATED O_3 REDUCTION

The estimated O_3 reduction can be converted by a series of assumptions and calculations into a rough estimate of the increase in biologically harmful ultraviolet (BHuv) radiation from the Sun. It is generally assumed that X percentage of O_3 reduction results in an approximately 2X increase in BHuv radiation for small O_3 reductions. Thus, a 0.1- to 0.3-percent reduction in O_3 results in a 0.2- to 0.6-percent increase in BHuv radiation. A 0.4-percent increase in BHuv radiation was chosen for assessing the potential impact on the biosphere.

Based on the limited available biological data, the impact on the biosphere of an assumed 0.4-percent increase in BHuv radiation has been assessed, and the following conclusions were drawn.

1. The effects on the biosphere of a 0.4-percent increase in BHuv radiation will not be detectable even after decades of observation; the natural BHuv irradiances are highly variable, and so are the responses of organisms and ecosystems to given doses of BHuv radiation at given dose rates. However, the fact that a cause-and-effect relationship of an increase in BHuv radiation cannot be established does not mean that an increase in BHuv radiation can be ruled out as a contributor to some deleterious future event; lack of detectability is not equatable with a lack of effect.

2. There is a very low probability that an average 0.4-percent increase in BHuv radiation will have any unacceptable effect on agricultural plants or natural ecosystems. This conclusion is based primarily on the wide range of BHuv irradiances to which agricultural and natural ecosystems are currently exposed without apparent impact and on the fact that more important and pervasive factors (e.g., temperature, precipitation, interspecies competition) generally limit the geographical distribution of vegetation types.

3. Some increase in the number of skin cancer cases may occur among susceptible individuals as a result of a 0.2-percent O_3 reduction; however, because of the great variability of normal BHuv radiation and biological responses mentioned previously, the long latent period (20 to 60 years) for the appearance of skin tumors, and the many other factors that already may be tending to increase or decrease the number of skin cancer cases (both reported and unreported), the increase will not be detectable.

4. The number of skin cancer cases resulting from a 10-year-duration, 0.2-percent O_3 reduction is not realistically predictable. (The widely publicized "prediction" that a 1-percent decrease in stratospheric O_3 will lead to approximately 6000 more cases of skin cancer each year in the United States alone is based on questionable data and refers to a lifetime exposure). The extant experimental and epidemiological data, although clearly suggesting a contribution of solar radiation exposure to skin cancer incidence, are inadequate for making quantitative predictions with reasonable limits of uncertainty for the Shuttle case.

Three reasons why the data are inadequate for quantitatively predicting the additional number of individuals developing skin cancer as a result of a 0.2-percent O_3 reduction are as follows.

1. The true current baseline annual incidence is not accurately known, and the number of cases reported does not necessarily reflect the number of cases that occur; moreover, the reported incidence is increasing rapidly even in the absence of any apparent O_3 reduction.

2. The reported annual incidence data apply to cases, not to patients; a sizable number of new cases occur in previously affected susceptible individuals.

3. The analyses of the epidemiological data do not adequately consider other contributing factors such as carcinogenic chemicals in the environment, changes in lifestyle (increased outdoor living and changes in clothing and hair style), geographic location of domicile prior to the development of skin cancer, and ethnic character.

Finally, the basic epidemiological data for skin cancer incidence are obviously for a full lifetime exposure to sunlight. The induction period for skin cancer is 20 to 60 years, averaging near 40 years. The Shuttle effects will last about 10 years. Current predictive models for skin cancer do not take the exposure period into account and therefore cannot be applied correctly to the Shuttle case.

TABLE 2-I.- ATTENDEES OF THE WORKSHOP

Attendee	Agency
J. Q. Miller	NASA MSFC[a]
J. B. Stephens	NASA MSFC
R. D. Hudson	NASA GSFC[b]
R. S. Stolarski	NASA JSC
C. E. Baker	NASA Lewis Research Center
R. D. Rundel	NASA JSC
S. C. Liu	University of Michigan
D. M. Butler	Rice University
D. E. Robbins	NASA JSC
G. Varsi	NASA JPL[c]
A. E. Potter	NASA JSC
J. Stanley	NASA JSC
G. L. Pellett	NASA Langley Research Center
R. Stanley	NASA Langley Research Center
I. G. Poppoff	NASA ARC[d]
M. H. Farlow	NASA ARC
R. C. Whitten	NASA ARC
O. B. Toon	NASA ARC
D. Davis	University of Maryland

[a]George C. Marshall Space Flight Center.

[b]Goddard Space Flight Center.

[c]Jet Propulsion Laboratory.

[d]Ames Research Center.

TABLE 2-I.- Concluded

Attendee	Agency
R. Cicerone	University of Michigan
J. S. Chang	LLL ERDA[e]
D. S. Nachtwey	NASA JSC
L. R. Greenwood	NASA Langley Research Center
P. Wetzel	NASA Headquarters
R. T. Watson	JPL[c]
L. Keyser	JPL
W. B. Moore	JPL
P. J. Armitage	NASA JSC
H. S. Pergament	AeroChem
B. G. Cour-Palais	NASA JSC
D. J. Kessler	NASA JSC
R. P. Turco	R&D Associates
C. Riegel	San José State University
R. Prinn	MIT[f]
P. B. Burband	NASA JSC
H. Rudolph	NASA KSC[g]
J. King	NASA Headquarters

[c]Jet Propulsion Laboratory.

[e]Lawrence Livermore Laboratory Energy Research and Development Administration.

[f]Massachusetts Institute of Technology.

[g]John F. Kennedy Space Center.

3. BASELINE AND ALTERNATE PROPELLANTS:

BALLISTICS AND EXHAUST COMPOSITION

A study of low-Cl solid propellants was initiated in August 1974 with the objective of defining possible alternates to the baseline propellant. Complete replacement of the perchlorate propellant with a nitrate-based propellant causes unacceptable ballistic performance. Consequently, a composite propellant grain was considered in which the baseline propellant is burned out at a maximum altitude of 20 kilometers (63 000 feet). Then, the burn changes to an alternate low-Cl formulation for passage through the stratosphere.

Approximately 250 different possible alternate propellant formulations were evaluated. These formulations included various combinations of AP and non-HCl-producing oxidizers such as ammonium nitrate (AN), cyclotetramethylenetrinitramine (HMX), trimethylethanitrinitrate, nitrocellulose, nitroglycerine, and cyclotrimethylenetrinitramine. Formulations were first evaluated on a theoretical basis in comparison with the baseline AP-oxidized propellant. From this comparison, the most promising alternate propellant formulations were selected for preliminary process, compatibility, hazard, burn rate, pressure exponent, and density impulse characterization. Based on results from these characterizations, the best HMX- and non-HMX-containing alternate propellant formulations were selected for additional evaluation. A formulation and ballistic property comparison of these two alternate formulations ("A" and "B") with the baseline formulation is presented in table 3-I. To achieve acceptable ballistic properties, both alternate formulations require the addition of AP. The theoretical exhaust composition for the baseline and alternates "A" and "B" is presented in table 3-II.

The most promising design concept developed was a double-web star propellant grain configuration (dual-grain concept). With this concept, the baseline propellant is completely burned out at an altitude of approximately 20 kilometers (63 000 feet) and the alternate propellant (low HCl) is burned at altitudes above 20 kilometers (63 000 feet); thus, minimum cost and performance impacts result. Alternate propellant formulations "A" and "B" were separately used with the baseline propellant to design two booster solid rocket motors incorporating the dual-grain concept. Figures 3-1, 3-2, and 3-3 contain data on thrust as a function of time and mass flow characteristics for the baseline, alternate "A," and alternate "B" designs, respectively.

Results from preliminary burn rate tests conducted on the alternate "B" propellant indicate that AP levels as high as 20 percent by weight may be required to obtain acceptable burn rates and combustion efficiencies. This change will increase the HCl percentage weight in the exhaust from 3.1 to approximately 5.8. Other exhaust constituent percentage weights are not significantly affected by this change. Therefore, for current environmental assessments, it is recommended that an HCl percentage weight range of 3.1 to 5.8 be used for alternate propellants. Use of this concept results in a ballistic performance loss estimate of approximately 3 percent for the entire grain (i.e., 25 percent of the grain consists of propellants having approximately 10 percent less specific impulse).

TABLE 3-I.- PROPELLANT FORMULATION AND BALLISTIC PROPERTY DATA

Constituent or property	Propellant		
	Baseline	Alternate "A"	Alternate "B"
Propellant formulation, wt %			
AP	70	10	10
AN	--	44	61
Al	16	15	15
HMX	--	17	--
Binder and additives	14	14	14
Ballistic properties			
Burn rate at 6895 kPa (1000 psia), cm/sec (in/sec)			
Measured	1.07 (0.42)	0.79 (0.31)	0.53 (0.21)
Estimated	1.07 (0.42)	0.89 (0.35)	0.76 (0.30)
Pressure exponent			
Measured	0.35	0.28	0.28
Estimated	0.35	0.30	0.28
Density, kg/m^3 (lb/in^3)	1774.28 (0.0641)	1652.49 (0.0597)	1646.95 (0.0595)
Flame temperature at 4826 kPa (700 psia), K (°F)	3411 (5680)	2690 (4382)	2750 (4490)
Theoretical vacuum specific impulse, sec	275.1	267.3	266.6
Initial vacuum delivered specific impulse, sec			
Measured	263.5	242.2	231.8
Estimated	263.5	247.6	242.5

TABLE 3-II.- THEORETICAL PROPELLANT EXHAUST COMPOSITION

[Percentage weight]

Constituent	Baseline	Alternate	
		"A"	"B"
HCl	20.9	3.1	3.1
Molecular hydrogen (H_2)	2.1	3.7	2.9
Water (H_2O)	9.4	6.1	16.2
Carbon monoxide (CO)	24.1	31.8	19.6
Carbon dioxide (CO_2)	3.5	3.8	6.5
Molecular nitrogen (N_2)	8.7	22.9	23.2
Al_2O_3	30.2	28.2	28.3
Other	1.1	.4	.2

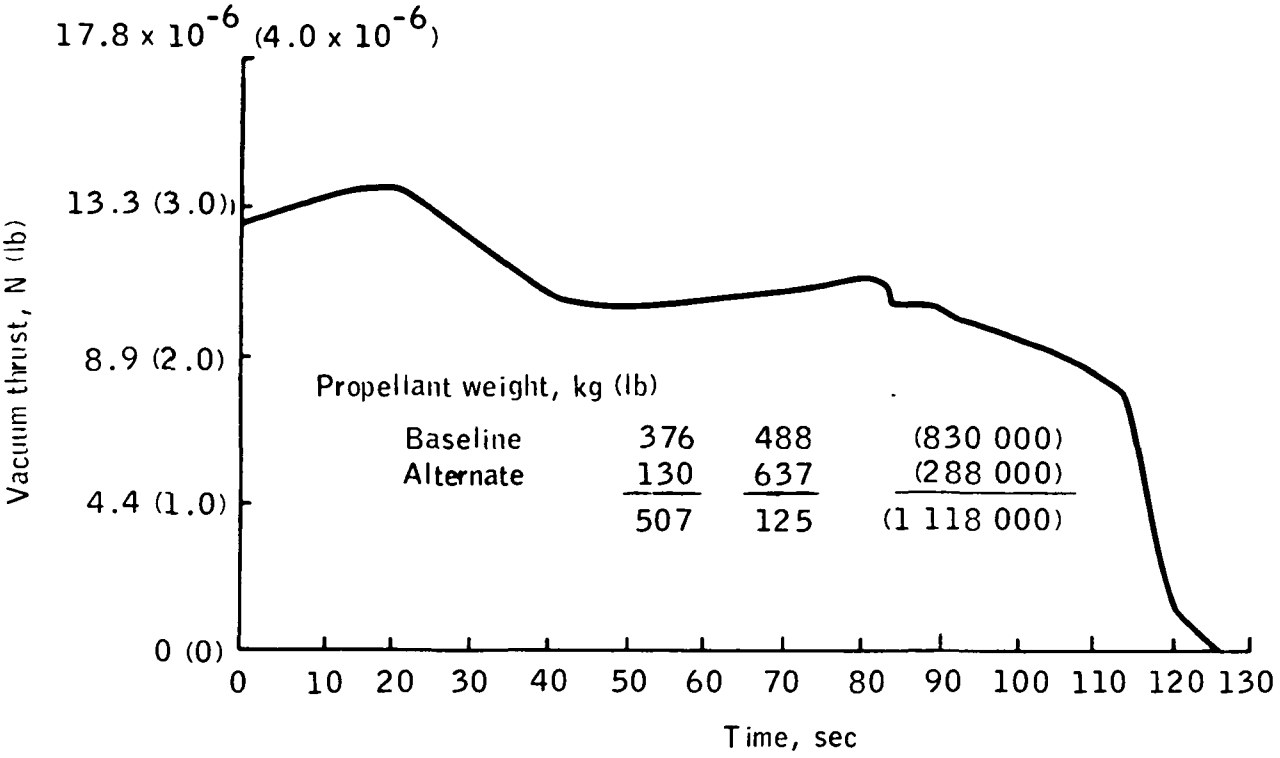

Time, sec	Altitude, m (ft)	Mass flow rate, kg/sec (lb/sec)
0	0	0
10	305 (1 000)	5 263 (11 603)
20	1 372 (4 500)	5 441 (11 996)
30	2 896 (9 500)	4 735 (10 439)
40	4 877 (16 000)	4 166 (9 185)
50	7 315 (24 000)	4 050 (8 929)
60	10 363 (34 000)	4 091 (9 020)
70	14 326 (47 000)	4 198 (9 255)
80	18 288 (60 000)	4 396 (9 692)
[a]83.36	19 507 (64 000)	4 301 (9 483)
90	22 860 (75 000)	4 232 (9 329)
100	28 651 (94 000)	3 833 (8 450)
110	34 442 (113 000)	3 456 (7 620)
120	41 453 (136 000)	505 (1 114)
125	44 196 (145 000)	115 (253)

[a] Transition to alternate propellant.

Figure 3-1.- Baseline thrust as a function of time and mass flow characteristics.

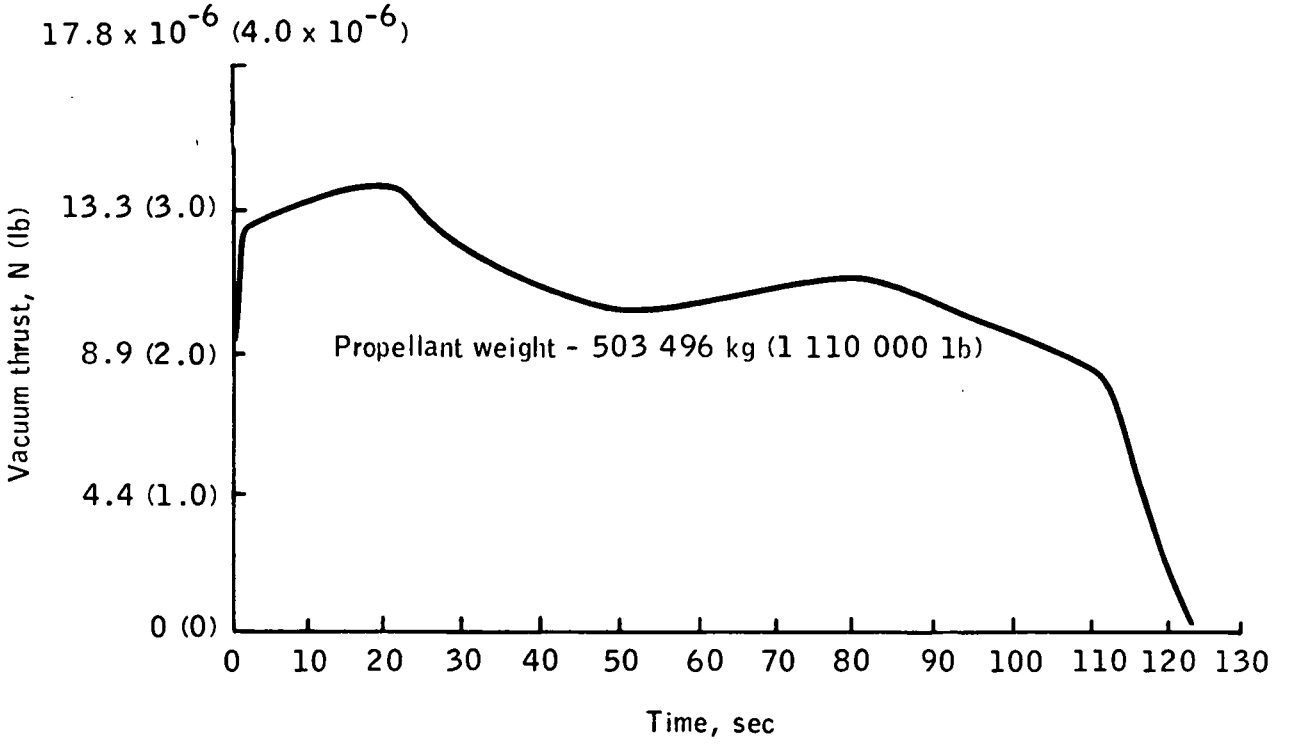

Time, sec	Altitude, m (ft)	Mass flow rate, kg/sec (lb/sec)
0	0	0
10	305 (1 000)	5 325 (11 740)
20	1 372 (4 500)	5 478 (12 076)
30	3 048 (10 000)	4 751 (10 475)
40	5 182 (17 000)	4 274 (9 423)
50	7 620 (25 000)	3 947 (8 702)
60	10 363 (34 000)	4 070 (8 972)
70	14 326 (47 000)	4 295 (9 469)
80	18 288 (60 000)	4 414 (9 731)
90	23 774 (78 000)	4 080 (8 995)
100	28 956 (95 000)	3 634 (8 011)
110	35 357 (116 000)	3 304 (7 283)
120	42 672 (140 000)	735 (1 621)
125	45 720 (150 000)	24 (52)

Figure 3-2.- Alternate "A" thrust as a function of time and mass flow characteristics.

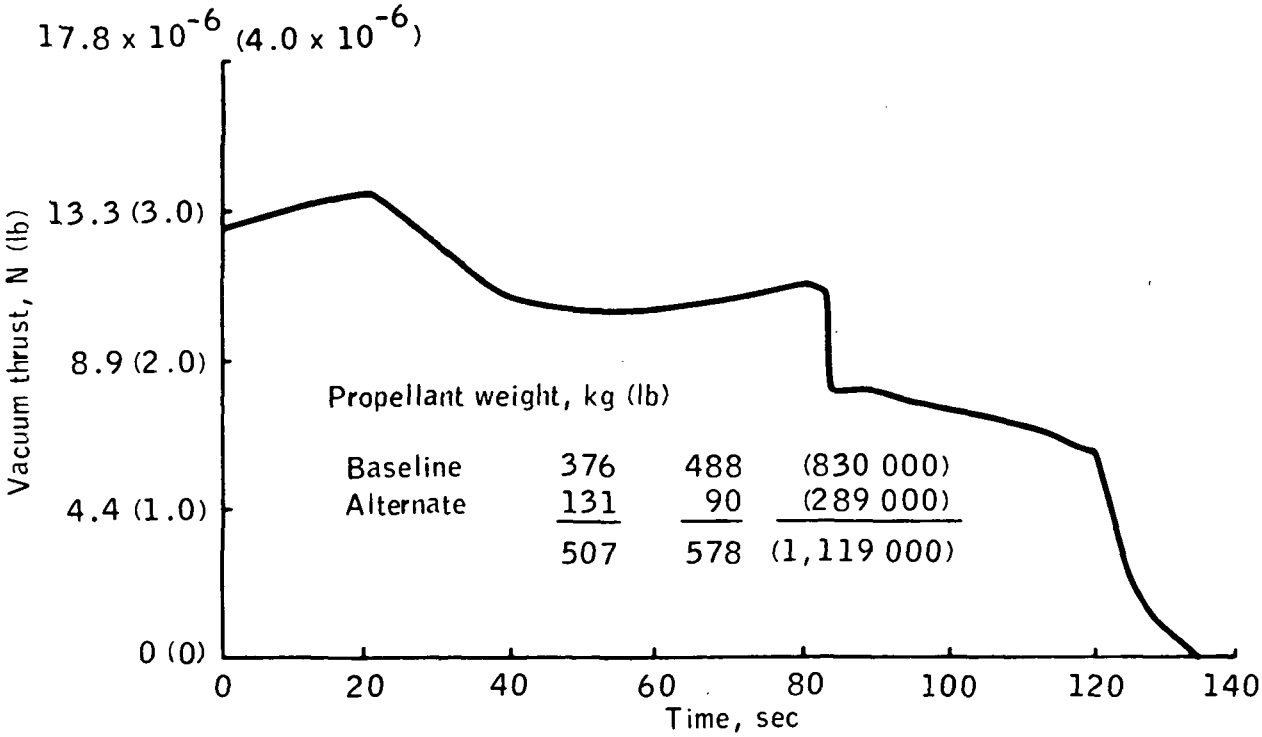

Time, sec	Altitude, m (ft)	Mass flow rate, kg/sec (lb/sec)
0	0	0
10	305 (1 000)	5 263 (11 603)
20	1 372 (4 500)	5 441 (11 996)
30	2 743 (9 000)	4 735 (10 439)
40	4 724 (15 500)	4 166 (9 185)
50	7 163 (23 500)	4 050 (8 929)
60	10 211 (33 500)	4 091 (9 020)
70	14 326 (47 000)	4 198 (9 255)
80	18 288 (60 000)	4 396 (9 692)
83.4	19 507 (64 000)	3 472 (7 654)
90	22 860 (75 000)	3 481 (7 675)
100	28 346 (93 000)	3 248 (7 160)
110	34 138 (112 000)	3 039 (6 700)
120	40 538 (133 000)	2 694 (5 940)
130	46 634 (153 000)	328 (723)
135	49 682 (163 000)	119 (262)

[a]Transition to alternate propellant.

Figure 3-3.- Alternate "B" thrust as a function of time and mass flow characteristics.

4. STRATOSPHERIC MODELING

Compounds of Cl and nitrogen (N) catalyze the reaction of O_3 with atomic oxygen (O). Therefore, HCl and NO_x released from the Space Shuttle exhaust into the stratosphere can result in a net reduction of O_3 and consequently increase the amount of solar uv radiation at the Earth surface.

The O_3 depletion effects of exhaust products may be estimated by use of theoretical stratospheric models. In these models, two major factors are considered: (1) the transport of chemical compounds into and out of the stratosphere and (2) chemical reactions in the stratosphere. Transport coefficient input data for the models are estimated by the analysis of vertical concentration profiles through the stratosphere. The relative importance of various chemical reactions in the models is estimated from laboratory measurements and, in special cases, from stratospheric measurements of the concentrations of intermediate species, such as hydroxyl (OH).

In the sections which follow, the current situation with respect to chemical rates and stratospheric measurements will be surveyed. Following this survey will be discussions of various models and their O_3 depletion predictions.

STRATOSPHERIC REACTION RATES

The complex network of chemical reactions involved in O_3 depletion is illustrated in figure 4-1, wherein C is carbon, F is fluorine, ^1D is an energy state, $H\nu$ is photon energy, and M is an energy-providing molecule. Not all the possible reaction processes are shown — only those believed to be most important. Recently measured rate expressions for 18 reactions are listed in table 4-I (refs. 4-1 to 4-5). This table also shows the estimated precision (as opposed to accuracy) where such information is available. Additional data are contained in reference 4-6 and an unpublished article.[1]

Despite recent advances in reaction rate measurements, not all the required data are available. Improved data are particularly needed for reactions involving HO_2, of which the most important are two:

$$OH + HO_2 \rightarrow H_2O + O_2 \qquad (4\text{-}1)$$

$$O + HO_2 \rightarrow OH + O_2 \qquad (4\text{-}2)$$

---

[1] R. T. Watson: Rate Constants of ClO_x of Atmospheric Interest. To be published in the Journal of Physical Chemistry.

Programs to measure these rate constants are underway in several laboratories.

Other reactions for which improved measurements are needed are those involving formation and destruction of chlorine nitrate ($ClNO_3$), oxidation of methane (CH_4), and formation of HCl. Specific reactions include the following.

$$NO + HO_2 \rightarrow NO_2 + OH \qquad (4\text{-}3)$$

$$Cl + CH_4 \rightarrow HCl + CH_3 \qquad (4\text{-}4)$$

$$Cl + HO_2 \rightarrow HCl + O_2 \qquad (4\text{-}5)$$

$$CH_3O_2 + NO \rightarrow \text{products} \qquad (4\text{-}6)$$

$$CH_3O_2 + HO_2 \rightarrow \text{products} \qquad (4\text{-}7)$$

$$ClO + NO_2 + M \rightarrow ClNO_3 + M \qquad (4\text{-}8)$$

$$ClNO_3 + O \rightarrow \text{products} \qquad (4\text{-}9)$$

$$ClNO_3 + OH \rightarrow \text{products} \qquad (4\text{-}10)$$

Photochemical studies of the following processes are also needed.

$$ClNO_3 + h\nu \rightarrow \text{products not defined} \qquad (4\text{-}11)$$

$$HOCl + h\nu \rightarrow \text{products not defined} \qquad (4\text{-}12)$$

$$HO_2 + h\nu \rightarrow \text{products not defined} \qquad (4\text{-}13)$$

$$CH_2O + h\nu \begin{array}{l} \nearrow \; CO + H_2 \\ \searrow \; H + HCO \end{array} \qquad (4\text{-}14)$$

where h is the Planck constant and ν is photon frequency.

A continuing investigation should be maintained to identify any possible reactions of significance which may have been omitted from the present stratospheric chemical models.

MEASUREMENT OF STRATOSPHERIC MINOR CONSTITUENTS

Stratospheric measurements are needed to provide experimental estimates of eddy diffusion coefficients, to narrow the uncertainty range of important reaction rates, and to evaluate the general validity of the stratospheric models. In general, transport terms can be derived from measurements of the vertical concentration profiles of sources and sinks which have clearly defined loss rates in the stratosphere (as CH_4 and ^{14}C), although terms derived in this way do depend on the details of the model used.

Important reaction rate information has been derived from measurements of unstable species, such as OH. Measurements aimed at verification of the complex of reactions shown in figure 4-1 have not been made, with the possible exception of NO/nitrogen peroxide (NO_2). For this reaction, simultaneous measurements of associated species must be made. Thus, for the Cl chemistry associated with the Space Shuttle problem, simultaneous measurements of ClO, HCl, OH, NO, O_3, O, uv flux, and a transport tracer, such as CH_4 or nitrous oxide (N_2O), are needed.

Chlorine Compounds

Chlorine compounds to be measured are HCl, ClO, Cl, halocarbons (both natural and manmade), and particulate chloride. Measurements of HCl have been done; these show increases from less than 0.1 part per billion by volume (ppbv) near an altitude of 15 kilometers (47 000 feet) to 0.5 to 1 ppbv at an altitude of 25 to 30 kilometers (82 000 to 98 000 feet). This altitude profile is attributed to a stratospheric source (probably photodissociation of halocarbons) and a tropospheric sink (rainout). No satisfactory measurements of ClO or Cl exist at this time, although ClO measurements are in progress by several investigators.

Altitude profiles have been measured for several halocarbons (e.g., CF_2Cl_2 and $CFCl_3$) with results that are consistent with photodissociation at altitudes above 20 kilometers (63 000 feet). Particulate matter suspended in the stratosphere has been analyzed and found to contain negligible amounts of chloride. Consequently, these particles do not appear to be important sources or sinks for Cl.

Hydrogen Compounds

Vertical profiles for H_2O and CH_4 have been measured by several investigators; the CH_4 profiles have been used in the estimation of transport coefficients. Different investigators have measured OH in different altitude ranges. The most significant measurements relative to the stratospheric problem (ref. 4-7) are in the range of 30 to 43 kilometers (98 000 to 140 000 feet). These results have been used to "tune" some stratospheric chemistry models by adjusting uncertain rate constants to match the observed altitude profile. Recent ground-based measurements (R. Burnett, private communication) are significant because they show the total OH concentration (vertical column content) to be "patchy," varying by almost an order of magnitude.

Nitrogen Compounds

Odd-N composites (NO, NO_2, and nitric acid (HNO_3)) are produced by reaction of $O(^1D)$ with N_2O. There are numerous measurements at different times and places of NO, NO_2, HNO_3, and N_2, but in situ simultaneous measurements are lacking. Below an altitude of approximately 40 kilometers (131 000 feet), the chemistry is such that odd-N compounds are split somewhat evenly among the three species, so that individual measurements of one or even two of these species in this region do not yield accurate estimates of the total odd-N content of the stratosphere to which a model can be adjusted. This fact is important to the Space Shuttle problem since predicted Cl perturbations are quite sensitive to the amount of NO present. Various measurements of NO differ by as much as an order of magnitude. Estimates of odd-N mixing ratios in the near-asymptotic region above 30 kilometers (98 000 feet) made from the existing measurements range from a few parts per billion by volume to a few tens of parts per billion by volume. Most models contain asymptotic odd-N mixing ratios of 10 to 20 ppbv. More high-altitude NO measurements are necessary, in addition to in situ simultaneous measurements of all the major odd-N constituents, to test the chemical reaction schemes.

The major source of odd-N compounds in the stratosphere is N_2O. Ground-level measurements of N_2O (R. A. Rasmussen, private communication) yield results in the range of 0.3 to 0.35 part per million by volume (ppmv) of N_2O. These are higher than earlier measurements (ref. 4-8), which were 0.25 to 0.27 ppmv. In contrast to previous measurements, the measurements in remote areas show almost no random variation. This uniformity possibly indicates a longer atmospheric residence time. If the stratosphere is the only sink and if the longer residence time is real, a source/sink balance problem, which is currently being debated, still remains.

New stratospheric profiles of N_2O (A. L. Schmeltekopf, private communication) show a much more rapid decrease with altitude than did previous results.

This difference may be a manifestation of the variability of atmospheric dynamics.

Transport Terms

Effective vertical eddy diffusion coefficients have been derived from the analysis of vertical concentration profiles for substances with known loss rates in the stratosphere. For example, the vertical distribution of CH_4 is determined by the effective upward transport rate and the reaction of CH_4 with $O(^1D)$, OH, and Cl. The loss rate by chemical reaction can be estimated and used with the profile data to obtain an effective vertical eddy diffusion coefficient.

Different species (as carbon-14), seasons, or locations yield different eddy diffusion coefficients. This conclusion is illustrated in figure 4-2, in which six different profiles proposed by different investigators are compared. Substantial differences are seen, and these are reflected in results from stratospheric models. It is evident that work is needed to reduce or to understand the uncertainties associated with vertical transport.

MODELING OF O_3 DEPLETION BY HCl DEPOSITION FROM SPACE SHUTTLE

Hydrogen chloride deposition by Space Shuttle booster combustion commences at launch and continues until burnout at 45 kilometers (155 000 feet). The rate of HCl emission in metric tons per kilometer (ref. 4-9) is shown in figure 4-3. At peak operational activity, 60 launches per year are planned. Launch operations are expected to commence in 1978; they build up to 60 per year by 1984 according to the schedule shown in figure 4-4. The rate of HCl emission from the alternate propellants described in the previous section can be obtained by multiplying the baseline emission rate by appropriate factors derived from table 3-II.

Five groups of investigators, each with a different one-dimensional stratospheric model, were represented at the workshop. Present were R. C. Whitten from the NASA Ames Research Center (ARC), R. Turco from R&D Associates, R. Cicerone and S. C. Liu from the University of Michigan, J. Chang from the Lawrence Livermore Laboratory (LLL), and R. Rundel and R. Stolarski from JSC. In addition, written and verbal (telephone) information was provided by S. Wofsy of Harvard University. These groups were asked to run their models for Space Shuttle injection of Cl at the rate of 60 launches per year, with north/south transport rates taken crudely into account by assuming the source to be averaged over the Northern Hemisphere.

Although all the models used the same amount of added Cl, they differed in the details of the reaction schemes; in choice of rate constants and cross sections, boundary conditions, and transport parameters; and in details of the mathematical manipulations. The results are shown in the third column of

table 4-II. A range of calculated O_3 depletions from 0.1 to 0.3 percent for the hemispherically averaged Space Shuttle source is found.

In the following sections of this report, more detailed comparisons of the various models are described. For this purpose, an attempt was made to separate the Cl perturbation predictions into effects caused mostly by transport (and boundary conditions) and those caused mostly by chemistry. The calculated asymptotic (i.e., above approximately 35 kilometers (114 000 feet)) mixing ratio of total Cl (Cl_x) is listed in the second column of table 4-II, and the efficiency of the perturbing Cl_x in terms of percentage change of O_3 per part per billion by volume of added Cl_x, is shown in the fourth column. The former depends only on transport, whereas the latter indicates to a large extent differences in assumed chemistry.

Model Comparison

Differences in the models used are discussed in the following paragraphs.

Transport parameters.- Most of the models employed to evaluate the effect on the O_3 layer of HCl emitted by Space Shuttle launch vehicles are one dimensional. Transport is thus confined to the vertical dimension and must be parameterized by an "eddy diffusion coefficient" profile. The physical basis for such a set of parameters is weak. In practice, one can make use of the concept by adjusting the eddy diffusivity profile such that it leads to predictions of vertical distributions of tracers such as carbon-14, CH_4, and total odd N that are close to observed values. Vertical eddy diffusion, then, represents the real transport with all its spatial and temporal variability averaged over the globe or hemisphere and over a long time period.

The eddy diffusion profiles used by various groups to study Space Shuttle effects on O_3 are shown in figure 4-2. To predict measured tracer distributions adequately, eddy diffusivity profiles must have the following characteristics.

1. A rapid decrease from large tropospheric values to a deep minimum located between 13 and 15 kilometers (42 000 and 47 000 feet)

2. A value at the minimum ranging from 1×10^3 to 5×10^3 cm^2/sec

3. A rapid increase from the minimum to a value of $>10^5$ cm^2/sec at 50 kilometers (163 000 feet)

Beyond these broad characteristics, the various model eddy diffusivities differ in that they predict somewhat different tracer distributions and are dependent on model structure.

It was generally felt that uncertainties were approximately ±2 near the minimum and ±3 near 50 kilometers (163 000 feet). The coefficients referred

to in table 4-II are shown in figure 4-2. The labels in figure 4-2 refer to those in the second column of table 4-II for each model. Relatively large volumes of the coefficients result in small values for the steady-state asymptotic Cl_x mixing ratios from the Space Shuttle and vice versa.

Boundary conditions.- It was generally agreed that, within the realm of reasonable choices, boundary conditions were not particularly crucial to the Space Shuttle problem. The problem of choosing an upper boundary condition for CH_4 flux was discussed. This value assumes importance when CH_4 is being used to deduce an eddy coefficient. Boundary conditions for the Cl injected by Space Shuttle should be a very small or zero mixing ratio at the tropopause and zero flux at some altitude above 45 kilometers (155 000 feet).

Effect of oxides of hydrogen on Cl perturbations of O_3.- In this and the next two subsections, aspects of the chemistry of the models which determine the efficiency of O_3 perturbation as given in the fourth column of table 4-II are discussed. Some of the differences can be ascribed to the choices made in calculating the oxides of hydrogen (HO_x). The key constituent is OH because its direct reaction with HCl forms Cl, which participates in the catalytic O_3 destruction cycle. Computed values of the concentration of OH at 35 to 40 kilometers (114 000 and 131 000 feet) are shown in the seventh and eighth columns of table 4-II. The estimates used for two crucial rate parameters, $OH + HO_2 \rightarrow H_2O + O_2$ and $O + HO_2 \rightarrow OH + O_2$, are given in the fifth and sixth columns. These rates are crucial because they exert a controlling influence on the calculated OH concentration and because their rates are virtually unknown. One technique is to adjust these rates within a limited range to fit the recent OH measurements (ref. 4-10), $\sim 2 \times 10^7$ cm^{-3} at 40 kilometers (131 000 feet). This "tuning" process was discussed together with the uncertainties caused by the apparent variability of OH as indicated in Burnett's column content measurements. It was agreed that the calculated OH shown in the table fairly closely reflects the choice of rates in the fifth and sixth columns and that the efficiency is directly related to the computed OH around 40 kilometers (131 000 feet).

Effect of No_x on Cl perturbations of O_3.- An inverse relationship exists between NO_x concentrations and the efficiency of Cl perturbations. This relationship occurs for two reasons.

1. The NO_x catalytic cycle is the principal destruction mechanism for O_3 in the stratosphere. Larger NO_x concentrations produce a larger O_3 destruction rate; hence, the fractional effect of a given Cl_x concentration is less.

2. The ClO reacts with both O and NO, but the latter leads to no net O_3 destruction; hence, increased NO leads to a lower efficiency of O_3 destruction.

Column 10 of table 4-II shows the calculated asymptotic mixing ratio of total odd N ($NO + NO_2 + HNO_3$) for each of the models. Two factors exert the major control over the differences. One is the eddy diffusion coefficient and the other is the choice of O^1D reaction rates. The effect of the eddy diffusion coefficient is such that a larger coefficient tends to diffuse more N_2O to altitudes where it can react with O^1D to produce NO; thus, a larger source is provided while the produced NO is diffused more rapidly toward its sink in the troposphere. The net effect is calculated to be in the same direction as that for the Space-Shuttle-injected Cl_x; that is, faster diffusion implies less odd N. However, because of the competing N_2O diffusion, the odd-N concentration is not as sensitive to the eddy diffusion coefficient as is the Cl_x concentration. This fact is clearly illustrated in columns 2 and 10 of table 4-II.

It was generally agreed that the gross features of the differences in Space Shuttle perturbation calculations were explained on the basis of the differences in the eddy coefficients and the choice of reaction rates including OH and O^1D. The OH and the odd-N contents reflect these differences.

Chlorine nitrate formation.- It has been suggested that the formation of $ClNO_3$ could be important to the stratospheric chemistry of Cl. Its formation by way of a three-body reaction ($ClO + NO_2 + M \rightarrow ClNO_3 + M$), its destruction by way of photodissociation, and its reaction with O or OH were hypothesized. If this suggestion is correct, the net effect is to tie up both Cl_x and NO_x in a temporary nonreactive compound and to reduce the expected O_3 perturbation.

At the stratospheric workshop, none of the model calculations reported included possible effects caused by $ClNO_3$; no generally accepted measurement of its formation rate has been made. However, calculations made after the workshop by the JSC and University of Michigan groups indicate that if the formation rate of $ClNO_3$ is approximately 10^{-31} cm^6/sec, reported O_3 depletions are reduced by a factor of approximately 2. The ARC group calculated a factor of 2 to 4 (appendix D).

Application of Models to the Space Shuttle Program

The various models were applied to questions related to the Space Shuttle, as shown in the following paragraphs.

Evaluation of suggested alternate propellants.- Three of the models were used to evaluate the change in the estimated O_3 depletion which would result from a switch from the baseline propellants to the alternates "A" and "B" described earlier in this report. The improvement factor for each alternate calculated by the various models is shown in table 4-III. There is general

agreement that a switch to alternate "A" at 20 kilometers (63 000 feet) will decrease the predicted O_3 depletion by a factor of 4 to 5 if alternate "A" has 3.1 percent HCl at the exit plane and a factor of 3 if it has 5.8 percent HCl at the exit plane. For alternate "B," the improvement is slightly less, a factor of 4 for a 3.1 percentage and a factor of 2.5 for a 5.8 percentage. Alternate "B" is slightly worse than alternate "A" because the decrease in burn rate is more than compensated for by the increase in the altitude of burnout.

A parametric study was conducted for the alternate propellants as a function of switchover altitude. These results, shown in figure 4-5, are not substantially different from the previous studies by JSC and ARC in which a switchover to a completely clean propellant was studied. The detailed shape of this curve will vary with exactly which eddy coefficient is chosen. Results indicate that increasing the altitude of switchover to 25 kilometers (82 000 feet) would not greatly change the O_3 depletion effects.

Corridor effect.- The latitude variation of O_3 reduction was approximated with the one-dimensional models by assuming the exhaust products to be distributed uniformly over the Northern Hemisphere only. A more exact calculation of the latitude variation of O_3 reduction was made by using the Massachusetts Institute of Technology three-dimensional model and the ARC two-dimensional models.

The largest effect is during the Northern Hemisphere summer, when the depletion near latitude 30° N is approximately a factor of 2 larger than in the remainder of the Northern Hemisphere. The Northern Hemisphere depletion is a factor of 2 to 3 larger than in the Southern Hemisphere. During the spring, the latitude 30° N to Northern Hemisphere average ratio is approximately 1.5, whereas the Northern Hemisphere average to Southern Hemisphere average is approximately 2.

If these ratios are applied to the one-dimensional hemispherically averaged calculations, it would mean that 20 to 30 percent of the O_3 depletion will occur in the Southern Hemisphere and that the Northern Hemisphere depletion can be correspondingly decreased by this amount. This resulting Northern Hemisphere value will have a factor of $\sim$1.5 enhancement in the summer in a corridor around latitude 30° N and a factor of $\sim$0.5 reduction in the spring. These remarks are illustrated in figure 4-6, in which the summer and winter latitude distributions are shown. The curves labeled "summer" and "winter" have been adjusted so that the area under them is equal to the area under the broken line labeled "one-dimensional approximation."

Time dependence.- A time-dependent calculation of the buildup and decay of O_3 perturbations caused by Space Shuttle launches is shown in figure 4-7. The delay in buildup reflects the slow buildup in the launch schedule. The time constant for ozone recovery if operations should cease may be as short as 2 years and as long as 6 years, depending on the choice of eddy diffusion parameters.

REFERENCES

4-1. Brown, Raymond D. H.; and Smith, Ian W. M.: Absolute Rate Constants for the Reactions of $O(^3P)$ Atoms With Hydrogen Chloride and Hydrogen Bromide. Int. J. Chem. Kinet., vol. 7, no. 2, 1975, pp. 301-315.

4-2. Zahniser, M. S.; Kaufman, F.; and Anderson, J. G.: Kinetics of the Reaction of OH With HCl. Chem. Phys. Letters, vol. 27, no. 4, 1974, pp. 507-510.

4-3. Smith, Ian W. M.; and Zellner, Reinhard: Rate Measurements of Reactions of Hydroxyl Radical by Resonance Absorption. 3. Reactions of Hydroxyl With Dihydrogen, Dideuterium, and Hydrogen and Deuterium Halides. J. Chem. Soc. Faraday Trans. II, vol. 70, no. 6, 1974, pp. 1045-1056.

4-4. Clyne, Michael A. A.; and Walker, Ronald F.: Absolute Rate Constants for Elementary Reactions in the Chlorination of Methane, Methane-d_4, Methyl Chloride, Methylene Chloride, Chloroform, Chloroform-d, Bromotrichloromethane. J. Chem. Soc. Faraday Trans., vol. 69, no. 9, 1973, pp. 1547-1567.

4-5. Davidson, J. A.; Sadowski, C. M.; et al.: Absolute Rate Constant Determinations for the Deactivation of $O(^1D)$ by Time Resolved Decay of $O(^1D) \rightarrow O(^3P)$ Emission. J. Chem. Phys., vol. 64, no. 1, Jan. 1, 1976, pp. 57-62.

4-6. Hampson, R. F.; and Garvin, D., eds.: Chemical Kinetic and Photochemical Data for Modeling Atmospheric Chemistry. NBS Tech. Note 866, June 1975.

4-7. Anderson, J. G.: The Absolute Concentration of $O(^3P)$ in the Earth's Stratosphere. Geophys. Res. Letters, vol. 2, no. 6, June 1975, pp. 231-234.

4-8. Junge, C.; Hahn, J.; et al.: N_2O Measurements in the North Atlantic. J. Geophys. Res., vol. 76, no. 33, Nov. 20, 1971, pp. 8143-8146.

4-9. Nozzle Exit Exhaust Products From Space Shuttle Boost Vehicle (November 1973 Design). JPL TM 33-712, Feb. 1975.

4-10. Anderson, J. G.: The Absolute Concentration of OH $(X^2\pi)$ in the Earth's Stratosphere. Atom-Radical Reaction Systems Final Tech. Rep. (NASA Grant NSG-9031), Univ. of Michigan (Ann Arbor), Aug. 1976.

TABLE 4-I.- RECENT MEASUREMENTS OF CRITICAL RATE CONSTANTS[a]

Reaction	Rate expression, cm^3/molecule-sec	Reference
$HCl + O \rightarrow Cl + OH$	$2.5\times10^{-12}\ \exp(-2900/T^b)$	4-1
$HCl + OH \rightarrow Cl + H_2O$	$2.0\times10^{-12}\ \exp(-313/T)$	4-2
	$4.1\times10^{-12}\ \exp(-500/T)$	4-3
$CH_4 + Cl \rightarrow CH_3 + HCl$	$5.1\times10^{-11}\ \exp(-1790/T)$	4-4
	$7.44\times10^{-12}\ \exp(-1226/T)$	
	$(1.2 \pm 0.3)\times10^{-13}$(295 K)	
$H_2 + Cl \rightarrow H + HCl$	$4.7\times10^{-11}\ \exp(-2340/T)$	--
$Cl + O_3 \rightarrow ClO + O_2$	$2.7\times10^{-11}\ \exp(-257/T)$	--
	$(1.3 \pm 0.3)\times10^{-11}$(295 K)	
$ClO + O \rightarrow Cl + O_2$	$1.07\times10^{-10}\ \exp(-224/T)$	--
	$3.36\times10^{-11}\ \exp(+76/T)$	
$ClO + NO \rightarrow Cl + NO_2$	1.9×10^{-11}	--
	$6.3\times10^{-12}\ \exp(+335/T)$	
$ClO + O_3 \rightarrow (Cl + 2O_2)$	8×10^{-19}(300 K)	--
$ClO + O_3 \rightarrow ClOO + O_2$	1.3×10^{-18}(300 K)	
$ClO + O_3 \rightarrow ClO_2 + O_2$		
$O(^1D) + H_2O \rightarrow$ products	$(2.1 \pm 1.0)\times10^{-10}$(298 K)	4-5
$O(^1D) + CH_4 \rightarrow$ products	$(1.3 \pm 0.3)\times10^{-10}$(298 K)	4-5
$O(^1D) + H_2 \rightarrow$ products	$(1.3 \pm 0.05)\times10^{-10}$(298 K)	4-5
$O(^1D) + N_2 \rightarrow$ products	$(3.0 \pm 0.01)\times10^{-11}$(298 K)	4-5

[a]This table contains measured rates of important stratospheric reactions which have appeared subsequent to the Climate Impact Assessment Program (CIAP) table of recommended rates.

[b]T = ambient temperature.

TABLE 4-I.- (Concluded)

Reaction	Rate expression, cm^3/molecule-sec	Reference
$O(^1D) + O_2 \rightarrow$ products	$(4.1 \pm 0.05)\times10^{-11}(298\ K)$	4-5
$O(^1D) + N_2O \rightarrow$ products	$(1.4 \pm 0.1)\times10^{-10}(298\ K)$	4-5
$Cl + H_2O_2 \rightarrow HCl + HO_2$	$(6.2 \pm 1.5)\times10^{-13}(295\ K)$	--
$Cl + HO_2 \rightarrow HCl + O_2$	$(^{4\ +\ 4.5}_{3\ -\ 1.8})\times10^{-4}(295\ K)$	--
$Cl + HNO_3 \rightarrow$ products	$(6.8 \pm 3.4)\times10^{-15}(295\ K)$	--
$ClNO_3 + h\nu \rightarrow$ products	--	--

TABLE 4-II.- COMPARISON OF O_3 DEPLETION EFFECTS PREDICTED BY VARIOUS STRATOSPHERIC MODELS

Modeling group	Space Shuttle asymptotic Cl_x, ppbv (a)	Percentage O_3 depletion, 60 launches/yr	Efficiency, $\frac{\%\Delta O_3}{Cl_x}$	$k_{OH + HO_2}$, cm^3/sec	$k_{O + HO_2}$, cm^3/sec	Diurnal average		Sources for O^1D rates	Asymptotic odd N, ppbv	$CH_4(40)$, ppbv
						OH(35), cm^{-3}	OH(40), cm^{-3}			
NASA ARC	0.056 (B)	0.11	2	6×10^{-11}	6×10^{-11}	7×10^6	1.6×10^7	CIAP[b]	15	390
Univ. of Michigan	.15 (C)	.29	2	2×10^{-11}	6×10^{-11}	7.6×10^6	2.3×10^7	York/ NOAA[c]	24	300
LLL	.1 (D)	.26	2.6	2×10^{-11}	1.5×10^{-11}	6×10^6	1.2×10^7	York/ NOAA[c]	16	360
NASA JSC, GSFC	.16 (E)	.2	1.3	2×10^{-11}	$.3\times10^{-11}$	8×10^6	1.6×10^7	York NOAA[c]	24	260
Harvard Univ.	.08 (F)	.2	2.5	—	—	—	$\sim2\times10^7$	—	11	—

[a]Vertical eddy diffusion coefficients from figure 4-2 are designated by letters in parentheses.

[b]Climate Impact Assessment Program.

[c]The York/National Oceanic and Atmospheric Administration (NOAA) study was withdrawn.

TABLE 4-III.- IMPROVEMENT FACTORS FOR O_3 DEPLETION RESULTING FROM USE OF ALTERNATE PROPELLANTS

Modeling group	Alternate "A"		Alternate "B"	
	3.1 percent HCl	5.8 percent HCl	3.1 percent HCl	5.8 percent HCl
ARC	4	--	4	--
LLL	4.6	2.8	4.1	2.5
JSC	5	3.3	4	2.5

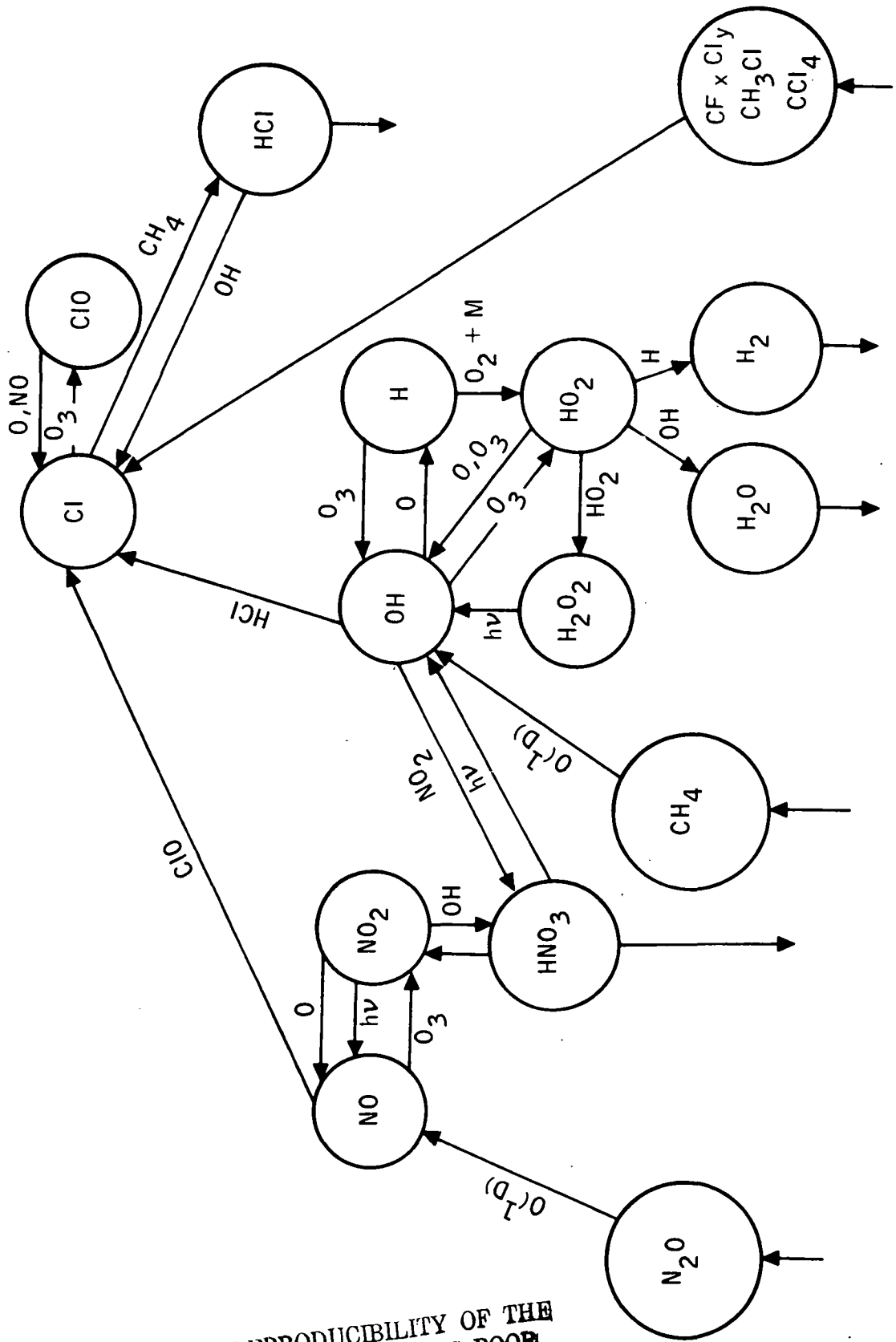

Figure 4-1.- Composite oxygen, hydrogen, nitrogen, and chlorine photochemistry.

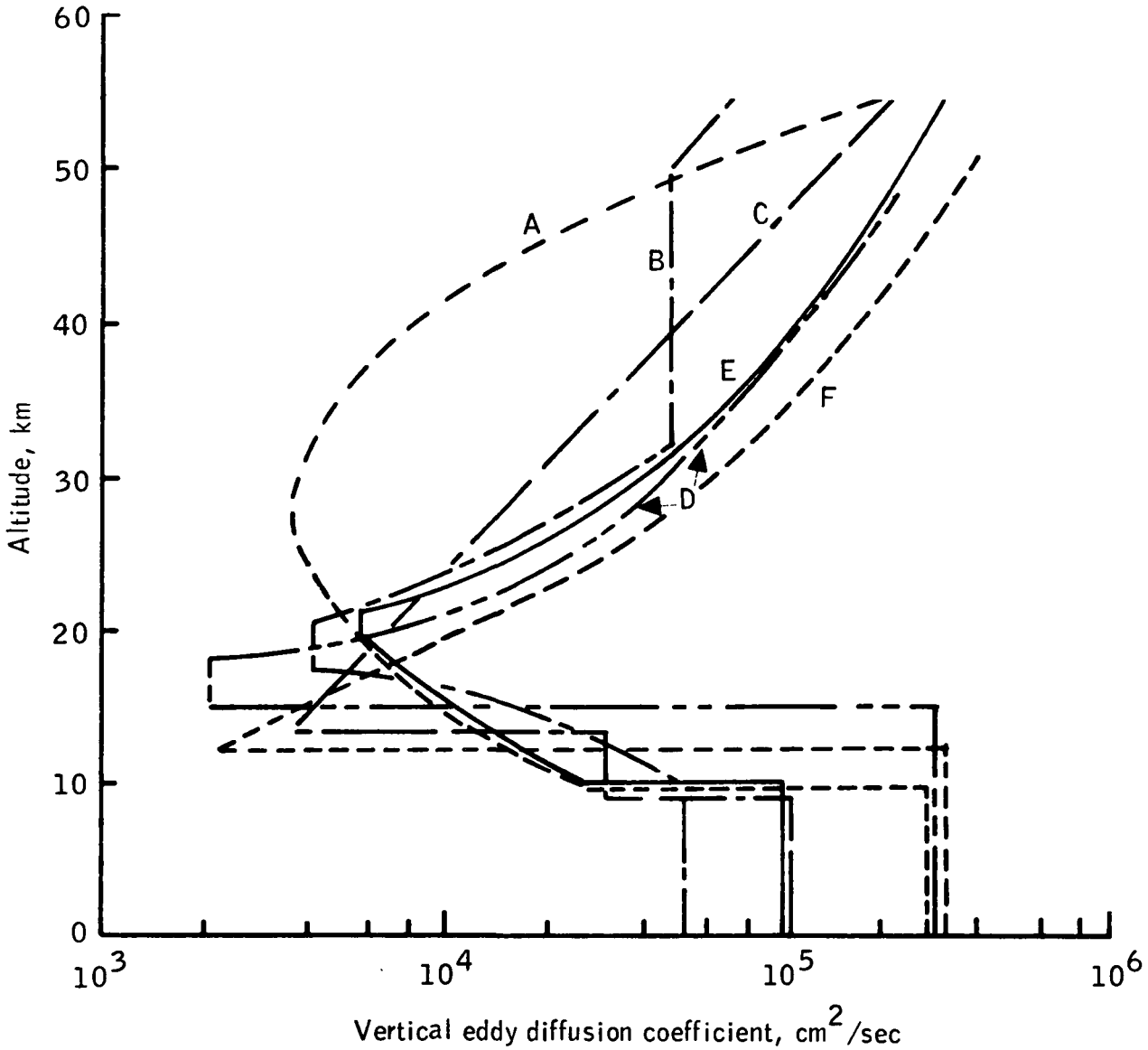

Figure 4-2.- Transport coefficients (profiles B to F taken from table 4-II).

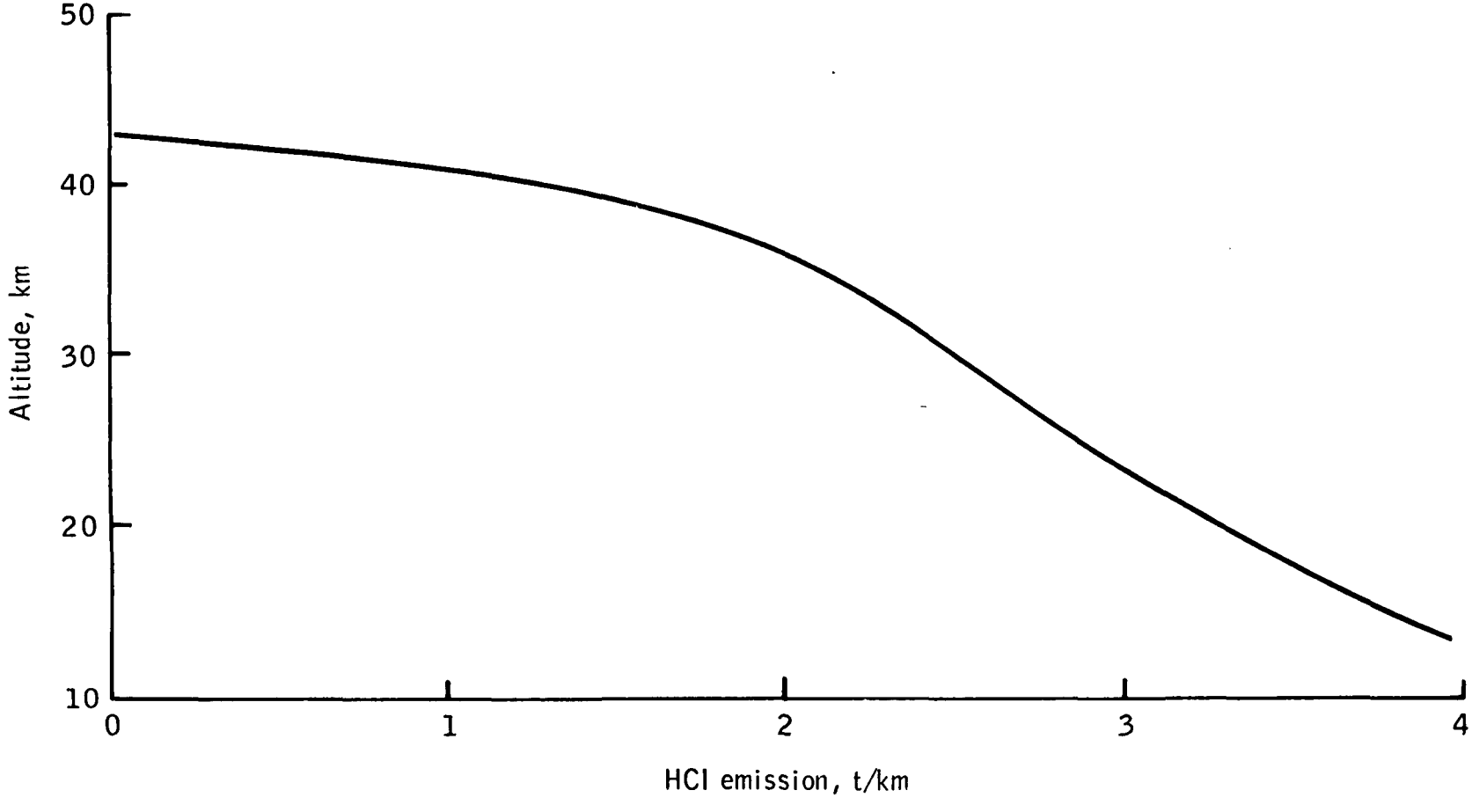

Figure 4-3.- Hydrogen chloride exhaust emissions as a function of altitude.

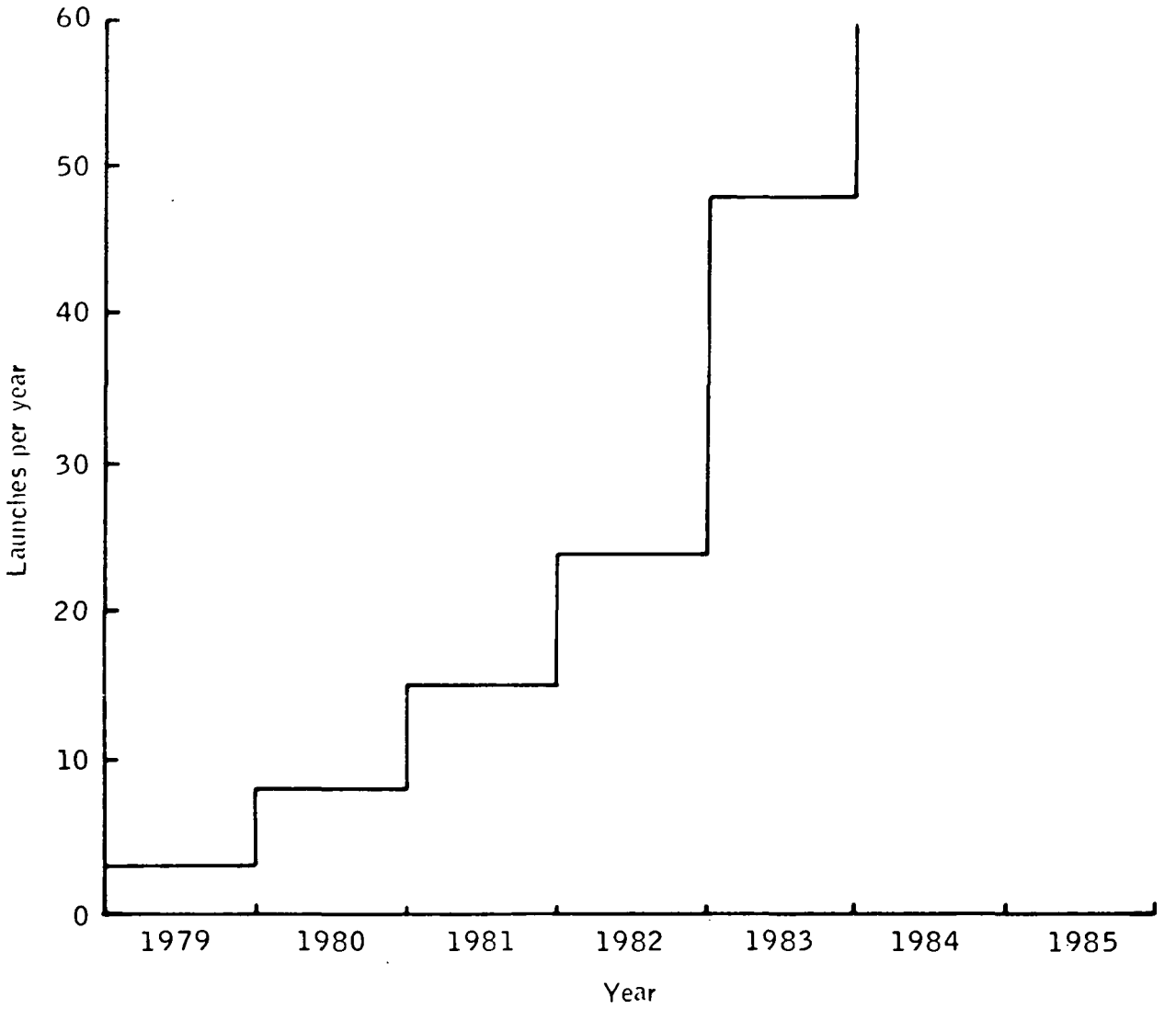

Figure 4-4.- Candidate Space Shuttle launch schedule.

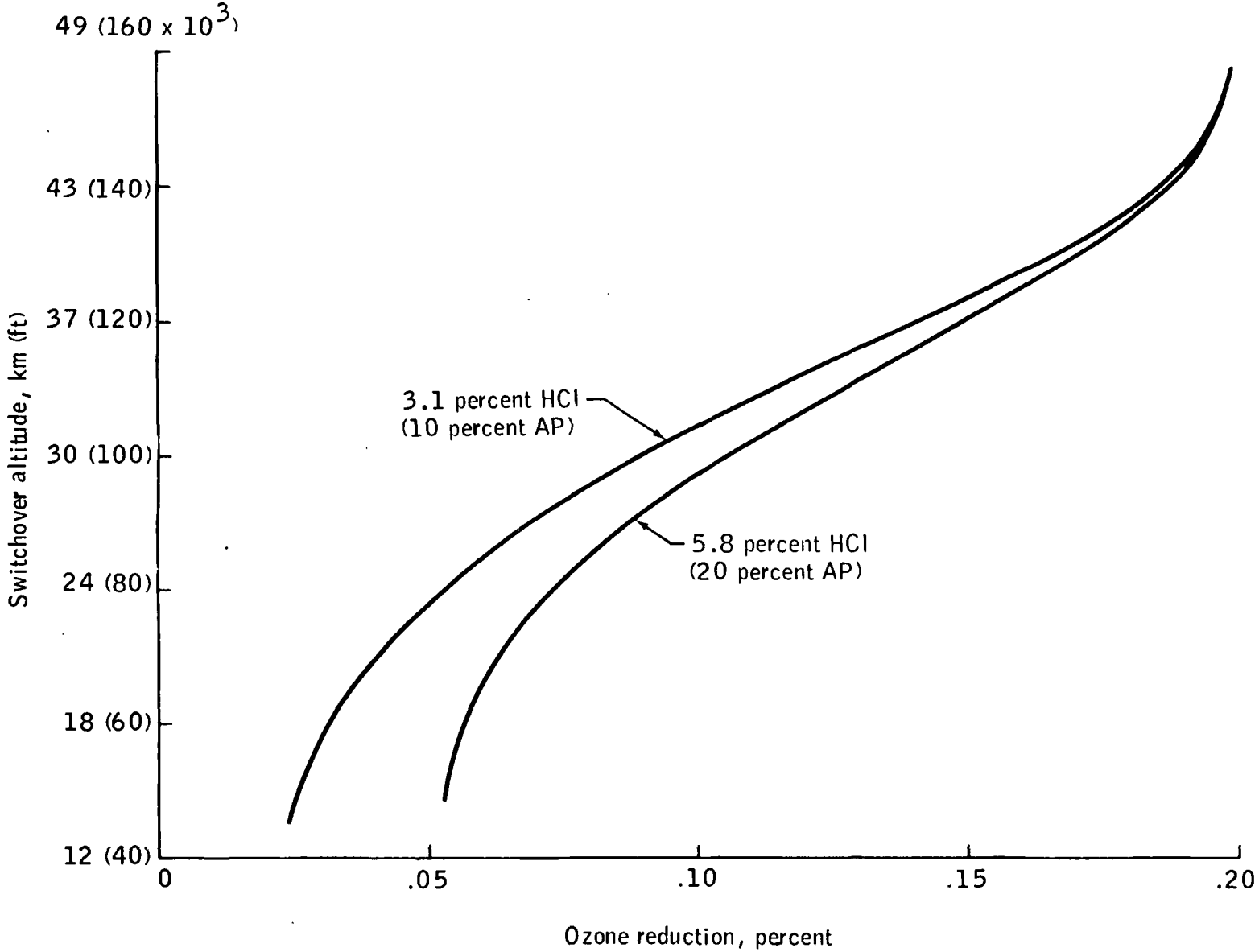

Figure 4-5.- Ozone reduction as a function of switchover altitude for two alternate propellants.

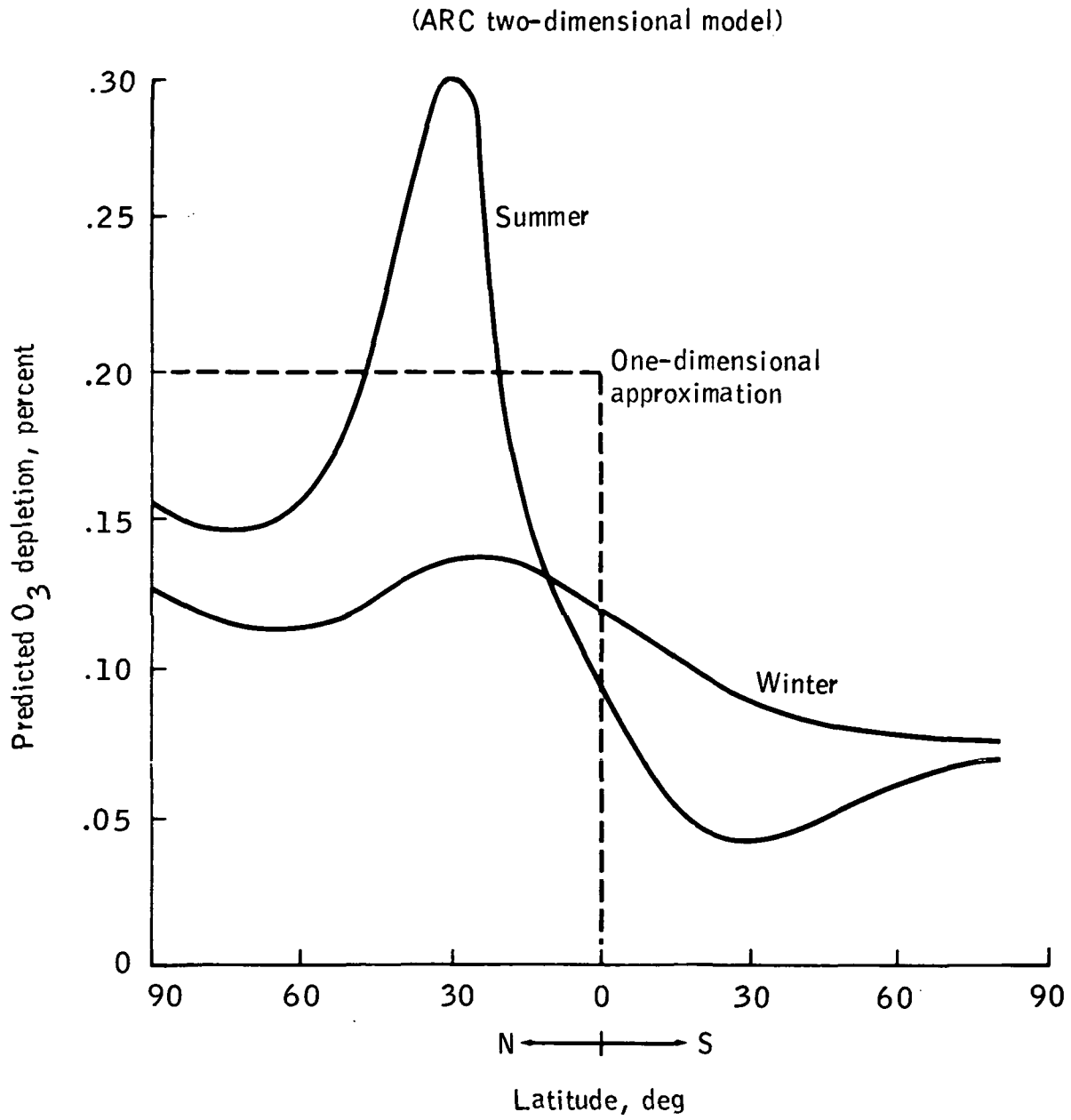

Figure 4-6.- Predicted latitude variations of ozone depletion for summer and winter.

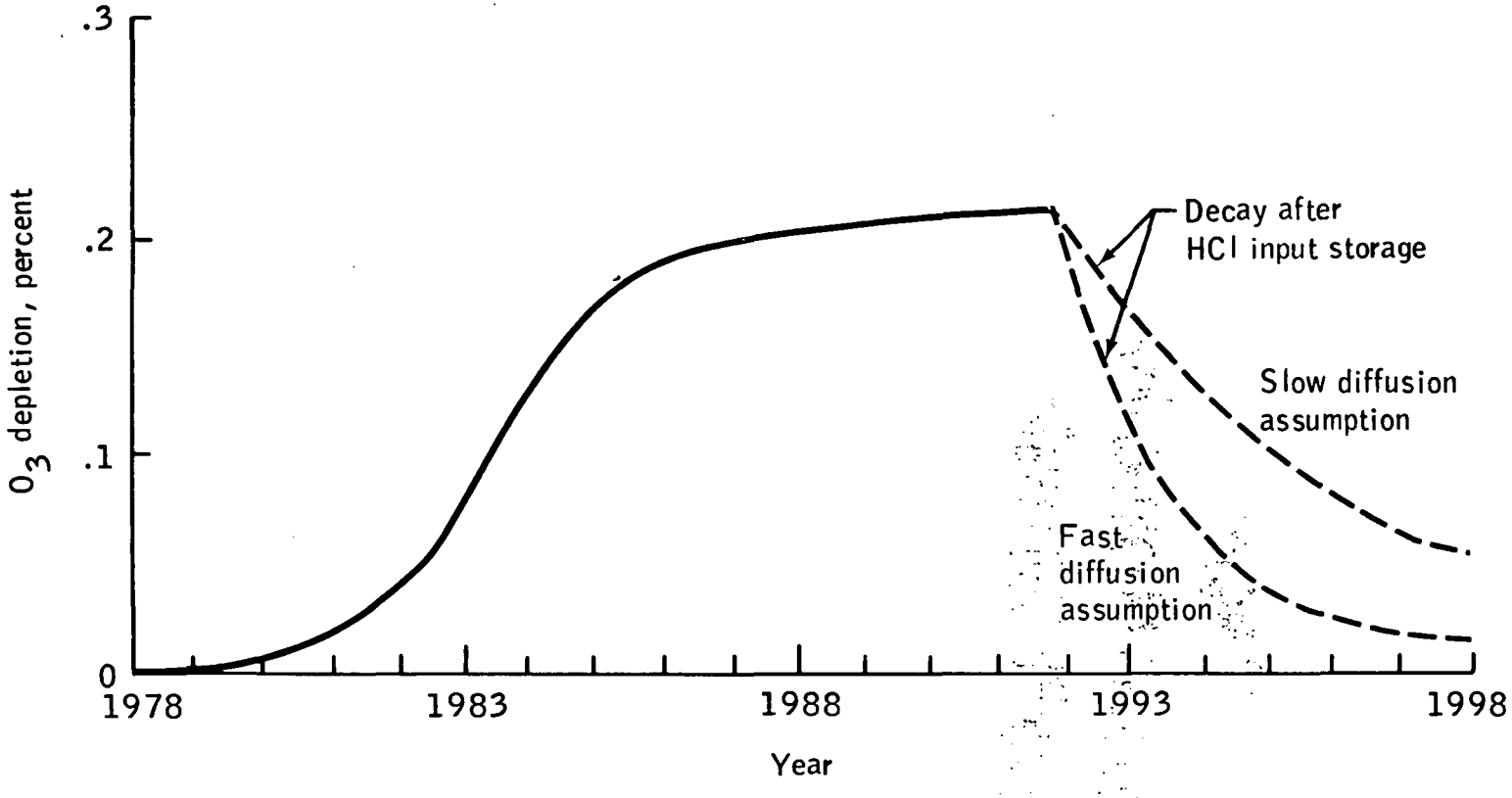

Figure 4-7.- Time dependence of ozone depletion from Space Shuttle operations.

Page
Intentionally
Left Blank

5. AFTERBURNING EFFECTS

Frozen chemical equilibrium in the rocket nozzle and interaction of the hot exhaust plume with the atmosphere result in the formation of NO. This compound also catalyzes the decomposition of O_3. The effect of NO from afterburning is assessed in the following paragraphs.

The NO produced by the Space Shuttle in the stratosphere has been calculated by using a model that includes the effect of the shock waves generated by plume interactions and afterburning. These results are given in table 5-I for the baseline AP propellant. The model is relatively new, and the figures quoted are from the initial run of the code. The calculation procedure is described in detail in references 5-1 and 5-2.[2] It should be noted that the chemistry in the stratosphere plume model is the same as that used for the troposphere plume and ground cloud. Aircraft measurements of the NO_x in the Titan ground cloud agree with the calculated values within 30 percent as reported in reference 5-3. The Titan propellant and the Space Shuttle baseline propellant are identical in composition.

The procedure used to evaluate the NO_x deposition rate from the alternate propellant was to establish the significant differences between the two propellants and to assess their influence on the mass of NO_x leaving the nozzle and the enhancement in the plume. The procedure used to obtain the values shown in table 5-II is a simplification of, and more conservative than, that used to generate the results of table 5-I. It is also given in references 5-1 and 5-2 and an unpublished article.[2]

The differences between the total amount of NO_x deposited by the baseline propellant and by the alternate "A" propellants are due to the following.

1. The lower chamber temperature for the alternate "A" propellant allows the NO mass fraction to reach its equilibrium value within the chamber. This value is approximately a factor of 50 less than the calculated NO mass fraction in the combustion chamber for the baseline propellant.

2. The alternate "A" propellant exhaust products contain more unburned fuel (H_2 + CO), which results in more intense afterburning.

3. The shock-induced NO_x enhancement in the plume should be similar for both types of propellant.

---

[2] R. D. Thorpe, H. S. Pergament, and B. Hwang: NO_x Deposition in the Stratosphere by the Space Shuttle Solid Rocket Motors. Proceedings 9th JANNAF Plume Technology Meeting, Feb. 1976, in press.

The total rate of NO_x deposited by the baseline and alternate propellants at 15 and 30 kilometers (47 000 and 95 000 feet) is compared with the HCl deposition rate in table 5-III. It is notable that the NO_x deposited in the stratosphere is not significant relative to the HCl for either propellant. Assuming approximately equivalent chemical efficiencies for NO_x and Cl_x, the effect of NO_x deposition on O_3 depletion is of the order of 0.005 times the effect of Cl_x deposition, or less than 0.001 percent O_3 depletion.

REFERENCES

5-1. Pergament, H. S.; and Thorpe, R. D.: NO_x Deposited in the Stratosphere by the Space Shuttle. NASA CR-132715, 1975.

5-2. Pergament, H. S.; Thorpe, R. D.; and Hwang, B.: NO_x Deposited in the Stratosphere by the Space Shuttle Solid Rocket Motors. NASA CR-144928, 1975.

5-3. Stewart, R. B.; and Gomberg, R. I.: The Production of Nitric Oxide in the Troposphere as a Result of Solid Rocket Motor Afterburning. NASA TN D-8137, 1976.

TABLE 5-I.- BASELINE PROPELLANT NO_x DEPOSITION

[Values in grams per second]

Parameter	Altitude	
	15 km	30 km
Nozzle	2 500	2500
Plume enhancement	9 500	1500
Total	12 000	4000

TABLE 5-II.- BASELINE AND ALTERNATE "A" PROPELLANT NO_x DEPOSITION

[Values in grams per second]

Parameter	Altitude	
	15 km	30 km
Nozzle		
Baseline	2 500	2500
Alternate "A"	55	55
Plume enhancement		
Baseline	9 500	1500
Alternate "A"	16 000	3000
Totals		
Baseline	12 000	4000
Alternate "A"	16 055	3055

TABLE 5-III.- COMPARISON BETWEEN NO_x AND HCl DEPOSITION RATES

Deposition rate	Altitude	
	15 km[a]	30 km[b]
No_x deposition, kg/km (ton/km)		
Baseline	20.865 (0.023)	3.629 (0.004)
Alternate "A"	28.123 (0.031)	2.722 (0.003)
NO_x/HCl deposition ratio		
Baseline	0.01	0.005
Alternate "A"	0.11	0.027

[a]Velocity = 561 m/sec.

[b]Velocity = 1140 m/sec.

6. EFFECTS OF PARTICULATE EMISSION FROM THE SPACE SHUTTLE EXHAUST

Concern has been expressed that the particulates formed from the Al_2O_3 emission of the Space Shuttle would remain suspended in the stratosphere and cause climatic changes in the troposphere. It has also been postulated that these particles would increase the O_3 destruction rate. To investigate these concerns, studies were carried out which included the analysis of particles from the Titan rocket exhaust, the measurement of O_3 surface reaction rates on Al_2O_3, and analysis of these results to predict the environmental consequences of Al_2O_3 dust in the stratosphere.

RADIATION SCATTERING BY THE EXHAUST PARTICLES

Estimates of the Earth mean temperature can be obtained by equating the amount of solar energy absorbed by the entire Earth with the amount of thermal radiation it emits to space (ref. 6-1). By performing such calculations for perturbed and unperturbed conditions, one can estimate the change in mean surface temperature produced as a result of the injection of Al_2O_3 particles by the Space Shuttle vehicle.

Mie scattering theory was used to relate the optical depth perturbation caused by the Space Shuttle to the steady-state mass loading of the added particles (ref. 6-1). These added particles are found from the mass of Al_2O_3 generated by a single Space Shuttle vehicle, the projected number of Space Shuttle flights, and the mean dwell time of particles in the stratosphere. For a projected traffic level of one Space Shuttle flight per week, an optical depth perturbation of 3.3×10^{-5}, an average albedo change of 4×10^{-6}, and a temperature decrease of 1.5×10^{-4} K for the Northern Hemisphere were found. The corresponding numbers for the Southern Hemisphere are 0.43 as large. These temperature changes are far smaller than those associated with significant observed climatic changes (ref. 6-2).

Kessler[3] studied the effect of Space Shuttle exhaust particles on the Earth's albedo and obtained an upper limit for the effect of 3×10^{-5}. From these results, it can be concluded that the uncertainty in the previous results, are approximately a factor of 4 due mainly to uncertainties in particle residence times in the stratosphere, particle scattering theory, and particle size distribution.

---

[3] D. J. Kessler: Current Assessment of the Effect of the Aluminum Compound Emission From the Space Shuttle. Rep. JSC-09913, Aug. 1975.

The preceding analyses are very sensitive to the number of particles in the size range between 0.05 and 1 micrometer. Although particles of 0.01-micrometer radii are too small to interact efficiently with light, they could serve as nucleation centers for H_2SO_4 and grow into larger H_2SO_4 droplets. It was found (ref. 6-3) that the number of Space-Shuttle-injected particles of this radius (and larger) would exceed or equal the number of particles of this size naturally found in the stratosphere. The growth of these particles has not yet been studied in detail, but any increase in the stratosphere sulfate layer could be more significant than the introduction of Al_2O_3 particles alone. Until the nucleation and growth is understood, the climatic effects cannot be easily estimated. Further studies are being performed at ARC.

DESTRUCTION OF O_3 BY SURFACE REACTIONS

Studies conducted at the NASA Jet Propulsion Laboratory (L. F. Keyser) and at ARC (T. Fujiwara) provide strong evidence that dispersal of Al_2O_3 in the stratosphere by the Space Shuttle rocket engines will not result in a significant depletion of O_3. The essential findings summarized in table 6-I are that the collision efficiency for O_3 destruction is 2×10^{-9} or less at room temperature and decreases with temperature. These values are approximately three orders of magnitude below the threshold of detectable long-range O_3 destruction rates (0.1 percent of the normal O_3 loss rate). The experimental studies further showed that there was no significant enhancement of catalytic activity by exposure to HCl, as might occur in the exhaust plume. Outgassing at temperatures between 600 and 1000 K activates Al_2O_3 for O_3 destruction. Collision efficiencies following outgassing are estimated to be as high as 10^{-6} to 10^{-5} for Al_2O_3 and 10^{-7} for samples of alumina from the solid rocket motor exhaust. Even at 10^{-7}, the destruction rate of stratospheric O_3 is a factor of 10 below the detectable threshold for O_3 destruction. Furthermore, exposure to air or O deactivates the alumina in less than 24 hours. The current assessment is that the long-term effect of alumina exhaust particles on the O_3 layer is negligible.

REFERENCES

6-1. Pollack, J. B.; Toon, O. B.; et al.: Estimates of the Climatic Effect of Aerosols Produced by Space Shuttles, SST's, and other High-Flying Aircraft. J. Appl. Meteorol., vol. 15, no. 3, Mar. 1976, pp. 247-258.

6-2. Pollack, James B.; Toon, Owen B.; et al.: Volcanic Aerosols and Climatic Change: A Theoretical Assessment. J. Geophys. Res., vol. 81, no. 6, Feb. 20, 1976, pp. 1071-1083.

6-3. Hofmann, D. J.; Carroll, D. E.; and Rosen, J. M.: Estimate of the Contribution of the Space Shuttle Effluent to the Natural Stratospheric Aerosol. Geophys. Res. Letters, vol. 2, no. 3, Mar. 1975, pp. 113-116.

TABLE 6-I.- OZONE DECAY RATES AND COLLISION EFFICIENCIES ON Al_2O_3

Designation	Sample	Form[a]	Crystallite size, μm (Å)	Specific surface area, m^2/g	Collision efficiency
A	Laboratory preparation	Gamma	0.0050 (50)	123	7.8×10^{-10}
B	Degussa aluminum oxide-C	Gamma	.0065 (65)	116	1.6×10^{-10}
C	Alcoa F-1 activated alumina	Boehmite, major; Gamma, minor	.0050 (50)	208	1.1×10^{-9}
D	Baker reagent powder	Alpha, major; Theta, trace	--	9.1	2.8×10^{-10}
SRM-A[b]	JPL SRM inside tank	Alpha, major; Gamma, Delta minor	--	4.8	4.0×10^{-10}
SRM-B	JPL open burn inside tank	Theta, major; Gamma, Delta, Alpha, minor	--	5.4	1.9×10^{-10}
SRM-C[b]	JPL SRM inside tank	Alpha, major; Gamma, Delta, minor	--	1.8	1.7×10^{-9}

[a]Analyses performed by Technology of Materials, Santa Barbara, California.

[b]Gaseous residence time in the solid rocket motor (SRM) was approximately 15 milliseconds for SRM-A and approximately 90 milliseconds for SRM-C. Motor SRM-C more closely approaches conditions expected for Space Shuttle solid booster rockets.

7. BIOSPHERIC IMPACT OF uv RADIATION INCREASE RESULTING FROM O_3 DEPLETION

The estimated average percentage of O_3 depletion presented in section 4 can be converted by a series of assumptions and calculations into an estimate of the increase in BHuv radiation from the Sun. Most estimates indicate that a 1-percent O_3 reduction results in a 2-percent increase in BHuv radiation. Considering the uncertainty in the estimate of O_3 depletion, the attendees of the workshop adopted a 0.2-percent O_3 depletion and a 0.4-percent increase in BHuv radiation as a worst-case situation for an assessment of the biospheric impact of the projected Space Shuttle operations outlined in the previous section.

Based on the limited available biological data, the impact on the biosphere of an assumed 0.4-percent increase in BHuv radiation was considered (appendix H), and the following conclusions were drawn.

1. The effects on the biosphere of a 0.4-percent increase in BHuv radiation will not be detectable with decades of observation because the natural fluctuations of BHuv radiation and the ecosystem are so much larger than this increase. These fluctuations include (1) greater variability of BHuv irradiances; (2) statistical uncertainty involved in the responses of organisms and ecosystems to given doses of BHuv radiation at given dose rates; and (3) large normal variation in the response of organisms to other, more pervasive or important environmental factors to which they are exposed such as temperature, moisture, nutrition, competition, and predation. The fact that a cause-and-effect relationship of an increase in BHuv radiation cannot be statistically detected, however, does not mean that an increase in BHuv radiation can be ruled out as a contributor to some deleterious future event. Lack of detectability is not equatable with a lack of effect.

2. There is a very low probability that an average 0.4-percent increase in BHuv radiation will have any unacceptable effect on agricultural plants or natural ecosystems, independently of whether the effects of such an increase are detectable or not. The basis for this conclusion is outlined in appendix H.

3. There may be some increase in the number of melanoma and nonmelanoma skin cancer cases among susceptible individuals resulting from 0.2-percent O_3 depletion, but it will not be detectable because of (1) the natural variations of BHuv radiation and biological variability mentioned previously, (2) the long latent period (20 to 60 years) for induction of skin tumors, and (3) the many other factors that already may be tending to increase or decrease the number of reported skin cancer cases. Factors possibly leading to an increased number of melanoma cases in the United States include (1) the increased proportion of people in the population living long enough to contract skin cancer; (2) the increased reporting of skin cancer cases because of Medicare; (3) the changing of lifestyles, which, in recent years, involves more leisure time activity in

the sunshine; and (4) the net southward migration of the population. (Regarding the latter factor, between 1940 and 1970, the center of population of the United States moved west and approximately 35 miles south from approximately 39° N latitude; this amount of southward movement corresponds to a 2-percent increase in the annual dose of BHuv radiation.) Factors possibly leading to a decreased incidence include action based on publicity-induced recognition by the population of the dangers of overexposure to solar radiation and on more accurate identification of susceptible individuals as a result of research generated by the O_3 depletion problem.

4. The number of skin cancer cases resulting from a 0.2-percent O_3 reduction is not realistically predictable. The extant experimental and epidemiological data, although clearly suggesting some contribution of solar radiation exposure to skin cancer incidence, are inadequate for making quantitative predictions with reasonable limits of uncertainty. (See appendix H.)

APPENDIX A

ALTERNATE BOOSTER PROPELLANT STUDIES

By J. Q. Miller[a]

The alternate propellant study was initiated in August 1974 to define a solid-propulsion supporting development program for eliminating or significantly reducing the release of gaseous hydrogen chloride (HCl) in the upper atmosphere while minimizing Space Shuttle Program cost, performance, and schedule impacts. Activities included propellant formulation and characterization and solid rocket motor design development. The major ground rules for this study were as follows.

1. Conduct the first operational flight in 1983.
2. Eliminate or minimize HCl release above 20 kilometers (63 000 feet).
3. Consider class II propellants only.
4. Retain 1-1A configuration envelope (baseline).

Approximately 250 different propellant formulations containing various combinations of ammonium perchlorate (AP) and non-HCl-producing oxidizers such as ammonium nitrate, cyclotetramethylenetrinitramine (HMX), trimethylethanitrinitrate, nitrocellulose, nitroglycerine, and cyclotrimethylenetrinitramine were evaluated theoretically. These formulations were compared with the baseline AP-oxidized propellant. From this comparison, the most promising alternate propellant formulations were selected for preliminary process, compatibility, hazard, burn rate, pressure exponent, and density impulse characterization. Based on results from these characterizations, the best HMX- and non-HMX-containing alternate propellant formulations were selected for additional evaluation. A formulation and ballistic property comparison of these two alternate formulations ("A" and "B") with the baseline formulation is presented in table 3-I. To achieve acceptable ballistic properties, both alternate formulations require the addition of AP. The theoretical exhaust composition for the baseline and alternates "A" and "B" is presented in table 3-II.

The most promising design concept developed was a double-web star propellant grain configuration (dual-grain concept). With this concept, the baseline propellant is completely burned out at an altitude of approximately 20 kilometers (63 000 feet) and the alternate propellant (low HCl) is burned at altitudes above 20 kilometers (63 000 feet); thus, minimum cost and performance impacts are afforded. Alternate propellant formulations "A" and "B" were used in conjunction with the baseline propellant to design two booster solid rocket motors incorporating the dual-grain concept. Figures 3-1, 3-2,

---

[a]NASA George C. Marshall Space Flight Center.

and 3-3 contain thrust as a function of time and mass flow characteristics for the baseline, alternate "A," and alternate "B" designs, respectively. By comparing mass flow characteristics with exhaust compositions below and above the transition altitudes (change from baseline to alternate propellant burn), the predicted exhaust constituent weights can be established.

Results from preliminary burn rate tests conducted on the alternate "B" propellant indicate that AP levels as high as 20 percent by weight may be required to obtain acceptable burn rates and combustion efficiencies. This increase in AP level will increase the HCl percentage weight in the exhaust from 3.1 to approximately 5.8. Other exhaust constituent percentage weights are not significantly affected by this change. Therefore, for environmental assessments at this time, it is recommended that an HCl percentage weight range of 3.1 to 5.8 be used for the alternate propellant.

The alternate booster propellant studies are planned for continuation through December 1976. The data contained here concerning exhaust composition and mass flow characteristics are not expected to change significantly. Most of the data generated between now and December 1976 will be used to update Space Shuttle Program cost, payload, and schedule impacts.

APPENDIX B

STRATOSPHERIC REACTION RATES

By W. DeMore[a] and L. F. Keyser[a]

Current measurements of selected critical rate constants used for Space Shuttle exhaust modeling are summarized in table 4-I. Additional data are contained in reference 4-1. A recent review of rate data for oxides of chlorine has been prepared (ref. 4-2).

Studies conducted at the NASA Jet Propulsion Laboratory and the NASA Ames Research Center provide strong evidence that dispersal of aluminum oxide in the stratosphere by the Space Shuttle rocket engines will not result in significant ozone (O_3) depletion. The essential finding is that the collisional efficiency for O_3 destruction is in the range of 10^{-9} to 10^{-10} at room temperature and decreases with increased temperature. These values are approximately three orders of magnitude below the threshold of detectable long-range O_3 destruction rates (0.1 percent of the normal O_3 loss rate). The experimental studies showed further that there was no significant enhancement of catalytic activity by exposure to hydrogen chloride, as might occur in the exhaust plume.

---

[a]NASA Jet Propulsion Laboratory.

APPENDIX C

MEASUREMENTS OF STRATOSPHERIC MINOR CONSTITUENTS

By the Environmental Effects Project Office[a]

CHLORINE COMPOUNDS

Personnel at the National Center for Atmospheric Research now have three sets of hydrogen chloride (HCl) measurements obtained using the filter technique. The measurements made by balloons reveal a concentration ranging from less than 0.1 part per billion by volume (ppbv) near 15 kilometers (47 000 feet) to 0.5 to 1.0 ppbv at 25 to 30 kilometers (79 000 to 98 000 feet). These measurements clearly indicate a high-altitude (approximately 30 kilometers) (98 000 feet)) source and a lower altitude sink (almost certainly rainout in the troposphere). Remote infrared spectroscopic measurements (refs. C-1 and C-2) show the same general shape and also indicate an apparent approach to an asymptotic mixing ratio above 30 kilometers (98 000 feet). These measurements are all shown in figure C-1, together with a calculated profile (ref. C-3) based on a specific set of tropospheric halogen sources.

The Lazrus et al. measurements (ref. C-4) indicate an asymptotic mixing ratio in the range of 0.5 to 1.0 ppbv. Latitudinal measurements were also made at 15 and 18 kilometers (47 000 and 58 000 feet) from an airplane. As expected for a tracerlike species, these show poleward increase (fig. C-2).

Whereas measurements of HCl give a good indication of the total chlorine-containing molecules (Cl_x) and information about sources, sinks, and transport, a measurement of chlorine oxide (ClO) would tend to indicate the activity of Cl_x toward ozone (O_3) in the stratosphere. Results are thus far inconclusive. Waters (ref. C-5) has looked for ClO with his microwave spectrometer and can set an upper limit of 2 to 3 ppbv, more than an order of magnitude over predictions. Carlson (private communication) has a tentative detection of column content by way of solar absorption. The value ($\sim 9 \times 10^{14}$ cm^{-2}) is much larger than expected, but the error bars still encompass predicted values. Anderson (private communication) conducted his in situ measurement in March 1976.

HYDROXYL MEASUREMENTS

An important measure of the odd-hydrogen (H) content of the atmosphere is hydroxyl (OH), which can catalytically destroy O_3 in the stratosphere or which can alternatively tie up oxides of nitrogen (NO_x) as nitric acid (HNO_3).

---

[a]NASA Lyndon B. Johnson Space Center.

Previously, only Anderson's measurements at altitudes from 46 to 70 kilometers (147 000 to 237 000 feet) existed. Recently, there have been measurements at ground level (ref. C-6), at 7 and 12 kilometers (22 000 and 36 000 feet) (ref. C-7), and from 30 to 43 kilometers (95 000 to 137 000 feet) (ref. C-8) as shown in figure C-3. The lower altitude measurements are of great interest in dealing with such problems as the oxidation of sulfur dioxide (SO_2) to sulfuric acid (H_2SO_4) and the destruction of hydrogen-containing chlorocarbons in the troposphere. The stratospheric OH measurements are of direct use in the evaluation of Space Shuttle Cl injections. They have already been used in an attempt to tune a model for use in Cl perturbation predictions (ref. C-8).

Further information is provided by Burnett's ground-based OH column content measurements (ref. C-9). Burnett frequently sees column contents of several times 10^{14} cm^{-2}. However, the OH concentration seems to be patchy; and an upper limit can frequently be set to the column content at 2×10^{13} to 3×10^{13}, which is smaller than that implied in the in situ measurements. The situation is still uncertain but is many times improved by recent measurements.

MEASUREMENTS FOR OXIDES OF NITROGEN

The measurement situation for NO_x constituents is quite confused. There are numerous measurements at different times and places of nitric oxide (NO), nitrogen peroxide (NO_2), and HNO_3, which have been summarized in reference C-2. (See figs. C-4 to C-6.) Odd N ($NO + NO_2 + HNO_3$) is produced from nitrous oxide (N_2O) by reaction with $O(^1D)$, where ^1D represents an energy state. It is transported around the stratosphere and eventually back to the troposphere for loss by rainout. Below an altitude of approximately 40 kilometers (127 000 feet), the chemistry is such that odd N is split somewhat evenly among the three species. Individual measurements of one or two of these species in this region do not yield accurate estimates of the total odd-N content of the stratosphere to which a model can be adjusted. Predicted Cl perturbations are quite sensitive to the amount of NO present in the model. Measurements of NO range over about an order of magnitude and represent a combination of transport and chemical processes. Estimates of odd-N mixing ratios in the asymptotic region at an altitude above 30 kilometers (95 000 feet) made from the existing measurements range from a few parts per billion by volume to a few tens of parts per billion by volume.

Most models contain a combination of transport coefficients and $O(^1D)$ rate rate coefficients to yield asymptotic odd-N mixing ratios of 10 to 20 ppbv. The most direct measurement of odd N is the NO measurement by C. J. Mason and J. J. Horvath (private communication) at an altitude between 40 and 60 kilometers (127 000 and 185 000 feet), where chemistry predicts odd N to be virtually all NO — only about 5 ppbv. More high-altitude NO measurements are necessary in addition to in situ simultaneous measurements of all major odd-N constituents to test chemistry.

NITROUS OXIDE MEASUREMENTS

R. A. Rasmussen's ground-level measurements (private communication) yield results in the range of 0.3 to 0.35 part per million by volume (ppmv) of N_2O. These values are higher than the earlier measurements (refs. C-10 and C-11), which are approximately 0.25 to 0.27 ppmv. In contrast to previous results, measurements in remote areas (ref. C-12) show almost no random variation. This uniformity possibly indicates a longer atmospheric residence time. If the stratosphere is the only sink and the longer residence time is real, a source/sink balance problem, which is currently being debated, remains.

New stratospheric profiles of N_2O by A. Schmeltekopf (private communication) show a much more rapid decrease with altitude than previous results (ref. C-12), as shown in figure C-7. These profiles are probably a manifestation of the variability of atmospheric dynamics. On the same flight, two fluorocarbons (Freon-11 ($CFCl_3$) and Freon-12 (CF_2Cl_2)) were measured; both showed a sudden drop at an altitude of 18 kilometers (58 000 feet) as shown in figures C-8 and C-9. These are either due to some unknown dynamical effect or are a warning of the difficulty involved in these types of measurements.

REFERENCES

C-1. Farmer, C. B.; Raper, O. F.; and Norton, R. H.: Spectroscopic Detection and Vertical Distribution of HCl in the Troposphere and Stratosphere. Geophys. Res. Letters, vol. 3, no. 1, Jan. 1976, pp. 13-16.

C-2. Ackerman, M.; Fontanella, J. C.; et al.: Simultaneous Measurements of NO and NO_2 in the Stratosphere. Planetary Space Sci., vol. 23, no. 4, Apr. 1975, pp. 651-660.

C-3. Cicerone, R. J.; Stedman, D. H.; and Stolarski, R. S.: Estimate of Late 1974 Stratospheric Concentrations of Gaseous Chlorine Compounds (Cl_x). Geophys. Res. Letters, vol. 2, no. 6, June 1975, pp. 219-222.

C-4. Lazrus, A. L.; Gandrud, B. W.; Woodard, R. N.; Sedlacek, W. A.: Stratospheric Halogen Measurements. Geophys. Res. Letters, vol. 2, no. 10, Oct. 1975, pp. 439-441.

C-5. Waters, J.: Aircraft Measurements of Stratospheric Molecules. Paper presented at the Stratospheric Research Advisory Committee meeting, Jet Propulsion Laboratory, 1976.

C-6. Wang, Charles C.; Davis, L. I., Jr.; et al.: Hydroxyl Radical Concentrations Measured in Ambient Air. Science, vol. 189, no. 4205, Sept. 5, 1975, pp. 797-800.

C-7. Davis, D. D.; Heaps, W.; and McGee, T.: Direct Measurements of Natural Tropospheric Levels of OH via an Aircraft Borne Tunable Dye Laser. Geophys. Res. Letters, vol. 3, no. 6, June 1976, pp. 331-333.

C-8. Anderson, J. G.: The Absolute Concentration of OH ($X^2\pi$) in the Earth's Stratosphere. Geophys. Res. Letters, vol. 3, no. 3, Mar. 1976, pp. 165-168.

C-9. Burnett, Clyde R.: Terrestrial OH Abundance Measurement by Spectroscopic Observations of Resonance Absorption of Sunlight. Geophys. Res. Letters, vol. 3, no. 6, June 1976, pp. 319-322.

C-10. Schütz, K.; Junge, C.; Beck, R.; and Albrecht, D.: Studies of Atmospheric N_2O. J. Geophys. Res., vol. 75, no. 12, Apr. 20, 1970, pp. 2230-2246.

C-11. Hahn, Jürgen: The North Atlantic Ocean as a Source of Atmospheric H_2O. Tellus, vol. 26, no. 1-2, 1974, pp. 160-168.

C-12. Craig, H.; Weiss, R.; and Doud, W. L.: Paper presented at American Geophysical Union meeting, Washington, D.C., 1976.

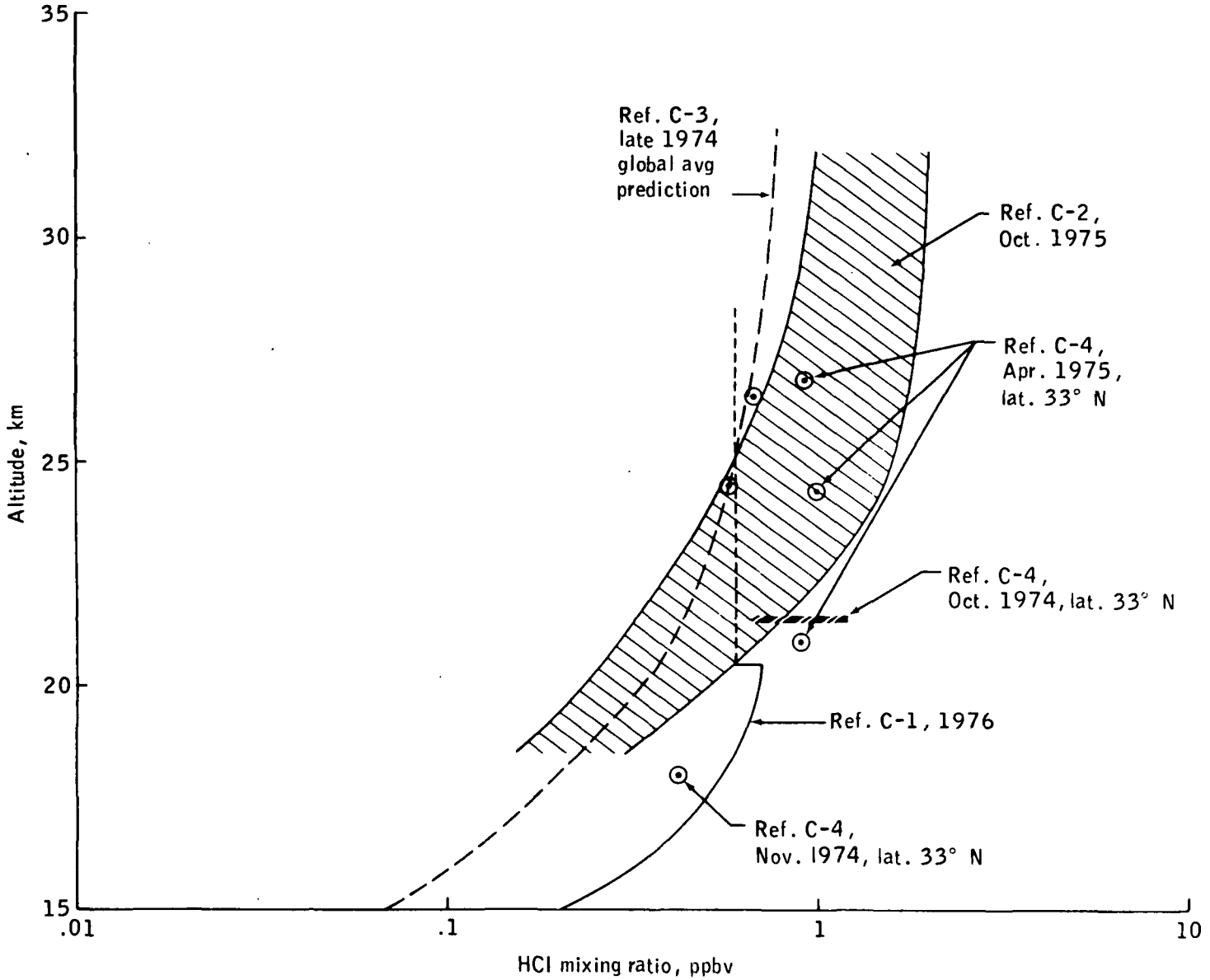

Figure C-1.- Remote infrared spectroscopic measurements with a calculated profile.

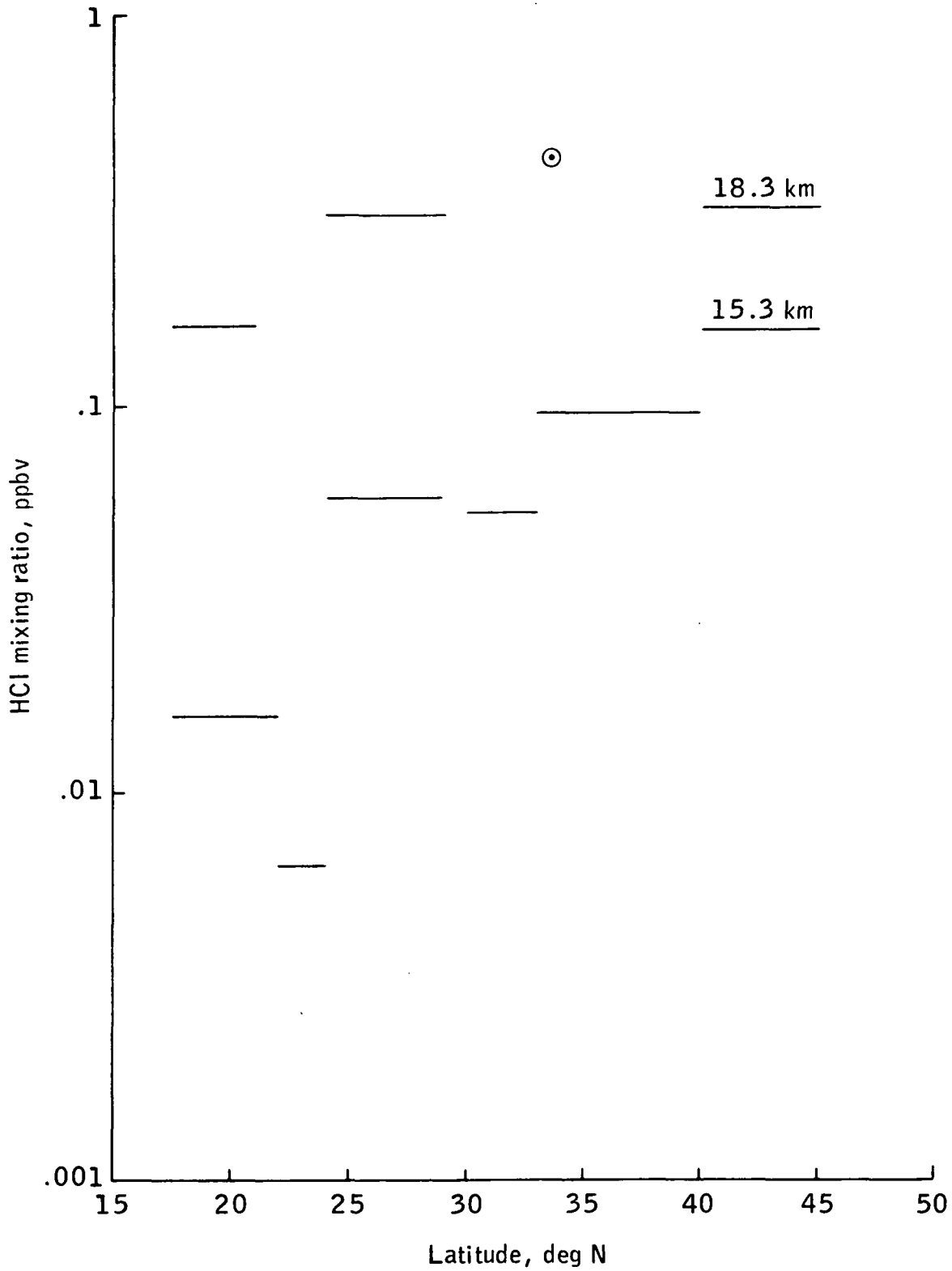

Figure C-2.- Latitudinal measurements from an aircraft at altitudes of 15 and 18 kilometers (47 000 and 59 000 feet).

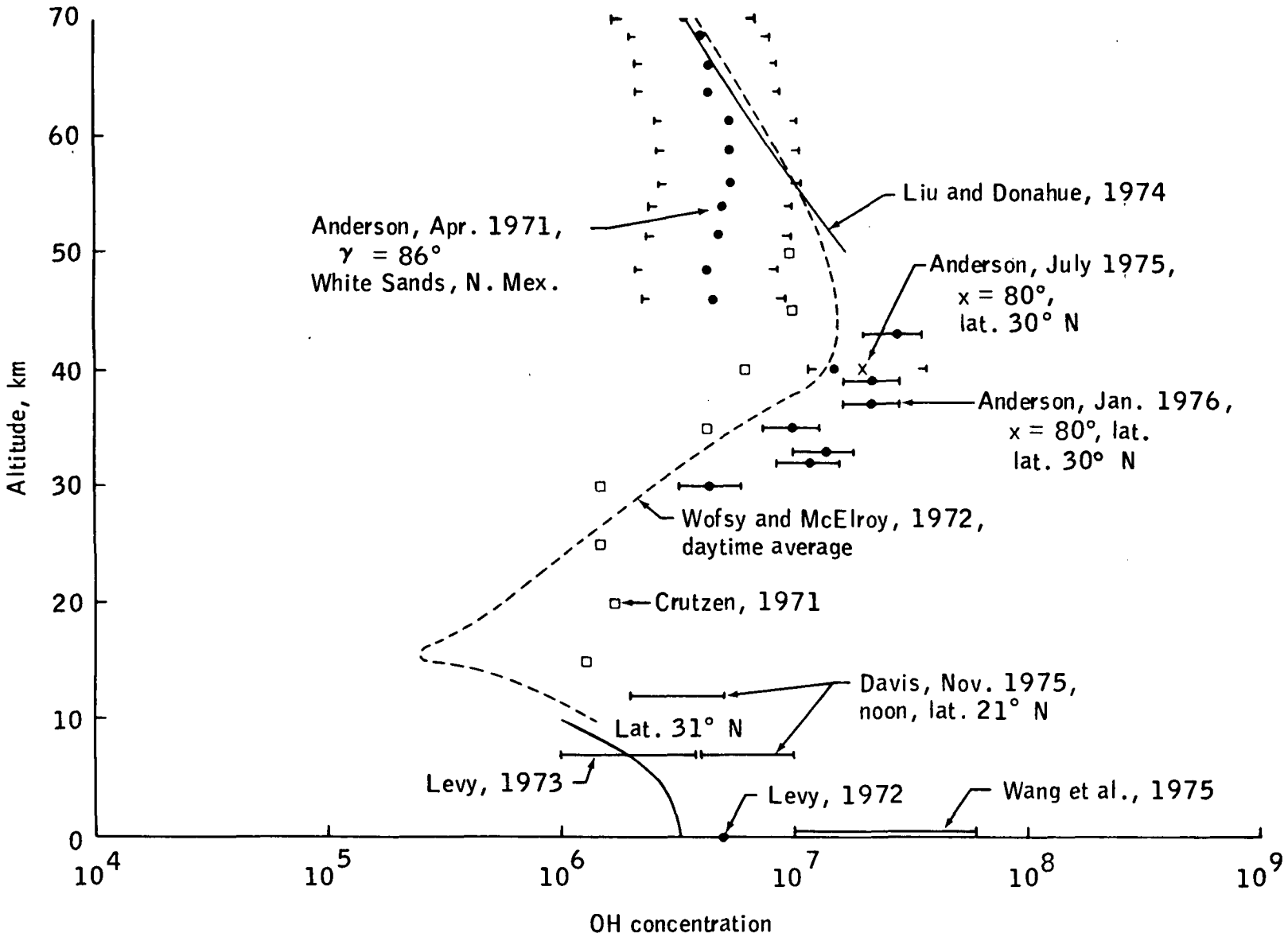

Figure C-3.- Ground-based measurements of OH concentration, where x is solar zenith angle.

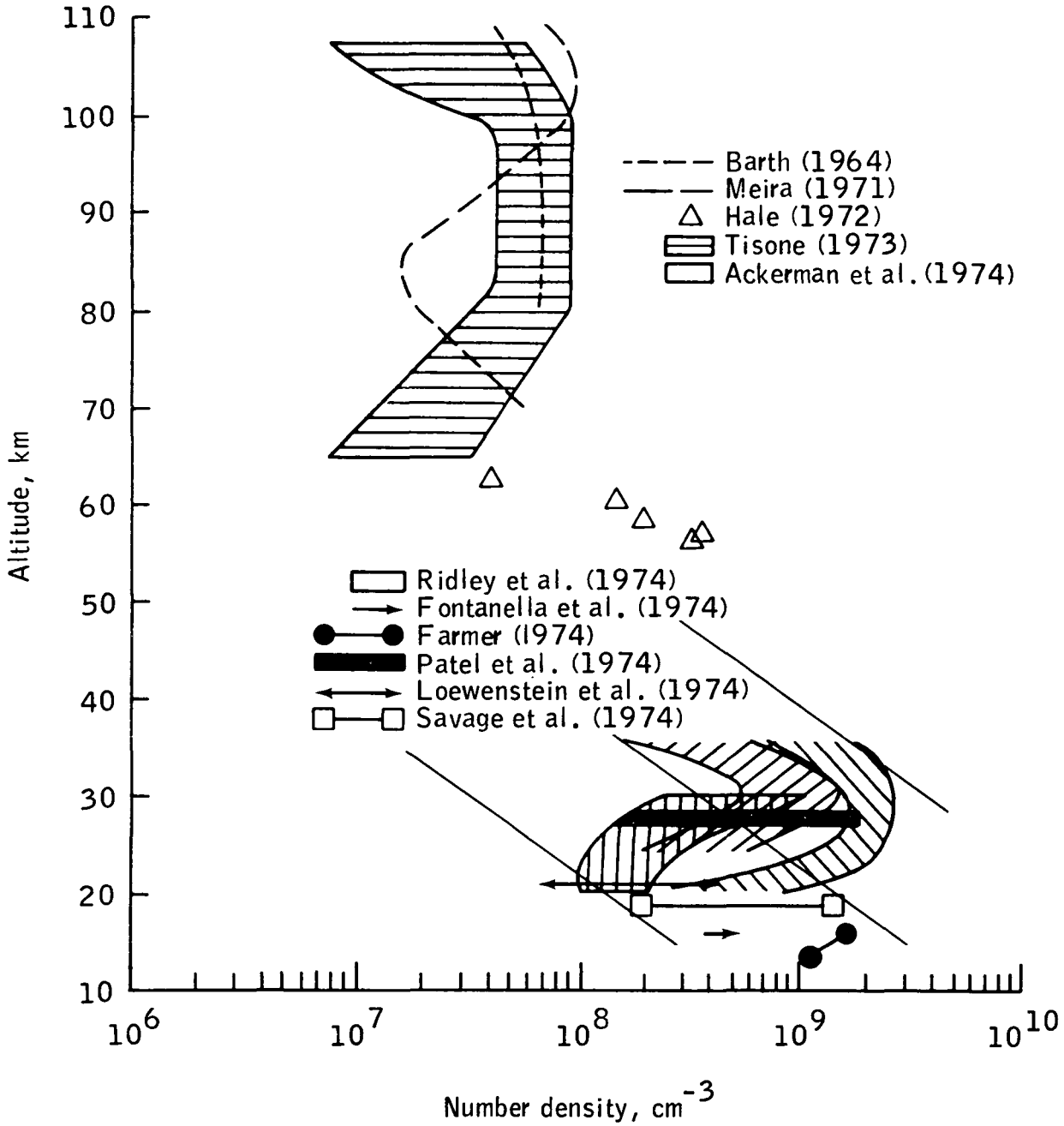

Figure C-4.- Height profiles of measured nitric oxide number densities in the chemosphere.

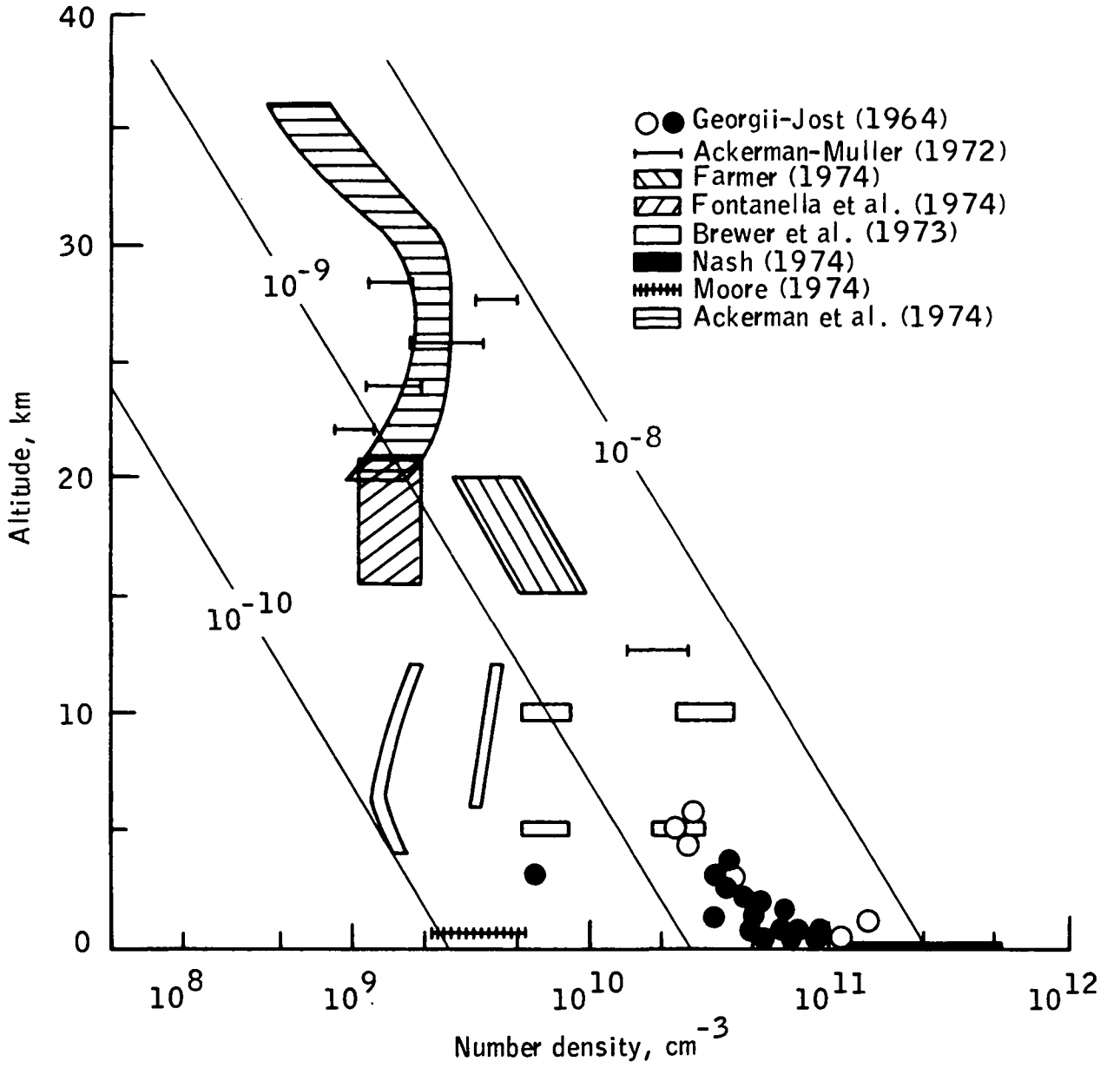

Figure C-5.- Height profiles of NO_2 number densities measured by ground-based aircraft and balloon-borne instruments. Constant volume mixing ratios are roughly indicated by the straight lines marked 10^{-8}, 10^{-9}, and 10^{-10}.

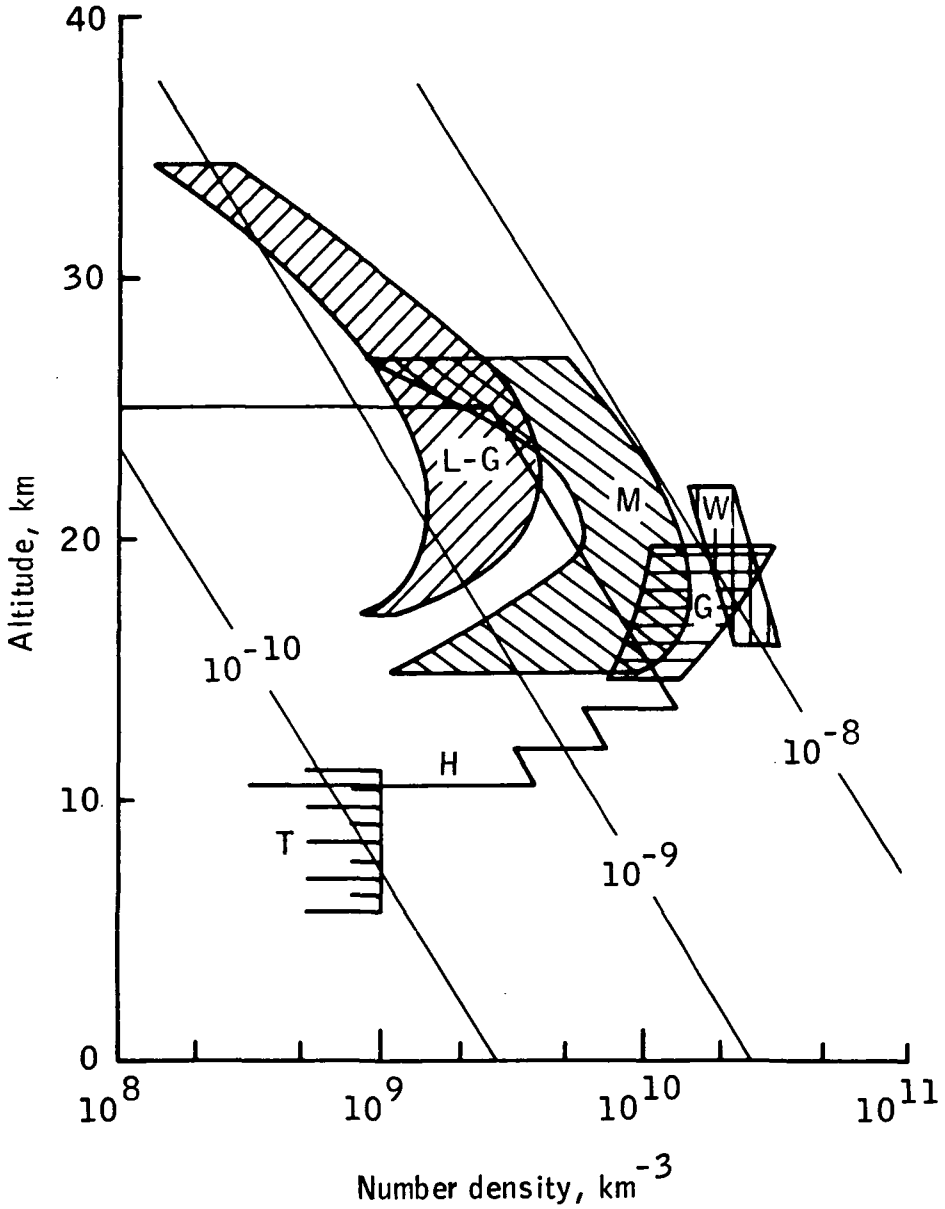

Figure C-6.- Envelopes representing the measured height profiles of nitric acid number densities. The envelope designated L-G corresponds to the data of Lazrus and Gandrud (1974), M to those of Murcray et al. (1974), G to those of Fontanella et al. (1974), W to those of Fried and Weinman (1970), and H to those of Harries et al. (1974). The values represented by the circles and by the upper limit designated T have been evaluated on the basis of the atmospheric experiments of Murcray et al. (1969) and of the laboratory data published by Fontanella et al. (1974). Constant volume mixing ratios are roughly illustrated by the straight lines marked 10^{-8}, 10^{-9}, and 10^{-10}.

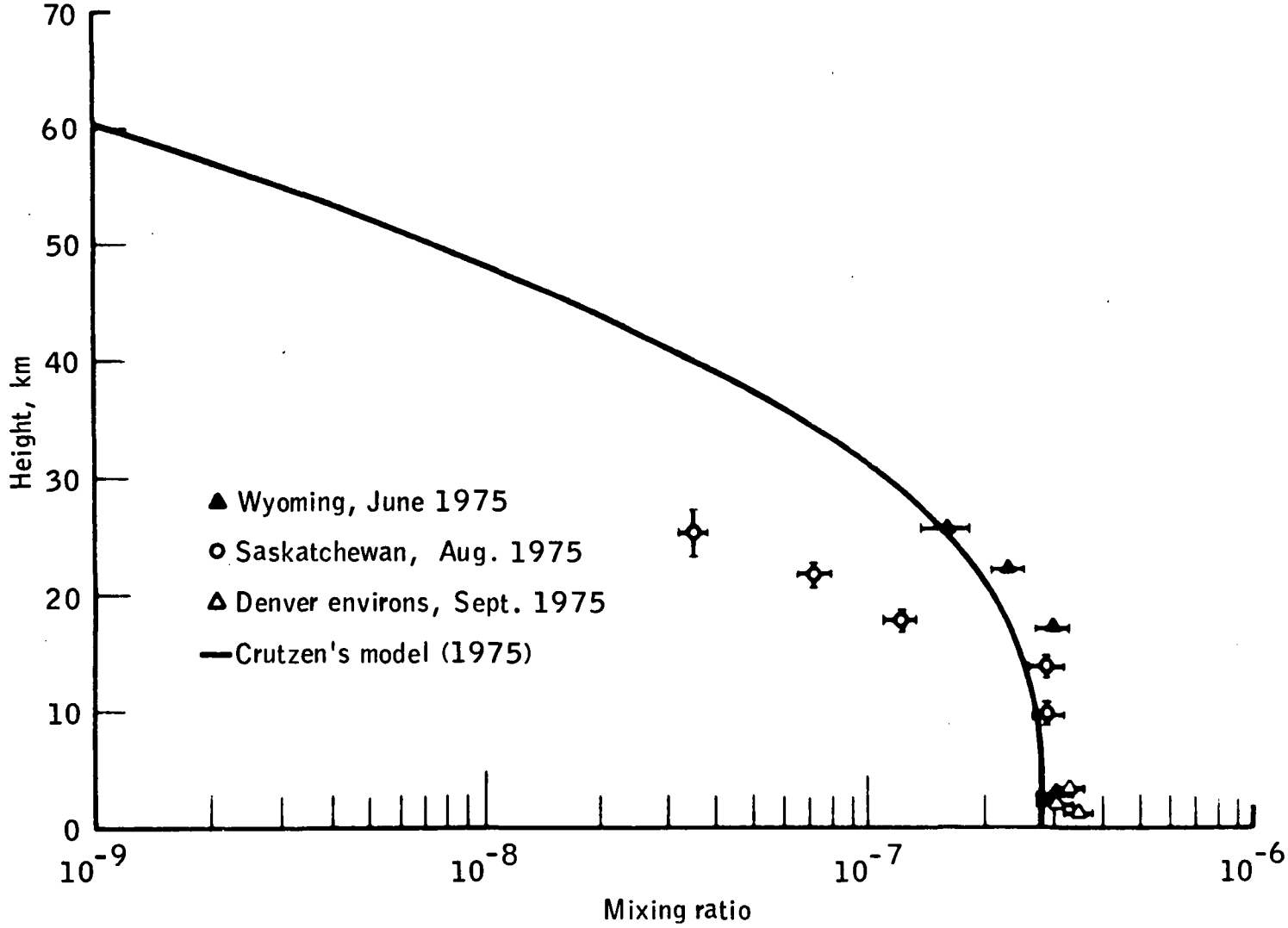

Figure C-7.- Altitude profiles of nitrous oxide obtained from stratospheric balloon flights (Wyoming and Saskatchewan) and tropospheric aircraft flights (Denver environs) compared to a theoretical photochemical model.

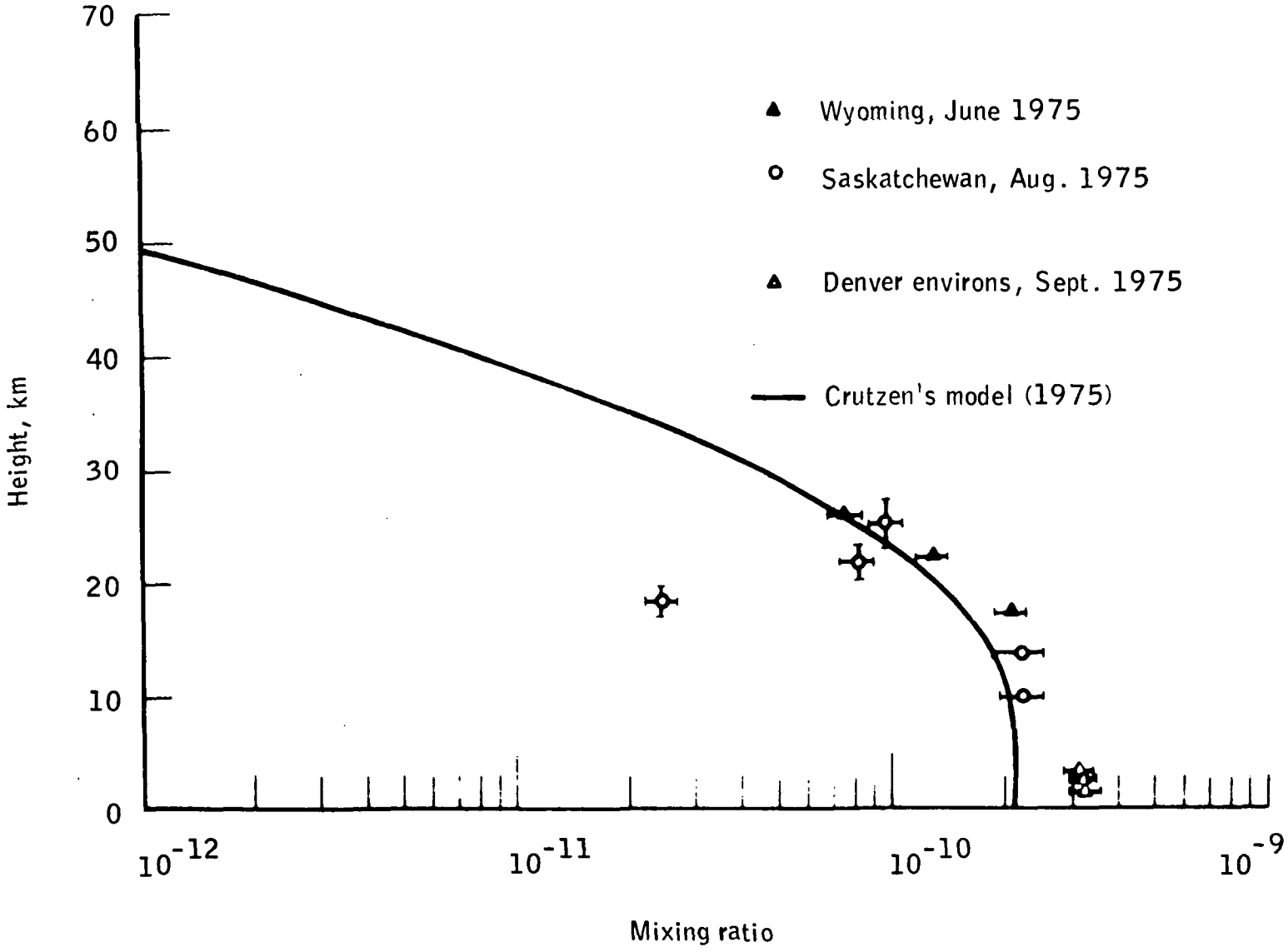

Figure C-8.- Altitude profiles of CF_2Cl_2 obtained from stratospheric balloon flights (Wyoming and Saskatchewan) and tropospheric aircraft flights (Denver environs) compared to a theoretical photochemical model.

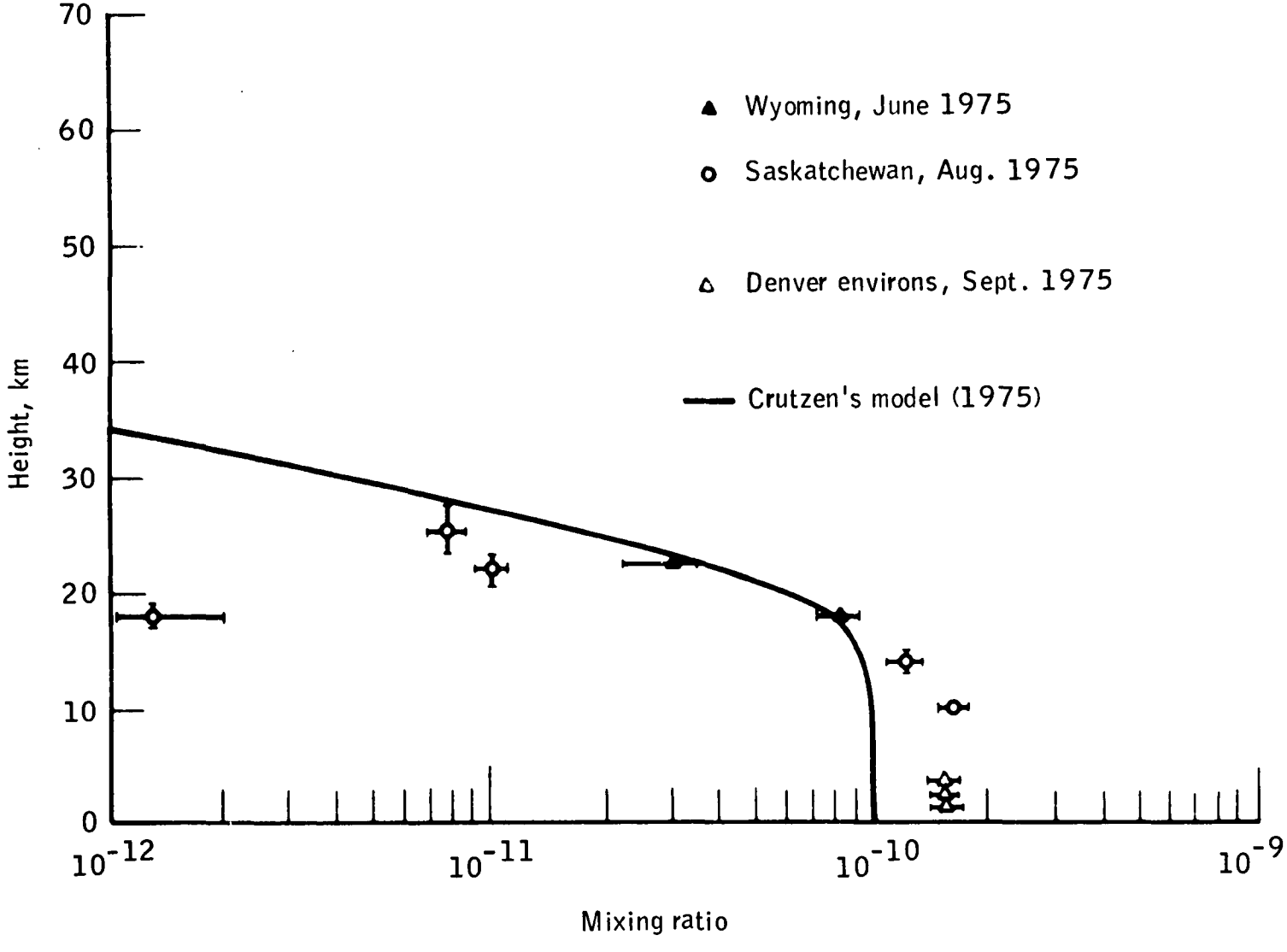

Figure C-9.- Altitude profiles of $CFCl_3$ obtained from stratospheric balloon flights (Wyoming and Saskatchewan) and tropospheric aircraft flights (Denver environs) compared to a theoretical photochemical model.

APPENDIX D

ASSESSMENT OF UPPER ATMOSPHERIC EFFECTS OF SPACE SHUTTLE OPERATIONS

By I. G. Poppoff,[a] R. C. Whitten,[a] J. B. Pollack,[a] and R. G. Prinn[b]

INTRODUCTION

Recent aeronomical investigations suggest that trace contaminants introduced into the air by anthropogenic activities may affect the stratospheric ozone (O_3) layer. Some of these substances can catalytically destroy O_3; that is, each molecule of pollutant gas can systematically remove any O_3 molecules. For example, global O_3 could be reduced by more than 10 percent by nitrogen oxides deposited in the stratosphere in the exhaust from a fleet of supersonic transports (refs. D-1 to D-4). Stratospheric O_3 is important as a natural molecular barrier against excessive solar ultraviolet (uv) radiation.

Concern has been expressed that hydrogen chloride (HCl) present in the exhaust plume of Space Shuttle launch vehicles could also deplete the O_3 layer. The mechanism for O_3 destruction is catalytic (ref. D-5),[4] just as in the case of the nitrogen oxide destruction cycle. Although HCl itself is quite inert with respect to off-oxygen allotropes (O and O_3), it is efficiently decomposed to chlorine (Cl) and water (H_2O) by reaction with hydroxyl (OH). The Cl then reacts with the odd O so that the overall effect is to accelerate the reaction:

$$O + O_3 \rightarrow 2O_2 \qquad \text{(D-1)}$$

As will be shown later, the Cl cycle is quite effective in converting odd O to even O.

The deposition of HCl by Space Shuttle launch vehicles commences at launch and continues until burnout at 45 kilometers (142 000 feet). The rate of HCl emission in metric tons per kilometer as recently determined (ref. D-6) is

---

[a]NASA Ames Research Center.

[b]Massachusetts Institute of Technology.

[4]S. C. Wofsy and M. B. McElroy, unpublished data, 1974.

shown in figure 4-3. At peak operational activity, it is expected that 60 launches per year would be carried out. Launch operations are expected to commence in 1978 and to build up to 60 per year by 1984. In some of the studies reported here, the launch schedule shown in figure 4-4 was employed.

During reentry of the Space Shuttle vehicle into the Earth atmosphere, substantial quantities of nitric oxide (NO) are produced in the shock-heated wake (ref. D-7). Estimates (refs. D-4 and D-8) of the accumulation of NO produced in this manner in the altitude range of 65 to 80 kilometers (211 000 to 268 000 feet) show that it does lead to a large local buildup of NO, which may last for a day. However, it spreads rapidly because of atmospheric motions, and in 1 week, the local NO concentrations are reduced nearly to the ambient condition. Calculations (ref. D-4) show that even if meridional spreading is very slow, the excess NO in the altitude region of 70 to 85 kilometers 237 000 to 274 000 feet) would be at most a few percent of the ambient concentration and would have no discernible effect on stratospheric NO. The NO produced during Space Shuttle vehicle reentry will not be considered further in this report.

Tiny particles, made chiefly of aluminum oxide (Al_2O_3), are contained in the exhaust products produced by the currently comtemplated fuel mixture for the Space Shuttle. Should future Space Shuttle vehicles use such a mixture, they will introduce particles into the stratosphere as they fly through this portion of the Earth atmosphere. As many of the added particles are smaller than a micrometer in size, they would typically remain in the stratosphere for periods on the order of a year; hence, a significant steady-state population of aerosols could be built up in the stratosphere.

The Al_2O_3 particles directly injected could serve as nucleation centers for sulfuric acid (H_2SO_4) vapor and thereby enhance the normal stratospheric sulfate layer. Current work[5] suggests that the particles in the normal stratospheric layer do form on preexisting particles. However, no studies have yet been performed that adequately consider the ways in which Al_2O_3 particles, serving as condensation nuclei, might alter the layer. Consequently, this discussion of Al_2O_3 effects will be restricted to the climatic effects of Al_2O_3 particles that have not interacted with H_2SO_4 vapor.

One of the most important effects that the added Al_2O_3 particles might have is to cause a change in the Earth's climate by interacting with both incident solar radiation and terrestrially generated thermal radiation. An attempt has been made to assess the importance of these effects. A series of radiative transfer calculations was performed to estimate the sensitivity of the mean global temperature to the introduction of these particles. The change in the atmospheric opacity and the resultant change in global temperature

---

[5]Hamill, Toon, and Kiang: A Physical Model of Stratospheric Aerosol Particles. To be published.

was compared with the optical depth changes that accompany particles introduced into the stratosphere by volcanic activity and with the temperature changes characteristic of past epochs of major climatic change.

CHEMISTRY

The HCl injected as rocket engine exhaust in the stratosphere can be converted into free Cl atoms principally by reacting with OH radicals:

$$OH + HCl \rightarrow H_2O + Cl \qquad (D\text{-}2)$$

The Cl atoms then react catalytically with odd O (O and O_3)

$$Cl + O_3 \rightarrow ClO + O_2 \qquad (D\text{-}3)$$

$$ClO + O \rightarrow Cl + O_2 \qquad (D\text{-}4)$$

to effectively remove O_3. Aeronomically, reaction (D-4) is the rate-limiting process in the O_3 destruction chain. Eventually, odd-O catalysis is terminated when Cl is converted into HCl, mainly by reacting with CH_4:

$$Cl + CH_4 \rightarrow HCl + CH_3 \qquad (D\text{-}5)$$

A secondary terminating reaction, similar to reaction (D-5), involves hydroperoxyl radicals.

$$Cl + HO_2 \rightarrow HCl + O_2 \qquad (D\text{-}6)$$

Although the HCl can be recycled into free Cl by way of reaction (D-2), a fraction of it is constantly being removed from the stratosphere by downward transport into the troposphere. Another important reaction in the Cl photochemical scheme involves the chemical dissociation of ClO by NO,

$$NO + ClO \rightarrow NO_2 + Cl \qquad (D\text{-}7)$$

which, followed by rapid nitrogen peroxide (NO_2) photolysis, effectively short-circuits the Cl catalysis chain.

For the sensitivity of computed Cl-induced O_3 reductions to variations in the rate coefficients and species concentrations for processes (D-2) to (D-7), it can be shown that for small perturbations, the fractional columnar O_3 decrease ΔO_3 is approximately proportional to the quantity:

$$\Delta O_3 \propto \frac{k_1 k_2 k_3 \, [\overline{O}] \, [\overline{OH}]}{\left(k_4[\overline{CH_4}] + k_5[\overline{HO_2}]\right)\left(k_6[\overline{NO}] + k_3[\overline{O}]\right)} \tag{D-8}$$

where an overbar denotes an average species concentration near the altitude of the greatest absolute O_3 decrement and k_1 to k_6 are rate coefficients. Some detailed calculations[6] support this simple O_3 reduction scaling rule, which can be used to obtain quick estimates of the changes in computer O_3 reduction resulting from changes in rate constants and ambient species abundances.

The methane (CH_4) is supplied to the stratosphere by upward transport from the troposphere and is decomposed mainly by way of the reaction

$$OH + CH_4 \rightarrow H_2O + CH_3 \tag{D-9}$$

Because of this simple chemistry, CH_4 serves as a convenient tracer for determination above an altitude of 30 kilometers (95 000 feet) of vertical eddy diffusivity for use in one-dimensional models. Thus, CH_4 plays an important role in Cl chemistry through reaction (D-5).

The chemistry of the oxides of hydrogen (HO_x) system is of great significance to the catalytic reduction of O by oxides of chlorine (ClO_x) because of reactions (D-2) and (D-6). The OH concentrations between 30 and 40 kilometers (95 000 and 126 000 feet) have been recently measured (ref. D-9) over Texas at a solar zenith angle of 80°. The measured value of approximately 2.2×10^7 molecules/cm^3 (±30 percent) at an altitude of 40 kilometers (126 000 feet) is substantially larger than previously predicted (e.g., ref. D-4).[4] The key odd-H (HO_2 and OH) reactions in this altitude range are the following.

---

[6] R. C. Whitten, I. G. Poppoff, and R. P. Turco: Comments on an Assessment of the Potential Impact on the Stratosphere of Solid-Fueled Rocket Engines. To be published.

[4] S. C. Wofsy and M. B. McElroy, unpublished data, 1974.

$$O(^1D) + H_2O \xrightarrow{k_8} 2OH \qquad \text{(D-10)}$$

$$OH + HO_2 \xrightarrow{k_9} H_2O + O_2 \qquad \text{(D-11)}$$

$$O + HO_2 \xrightarrow{k_{10}} OH + O_2 \qquad \text{(D-12)}$$

$$O_3 + OH \xrightarrow{k_{11}} HO_2 + O_2 \qquad \text{(D-13)}$$

$$O + OH \xrightarrow{k_{12}} H + O_2 \qquad \text{(D-14)}$$

$$HO_2 + h\nu \xrightarrow{J_{13}} OH + O \qquad \text{(D-15)}$$

$$HO_2 + h\nu \xrightarrow{J_{14}} H + O_2 \qquad \text{(D-16)}$$

where ^1D is an energy state, $h\nu$ is photon energy, and k_8 to k_{12}, J_{13}, and J_{14} are rate coefficients. The hydrogen peroxide (H_2O_2) reactions are omitted because they do not result in a significant net production or loss of odd-H species. For the atmospheric conditions that prevail between 34 and 40 kilometers (110 000 and 126 000 feet), one can easily show that in daylight, equation (D-17) is an excellent representation of calculated OH profiles when the reaction rate coefficients listed in table D-I and predicted $O(^1D)$, O, O_3, H_2O, and CH_4 concentrations are inserted.

$$[OH] \approx \left\{ \frac{\left(k_{10}[O] + J_{13}\right) k_8 [O(^1D)]\,[H_2O]}{k_9 \left(k_{11}[O_3] + k_{12}[O]\right)} \right\}^{\frac{1}{2}} \qquad \text{(D-17)}$$

The discrepancy between computed OH abundances and those measured by Anderson (ref. D-9) may be due to the rate coefficients k_9 and k_{10}, neither of which is known to be more accurate than an order of magnitude. For example, if these rate constants were equal (which is kinetically reasonable) and if rate coefficient J_{14} were zero, one would obtain OH concentrations very close to the lower uncertainty limit of Anderson's (ref. D-9) measured values. Additional uncertainties in the concentrations of O, O_3, $O(^1D)$, and H_2O and in the rates of the other photochemical processes (D-10) to (D-16) may account for residual differences in the OH abundance. Table D-I contains the important reactions and the most recent, available rate coefficient data (refs. D-10 to D-21).

DESCRIPTION OF TRACE CONSTITUENT MODELS

The large number of chemical species and their reactions have been approached by use of models. So far, these models range in complexity from one dimensional to three dimensional.

One-Dimensional Models

One-dimensional models of atmosphere trace constituents include vertical transport and photochemistry. Transport is parameterized by an eddy diffusivity which relates vertical mass flux to the vertical mixing ratio gradient. In reality, the motions which distribute the various constituents throughout the atmosphere cannot be represented by a single parameter. However, with the selection of a diffusivity profile which leads to agreement between calculated and observed vertical distributions of convenient tracers such as CH_4 and carbon-14, globally averaged vertical transport rates can be roughly simulated. The diffusivity profile shown in figure D-1 was employed[6]; this profile, a modified form of that suggested in reference D-22, has a 13-kilometer (42 000 foot) tropopause level characteristic of middle latitudes.

One-dimensional models consist of a set of coupled continuity equations:

$$\frac{\partial n_i}{\partial t} + \frac{\partial \phi_i}{\partial z} = P_i - \ell_i n_i \qquad \text{(D-18)}$$

---

[6] R. C. Whitten, I. G. Poppoff, and R. P. Turco: Comments on an Assessment of the Potential Impact on the Stratosphere of Solid-Fueled Rocket Engines. To be published.

where t is time, z is the vertical coordinate, n_i is the number density of the i-th constituent, and P_i and ℓ_i are the production and loss rates, respectively, for the i-th constituent. The flux ϕ_i in equation (D-18) can be written as

$$\phi_i = -K_e n_M \frac{\partial \frac{n_i}{n_M}}{\partial z} \qquad \text{(D-19)}$$

where K_e is the eddy diffusivity and n_M is the air density.

All chemistry is represented in terms of P_i and $\ell_i n_i$. Equation (D-18) is typically very "stiff"; that is, the characteristic time constants vary over many orders of magnitude. To overcome the problem of stiffness while still maintaining solution speed and precision, Turco and Whitten (ref. D-23) use the fact that in many aeronomic systems, there are families of species in which the members are rapidly intraconverted (or shuffled) but are only slowly converted to those outside the family. The family is conserved on a time scale much longer than the lifetime of many of its members. Accordingly, the equation governing the behavior of the total family concentration is more stable than the equations for its members and may be accurately solved over longer time steps. The concentrations of the family members themselves are first approximately determined by using a suitable stable numerical technique and are then adjusted to correspond to the more accurate total family concentration. As in all mathematical models, upper and lower boundary conditions must be specified. To model diurnal variations accurately without inordinate demands on computer time, it is necessary to average diurnally both photolytic rates and concentrations of species that undergo large variations between night and day.[6] These modifications have been included in the Whitten-Turco model. Wofsy used a similar model for Space Shuttle effects computations, and his work is summarized in the section of this appendix entitled "The Harvard Model."

The Ames Research Center Two-Dimensional Model Of Stratospheric Trace Constituents

In constructing a two-dimensional model (i.e., a model in a meridional plane) of trace constituents, one must modify equations (D-18) and (D-19) so that

---

[6] R. C. Whitten, I. G. Poppoff, and R. P. Turco: Comments on an Assessment of the Potential Impact on the Stratosphere of Solid-Fueled Rocket Engines. To be published.

$$\frac{\partial n_i}{\partial t} + \underset{\sim}{\nabla}\cdot\left(\underset{\sim}{V} n_i\right) + \underset{\sim}{\nabla}\cdot\underset{\sim}{\phi}_i = P_i - \ell_i n_i \qquad \text{(D-20)}$$

$$\underset{\sim}{\phi}_i = -\underset{\approx}{K}_e \cdot n_M \underset{\sim}{\nabla}\left(n_i / n_M\right) \qquad \text{(D-21)}$$

where the mass flux ϕ_i is now a vector quantity $\underset{\sim}{\phi}_i$, the eddy diffusivity is a tensor $\underset{\approx}{K}_e$, $\underset{\sim}{\nabla}$ is the gradient vector operator, and $\underset{\sim}{V}$ is the atmospheric advective or bulk velocity.

The transport computations are time-split into those for vertical and horizontal advection and diffusion. Solutions for the transport processes are obtained from a mass-conserving, forward-time, space-centered finite-difference formulation of the equations. To optimize speed and accuracy, an implicit formulation is used for the horizontal diffusion and an explicit formulation is used for all other transport processes. Spherical geometry is employed in equations (D-20) and (D-21) with the horizontal coordinates extending along a meridian from latitudes 80° S to 80° N in 5° intervals with the vertical coordinates extending from the surface to 60 kilometers (195 000 feet) in 2.5-kilometer (7000 foot) intervals. End boundaries are taken at latitudes 80° N and 80° S because meridional fluxes are expected to be small at these latitudes. The end boundary conditions are taken to be zero flux for all constituents across the vertical boundaries. The upper boundary conditions are set by putting the constituents in mixing equilibrium at a 60-kilometer (195 000 foot) altitude, whereas the lower boundary condition for all components except nitric acid (HNO_3), NO_2, O_3, HCl, and H_2O_2 is chemical equilibrium. Because HNO_3, HCl, and H_2O_2 are water soluble, the mixing fractions are set equal to zero at the lower boundary. The number density of NO_2 is fixed at 3×10^9 cm^{-3} at the lower boundary, whereas that for O_3 is fixed at 6×10^{11} cm^{-3}.

The mean meridional circulation is obtained by the kinematic method from the averaged equation of mass continuity. With the assumption that the density field is in a steady state, the approximate form of this equation in spherical coordinates is

$$\frac{1}{R \cos\phi}\frac{\partial\left(\overline{\rho v}\cos\phi\right)}{\partial\phi} + \frac{\partial\left(\overline{\rho w}\right)}{\partial z} = 0 \qquad \text{(D-22)}$$

where the overbar denotes an average with respect to time and longitude, $\bar{\rho}$ is the bulk density, $\bar{v}$ and $\bar{w}$ are the meridional and vertical velocity components, R is the radius of the Earth, and ϕ is the latitude. Equation (D-22) implies the existence of a "stream function" ψ for the total mass flux such that

$$2\pi R\bar{\rho}\bar{v} \cos \phi = - \frac{\partial \psi}{\partial z}$$

$$2\pi R\bar{\rho}\bar{w} \cos \phi = \frac{\partial \psi}{R \, \partial \phi} \qquad \text{(D-23)}$$

If the distribution of $\bar{\rho}$ and $\bar{v}$ is known, the first of these can be integrated vertically and $\bar{w}$ can be obtained from the second.

To altitudes of 20 kilometers (63 000 feet), the density was obtained from data presented in reference D-24. Above that altitude, the density was obtained from vertical integration of the hydrostatic equation by using mean (rocket) temperatures.

The $\bar{v}$ components were based on measured winds (ref. D-24) to altitudes of 20 kilometers (63 000 feet). These values were then extrapolated to the top of the model by imposition of a simple vertical profile that matched the 20-kilometer (63 000 foot) value. In addition, a meridional variation was imposed that resulted in a three-cell circulation structure (latitudes 80° N to 80° S) in the stratosphere and lower mesosphere during the summer and winter seasons and a four-cell structure in spring and fall. The first segment of equation (D-23) was then integrated vertically with the condition that $\psi = 0$ on all boundaries. This condition implies that no net mass flux exists across a vertical latitude wall; therefore, the specified values of $\bar{v}$ had to be slightly adjusted so that the boundary condition was satisfied at the top and bottom of the model. The resulting circulation patterns are reasonable in the troposphere and lower stratosphere but need further refinement in the upper portion of the model. Except in the upper equatorial troposphere, meridional windspeeds are generally less than 1 m/sec. Vertical windspeeds attain maximums in excess of 4 mm/sec in the equatorial troposphere but are usually less than 1 mm/sec except in the vicinity of cell boundaries.

The eddy fluxes are modeled by diffusion coefficients based on the method cited in reference D-25. The data given in reference D-26 were used at altitudes as high as 20 kilometers (63 000 feet). These values were extended to the higher levels by assuming that coefficient K_{yy} is proportional to the variance of the v component and that the slopes of the mixing surfaces are proportional to the slopes of the mean isentropic surfaces. Given K_{yy}, the other coefficients (ref. D-24) were obtained from

$$K_{yz} = \alpha K_{yy}$$
$$K_{zz} = \left(\bar{\alpha}^2 + \overline{\alpha'^2}\right) K_{yy} \tag{D-24}$$

where $\bar{\alpha}$ is the mean slope of the mixing surface and $\overline{\alpha'^2}$ is its variance. The value of $\overline{\alpha'^2}$ was assumed to be constant. The variances of the v component were taken from reference D-27.

The chemical rate equations are solved with an implicit technique. Omission of the transport term from equation (D-20) yields the finite-difference form

$$\frac{n_i^{j+1} - n_i^j}{\Delta t} = Q_i^{j+1} \tag{D-25}$$

which can be linearized by taking the first term in a Taylor series expansion of Q_i^{j+1} about Q_i^j.

$$\frac{n_i^{j+1} - n_i^j}{\Delta t} = Q_i^j + \sum_k \frac{\partial Q_i^j}{\partial n_k}\left(n_k^{j+1} - n_k^j\right) \tag{D-26}$$

The members of the set of mass conservation equations are coupled and require solution by matrix methods. With the implicit method, large time steps can be taken even though the equations are very stiff.

Massachusetts Institute of Technology Model

The Massachusetts Institute of Technology (MIT) three-dimensional model presently comprises 26 horizontal levels equally spaced in log pressure coordinates between the ground and 72-kilometer (237 000 foot) altitude. It solves a set of dynamical equations similar to the conventional midlatitude beta plane quasi-geostrophic equations except that it is global and allows for the variation of the Coriolis parameter with latitude. It also includes solution of the full continuity equation for O_3. In the horizontal direction, predicted quantities are expressed in terms of a series of spherical harmonics using planetary waves with maximum wave number six and six degrees of freedom in latitude (rhomboidal truncation). Northern and Southern Hemisphere orography and tropospheric heating rates are also expressed in series form. The chemical scheme presently requires specification of the distributions of certain odd-N

and odd-H species, but this limitation will be ultimately removed by inclusion of a larger set of chemical reactions. (This set is being implemented by recoding for the Illiac IV computer.) Allowance is made for radiative heating by O_3 and other gases. Chemical and heating computations are performed at a set of grid points chosen to filter aliasing errors during transformation from spectral to grid-point representations. Time integration of the model is performed using a Lorenz four-cycle scheme with four 1-hour steps in each cycle. This spectral model is extremely efficient computationally compared to existing stratospheric primitive equation grid-point models; it requires about 40 seconds of IBM 360/95 time per stratosphere day. A full description of the first version of the three-dimensional model appears in reference D-28. Further runs, including a simulation of the stratosphere perturbed by supersonic aircraft effluents, are described in reference D-29.

The MIT two-dimensional model extends from pole to pole and over the 8- to 68-kilometer (21 000 to 221 000 foot) region. Atmospheric motions are simulated by using mean vertical and meridional winds (presently obtained from the three-dimensional model), and eddy diffusion coefficients are deduced from observations (currently those computed by Luther, ref. D-26). A set of 36 chemical reactions involving odd-N, odd-H, and Cl species is included (table D-I). The full continuity equation for long-lived species is solved on grid points spaced 5° in latitude and 2 kilometers (6300 feet) in altitude; a photochemical steady state is assumed for very-short-lived species. The lower boundary condition for water-soluble species such as HNO_3 and HCl is formulated in terms of a tropospheric rainout time. A full description of the first version of the two-dimensional model is given in reference D-30.

Radiative Model

The addition of aerosols to the Earth atmosphere can produce either a net warming or cooling depending on their optical constants and their size distribution function. Measurements of the transmission and reflection characteristics of Al_2O_3, as given in the scientific literature, were used to derive their optical constants — the real and imaginary indexes of refraction — from the near uv to the middle infrared.[7] Estimates of the particle size distribution function were obtained from a combination of measurements of their size distribution in the exhaust wake and estimates of the change in the size distribution caused by sedimentation process (ref. D-31).

Estimates of the mean temperature of the Earth can be obtained by equating the amount of solar energy absorbed by the entire Earth with the amount of thermal radiation it emits to space (ref. D-31). With such calculations for perturbed and unperturbed conditions, it is possible to determine the change

---

[7] O. B. Toon, J. B. Pollack, and B. N. Khare: The Optical Constants of Several Atmospheric Aerosol Species: Ammonium Sulphate, Aluminum Oxide, and Sodium Chloride. Journal of Geophysical Research, in press.

in the mean surface temperature produced as a result of a given perturbation. To calculate the solar energy absorbed by the Earth, a computer program that permits an accurate solution of the multiple scattering problem was used. Allowance was made for scattering and absorption by both gases and aerosols, separate calculations were made at a number of wavelengths that spanned the near uv to the near infrared, and account was taken of partial cloud cover and the vertical inhomogeneity of the atmosphere. Mie scattering theory was used to derive the single scattering properties of the natural, background aerosols and the perturbing aerosols.

A separate computer program was used to evaluate the thermal radiation at the top of the atmosphere, and both gaseous and aerosol opacity were considered. Iteratively, this program also determined the surface temperature at which global heat balance was achieved.

Ambient Atmosphere

The Cl emitted in the stratosphere by the Space Shuttle will react with several ambient trace gases including O, O_3, OH, NO, and CH_4. Atomic O has been observed only once in the stratosphere (ref. D-32). Figure D-2 demonstrates that the measured data agree quite well with the NASA Ames Research Center (ARC) model predictions at altitudes above 35 kilometers (108 000 feet). At lower altitudes, O_3 layering and backscattering of sunlight may affect the atomic O concentration, which is proportional to the sunlight intensity and O_3 density. The only measured profile of stratospheric OH is that of Anderson (ref. D-9). His data for a solar zenith angle of 80° are shown in figure D-3, together with two profiles predicted by a one-dimensional model.[6] As discussed previously, the reasons for the discrepancy between prediction and observation are suspected but not yet definitely known.

Numerous measurements of NO have been made in the lower stratosphere, but only a few have been made near 30 kilometers (95 000 feet). The one-dimensional model predictions agree within the experimental spread with the observational data shown in figure D-4 (refs. D-24 and D-33 to D-38).

Figure D-5 (refs. D-39 to D-42)[8] shows the observed vertical CH_4 distribution and the one-dimensional model results obtained by using the eddy diffusivity profile shown in figure D-1. Figure D-6 (refs. D-43 to D-46)[6] illustrates the measured ambient abundances of HCl and the model calculation In both cases, the agreement is satisfactory.

---

[6] R. C. Whitten, I. G. Poppoff, and R. P. Turco: Comments on an Assessment of the Potential Impact on the Stratosphere of Solid-Fueled Rocket Engines. To be published.

[8] E. A. Martell, unpublished NCAR report, 1975.

Figures D-7 (refs. D-9 and D-47), D-8 (ref. D-32), and D-9 (refs. D-34, D-35, and D-48) show, respectively, some vertical profiles of OH, O, and NO at various latitudes as computed with the ARC two-dimensional model. As with one-dimensional model results, the OH concentration profiles are substantially lower than Anderson's (ref. D-9) measured values. The computed NO profiles are very close to the measured profiles. However, the atomic O predicted concentrations are smaller than those measured by Anderson (ref. D-32) because, unlike the ARC one-dimensional model, the two-dimensional model does not yet include diurnal averaging on concentrations.

The MIT three-dimensional model predictions of zonal winds, stratospheric temperature, meridional circulation, and O_3 density compared to altitude and latitude, or season and latitude, are shown in figures D-10 (ref. D-49), D-11 (ref. D-49), D-12, and D-13 (ref. D-50), respectively. Agreement with observations is good in each case.

RESULTS OF SPACE SHUTTLE IMPACT ASSESSMENT

The models have also been calculated using the estimated Space Shuttle exhaust products. Predictions from those calculations are described in the following section.

Results Of One-Dimensional Model

The potential effect of Space Shuttle exhaust on the O_3 layer was first estimated in reference D-51; an average hemispherical O_3 reduction of approximately 0.3 percent for 60 launches per year was calculated. The estimate has recently been lowered to approximately 0.1 percent,[6] based on the newly measured chemical reaction coefficient data presented in table D-I. The time-dependent O_3 reduction corresponding to the launch schedule shown in figure 4-4 is shown in figure D-14.

The new estimates[6] of the O_3 reductions beyond 1978 due to planned Space Shuttle launches are shown in figure D-14. Curve A represents the predicted O_3 reduction using the new rate coefficients for the reaction of Cl with O_3, Cl with CH_4, and ClO with NO (table D-I); the other rate coefficients are adopted from previous work. The eventual O_3 decrease, approximately 0.08 percent, is about one-fourth the estimated reduction (0.3 percent) reported previously.

---

[6] R. C. Whitten, I. G. Poppoff, and R. P. Turco: Comments on an Assessment of the Potential Impact on the Stratosphere of Solid-Fueled Rocket Engines. To be published.

It should be noted that the effect of diminishing the rate constant for reaction (D-3) by a factor of approximately 0.5 and increasing the rate constants for reactions (D-5) and (D-7) by factors of approximately 1.8 and 1.7, respectively, is to decrease the O_3 reduction by a factor of approximately 6. This reduction factor is raised to approximately 9 by an increase of approximately 50 percent in the predicted NO concentration resulting from the use of a new eddy diffusivity profile and to a diurnally averaged model. However, these downward adjustments are partly offset by increases in the computed O and OH abundances by approximately 50 percent each.

Curve B shows the O_3 reduction, approximately 0.11 percent at steady state, when the rate coefficient of the ClO + NO reaction (D-7) is reduced to its older value, 1.7×10^{-11} cm^3 sec^{-1}, with all other rate coefficients remaining unchanged. Comparison of curve B with curve A illustrates the large change in the predicted O_3 reduction caused by the new data on the important reaction (D-7) between NO and ClO.

Curve C shows the O_3 reduction when the rate coefficient for the OH + HO_2 reaction (D-11), which affects the OH concentration, is increased to the previously used value of 2×10^{-10} cm^3 sec^{-1}. However, in view of Anderson's recent OH measurements, this high value seems unrealistic.

Curve D shows the predicted O_3 reduction of approximately 0.11 percent when $k_{10} = k_{11} = 6 \times 10^{-11}$ cm^3 sec^{-1} is set, which leads to a better match with the OH distribution observed by Anderson; hence, curve D is probably a more realistic estimate of the potential O_3 reduction.

Curve E illustrates the O_3 reduction when the rate coefficient for reaction (D-6) is increased to 10^{-10} cm^3 sec^{-1}; this value is almost certainly an upper limit for this reaction. Adjusting the rate constant (reaction (D-5)) to its older value of 5.1×10^{-11} $e^{-1790/T}$ cm^3 sec^{-1} would lead to an increase of approximately 70 percent in the predicted O_3 reduction shown in figure D-14.

The set of O_3 reductions (curves A to E) presented in figure D-14 demonstrates the potential variability in predicted Space Shuttle effects. Although the cases treated are quite specific, they are all interesting because they illustrate the effects of important aeronomic uncertainties on calculated O_3 reductions. Consideration of the uncertainties in reaction rates and ambient species concentrations leads to the conclusion that current estimates have an uncertainty of approximately 3.

Figure D-15 shows the steady-state vertical distribution of the increments in the concentrations of Cl, ClO, and HCl (labeled [Cl], [ClO], and

[HCl], respectively). Because these incremental concentrations are approximately 0.1 of the computed ambient concentrations of the allotropes of chlorine (Cl_x) constituents (e.g., the HCl distribution in figure D-6), the steady-state O_3 reduction caused by Space Shuttle operations is approximately 0.1, the reduction caused by the ambient Cl_x.

To estimate the stratospheric O_3 recovery time, a case was considered in which all launches are ended after a steady-state condition is reached.[6] The corresponding O_3 reduction shown on figure D-14 (curve F) indicates that the recovery is very rapid; the ozone reduction decreases by a factor of 2 in approximately 1.8 years. The O_3 recovery is aided by the fast diffusive redistribution of the injected Cl after the end of launch operations; excess Cl above 30 kilometers (95 000 feet) is quickly transported to lower altitudes where HCl is not strongly dissociated. It is subsequently transferred across the tropopause at a slower rate. The characteristic O_3 recovery time will be sensitive to the eddy diffusivity profile and will become longer as the diffusivity near 30 kilometers (95 000 feet) is decreased.

Results of ARC Two-Dimensional Model

The two-dimensional model described in section 4 was adapted to assess the O_3 degradation by Space Shuttle launch vehicle emissions. The launch schedule shown in figure 4-4 was employed, and all launches were assumed to be performed at the NASA John F. Kennedy Space Center (KSC) (latitude 30° N). The latitude dependence of O_3 column reduction after 10 years of operations is shown in figure D-16 for the four seasons. The most remarkable feature is the strong corridor effect at latitude 30° N in summer. This seasonal effect is due mainly to larger OH and abundance O but smaller NO abundance during summer than during winter in the altitude range of 30 to 40 kilometers (95 000 to 126 000 feet). For the same reason, O_3 loss is greater during summer than during the winter throughout the Northern Hemisphere.

The buildup of the globally averaged O_3 distribution is shown in figure D-17. Notably, the globally averaged reduction after 10 years is very close to one-half that obtained with the ARC one-dimensional model for the hemispherically averaged case, as shown on curve A, figure D-14. However, the time required for buildup to a steady state is longer than 10 years. Hence, the calculated steady-state percentage of O_3 destruction will be somewhat larger than

---

[6] R. C. Whitten, I. G. Poppoff, and R. P. Turco: Comments on an Assessment of the Potential Impact on the Stratosphere of Solid-Fueled Rocket Engines. To be published.

that computed with the one-dimensional model. After 10 years of simulated Space Shuttle operations, further launches were stopped and the O_3 layer was allowed to recover. It was found that in approximately 3 years, the globally averaged O_3 column reduction had decayed to one-half its value when operations ceased; the decay time was approximately 50 percent longer than that obtained with the one-dimensional model. The investigation also showed that the predicted corridor effect centered at latitude 30° N had disappeared within 1 year after operations ceased.

Results of MIT Model

The MIT two-dimensional model has been run for a continuous insertion of HCL in a 5° latitude belt centered at latitude 30° N. The source magnitude was designed to simulate the effect of 50 Space Shuttle launches per year from KSC. From this run, an input distribution of ClO for the three-dimensional model was obtained. The three-dimensional model has not yet been run with this distribution of ClO.

Radiative Effects

The results of the radiative calculations (ref. D-31) are summarized as follows. Figure D-18 shows the dependence of the global albedo on the optical depth enhancement $\Delta\tau$ at 0.55 micrometer as a result of the added aerosols. The addition of Space-Shuttle-generated Al_2O_3 aerosols to the stratosphere would cause an increase in the Earth's albedo or, equivalently, the Earth would absorb less solar energy.

The resulting change in mean surface temperature ΔT as a function of $\Delta\tau$ is shown in figure D-19. The four curves of this figure illustrate the effect of alternative prescriptions for the change in water-vapor abundance and change in stratospheric temperature profile and the inclusion of the aerosol effect on the thermal radiation. Curve A was calculated for a constant relative humidity and a constant temperature lapse rate and is probably the most realistic of the cases shown. Curves B and C show the effects of assuming instead a constant absolute humidity and a constant stratospheric temperature profile, respectively. Finally, curve D shows what happens when the added aerosol opacity in the thermal infrared is neglected. Comparison of curves A and D shows that such a neglect is a poor approximation. Quite clearly, the aerosol effect at thermal wavelengths largely cancels the effect at visible wavelengths. The former causes a surface warming by enhancing the greenhouse effect.

To apply these results to determine the impact of Space Shuttle traffic during the next several decades, $\Delta\tau$ must first be evaluated. To do this, Mie scattering theory was used to relate $\Delta\tau$ values to the steady-state mass loading of the added particles. The latter parameter was found from the mass of Al_2O_3 generated by a single Space Shuttle vehicle as it traverses the stratosphere, from the projected number of Space Shuttle flights, and from

the mean dwell time of particles in the stratosphere (ref. D-32). For a projected traffic level of one Space Shuttle flight per week, it was found that $\Delta\tau = 3.3 \times 10^{-5}$ for the Northern Hemisphere; hence, according to curve A of figure D-14, $\Delta T = 1.5 \times 10^{-4}$ K. The corresponding number for the Southern Hemisphere is three-sevenths as large.

To assess the significance of these values, the $\Delta\tau$ values were compared with those produced as the result of volcanic eruptions and the ΔT values with those typical of epochs of major climatic change. Figure D-20 illustrates the $\Delta\tau$ values that have occurred during the last century, primarily as a result of the introduction of material into the stratosphere by volcanic explosions (ref. D-52). The $\Delta\tau$ values expected from the particles produced by Space Shuttle vehicles are several orders of magnitude smaller than those generated by volcanic explosions. In fact, even relatively minor volcanic explosions typically generate a $\Delta\tau$ on the order of 10^{-2}.

The difference in temperature between a major ice age and the current epoch is approximatley 5 K; and the difference between 1940 (the time of a recent temperature maximum) and the period from 1450 to 1915 (the time of the "Little Ice Age") is approximately 0.5 K (ref. D-52). During the Little Ice Age, glaciers tended to expand and famines were more frequent at some higher latitude locations than during the warmer, preceding epoch. Hence, a ΔT of 0.5 K would be a serious change, but a ΔT value of less than 0.1 K would be less significant. Since the ΔT expected from the Space Shuttle Al_2O_3 aerosols is about two orders of magnitude smaller than this limit, it seems unlikely that such a variation will cause a significant climatic change.

The basic reason for the slight climatic impact of the added Al_2O_3 particles is that there are very few particles large enough to interact efficiently with light. Unless the ratio $X = 2\pi(r/\lambda)$ (where r is particle radius and λ is the wavelength of light) is 1 or greater, particles are not efficient in scattering light. For visible light, therefore, r must be approximately 0.1 micrometer for X to be approximately 1. The Space Shuttle exhaust increases the number of 0.1-micrometer-sized particles in the stratosphere by approximately 1 percent (ref. D-53). Hence, $\Delta\tau$ is small and no significant climatic change results. As pointed out earlier, Al_2O_3 particles could serve as nucleation centers for H_2SO_4. This process could cause small Al_2O_3 particles with $X < 1$ to grow into added H_2SO_4 particles with $X > 1$. The number of Al_2O_3 particles with $r > 0.01$ micrometer will exceed or equal the number of natural nuclei of this size and will greatly exceed the number of natural particles with $r > 0.1$ micrometer; therefore, such growth could be significant (ref. D-53). The growth of these particles has not yet been studied in detail; but because any increases in the stratospheric sulfate layer could have climatic implications, the problem should be pursued. Until the nucleation and growth is understood, the climatic effects cannot be easily

estimated. Further studies to define the problem are being performed at ARC by using a model that has been developed for studying nucleation and growth of sulfate aerosol particles.

Results of Space Shuttle effects obtained by S. C. Wofsy are given in the following section.

THE HARVARD MODEL

To estimate the effect on stratospheric O_3, a model was adopted that provided for 60 Space Shuttle flights per year, steady-state conditions, and global spreading of the exhaust products. If one assumes that debris will be restricted to the Northern Hemisphere, the adjusted effect would be double the calculated global effect. Space Shuttle emission profiles from reference D-6 were used.

The global average source strength of CHl from 60 Space Shuttle launches is considerably smaller than that of the background sources caused by CH_3Cl, CCl_4, CF_2Cl_2, and $CFCl_3$. For example, at an altitude of 30 kilometers (95 000 feet), 60 launches give an average HCl source of 0.15 cm^3 sec^{-1} compared to approximately 6 cm^3 sec^{-1} from the other sources of Cl; that is, the Space Shuttle contribution is 2.5 percent. At lower altitudes, the Space Shuttle contribution is slightly more important; e.g., approximately 5.5 percent at 20 kilometers (63 000 feet). An O_3 reduction of 2 to 4 percent from CL is predicted because of the background sources; thus, Space Shuttle effects lie in the range of a few tenths of 1 percent, or less.

Making a quantitative estimate is hampered by the difficulty of suppressing numerical fluctuations of the order 0.1 percent for O_3 using a standard one-dimensional diffusion model. Nonlinearities of the O_3 equation are responsible for this problem. Therefore, the estimate is made indirectly by using another calculation in which the background sources were increased by approximately a factor of 5. The following table gives the results and a comparison with Space Shuttle.

Model	Total Ozones, cm^{-2}	Δ total O_3, percent	f_{Cl} mixing ratio of HCl + ClO	
			At 30 km, V/V	At f_{Cl}
Standard model	9.8×10^{18}	—	1.05×10^{-9}	—
Perturbation of Cl by 5×	8.67	12	4.75	3.7×10^{-9}

The Δf_{Cl} from 60 Space Shuttle flights is 2.8×10^{-11}(V/V) at 30 kilometers (95 000 feet); thus, a scaling of results from the table predicts 0.1 percent. If the effluent from Space Shuttle flights were restricted to the Northern Hemisphere, the Space Shuttle effect would be approximately 0.2 percent.

The 0.2-percent estimate is on the upper end of the range of values predicted by the model for three reasons.

1. There should be considerable interhemispheric exchange.

2. Steady-state conditions have been assumed. It is not clear whether flights will continue long enough to approach a steady state.

3. Nonlinear interactions exist between oxides of nitrogen (NO_x) and ClO_x systems which tend to decrease the ClO_x perturbation over certain limited concentration ranges. Neglect of these factors will tend to enhance the calculated perturbations.

SUMMARY

From the foregoing discussion, one can conclude the following about stratospheric effects of Space Shuttle vehicles.

1. The hemispherically averaged O_3 reduction is of the order 0.1 percent subject to a significant uncertainty (approximately a factor of 3) associated mainly with uncertainties in pertinent chemical rate coefficients and in vertical distributions of important atmospheric constituents (i.e., OH, O, NO, and CH_4). The ARC and Harvard University results agree within the uncertainty.

2. Studies using two-dimensional models revealed a strong corridor effect (centered at altitude 30° N) in summer but not in winter. The summertime O_3 reduction percentage at latitude 30° N is about twice that at latitude 50° N.

3. The reentry of Space Shuttle vehicles into the Earth's atmosphere will produce NO in the altitude range of 65 to 80 kilometers (211 000 to 268 000 feet). However, it will be rapidly dispersed (about 1 week) over the Earth, so that the long-term addition to the ambient mesospheric NO will be at most a few percent. The effect of such NO on stratospheric O_3 will be negligible.

4. The direct climatic effects of the Al_2O_3 aerosol are likely to be negligible. That is, the decrease of mean surface temperature resulting from the scattering of sunlight by Al_2O_3 particles is estimated to be of the order of thousandths of a degree. However, it is possible that the small particles may act as condensation nuclei and thereby significantly increase the abundance of large H_2SO_4 droplets. The condensation nuclei aspect of the problem is being assessed at ARC.

ADDENDUM

Since preparation of this paper, the importance of chlorine nitrate ($ClNO_3$) has become apparent. Odd N is responsible for approximately 25 percent of the total loss rate of stratospheric O_3. Were it not for the nitric acid reservoir, the destructive effect of NO_x on O_3 would be substantially greater; in the 20- to 30-kilometer (63 000 to 95 000 foot) region, $ClNO_3$ acts as an additional NO_x reservoir and thus decreases the O_3 loss rates caused by the presence of NO_x. Hence, Cl both reduces and increases O_3; the former effect occurs above 30 kilometers as stated in this paper and the latter effect below 30 kilometers. Because of the subtractive nature of the two effects, the total change in O_3 caused by the presence of stratospheric Cl is very sensitive to the rates of formation and destruction of $ClNO_3$. In a paper to be published elsewhere, one of the authors (Whitten) and his associates calculated that when $ClNO_3$ is included in the computations, O_3 loss caused by Cl will be between one-half and one-fourth the values obtained when $ClNO_3$ is not included.

REFERENCES

D-1. Johnston, Harold: Reduction of Stratospheric Ozone by Nitrogen Oxide Catalysts From Supersonic Transport Exhaust. Science, vol. 173, no. 3996, Aug. 6, 1971, pp. 517-522.

D-2. Crutzen, P. J.: SST's — A Threat to the Earth's Ozone Shield. AMBIO, vol. 1, no. 2, 1972, pp. 1-51.

D-3. McElroy, Michael B.; Wofsy, Steven C.; Penner, Joyce E.; and McConnell, John C.: Atmospheric Ozone: Possible Impact of Stratospheric Aviation. J. Atmos. Sci., vol. 31, no. 1, Jan. 1974, pp. 287-303.

D-4. Whitten, R. C.; and Turco, R. P.: Perturbations of the Stratosphere and Mesosphere by Aerospace Vehicles. AIAA J., vol. 12, 1974, pp. 1110-1117.

D-5. Stolarski, R. S.; and Cicerone, R. J.: Stratospheric Chlorine: A Possible Sink for Ozone. Canadian J. Chem., vol. 52, no. 8, 1974, p. 1610.

D-6. Nozzle Exit Exhaust Products from Space Shuttle Boost Vehicle. JPL TM 33-712, Feb. 1975.

D-7. Park, C.: Estimates of Nitric Oxide Production for Lifting Spacecraft Reentry. NASA TM X-62-052, 1972.

D-8. Stolarski, R. S.; Cicerone, R. J.; and Nagy, A. F.: Impact of Space Shuttle Orbiter Re-entry on Mesospheric NO_x. AIAA J., vol. 12, no. 3, 1974, pp. 395-397.

D-9. Anderson, J. G.: The Absolute Concentration of $OH(X^2\pi)$ in the Earth's Stratosphere. Geophys. Res. Letters, vol. 3, no. 3, Mar. 1976, pp. 165-168.

D-10. Watson, R. T.: Chemical Kinetics Data Survey VIII. Rate Constants of of ClO_x of Atmospheric Interest. NBSIR 74-516, 1974.

D-11. Zahniser, M. S.; Kaufman, F.; and Anderson, J. G.: Kinetics of the Reaction of OH With HCL. Chem. Phys. Letters, vol. 27, no. 4, 1974, pp. 507-510.

D-12. Bemand, P. P.; Clyne, M. A. A.; and Watson, R. T.: Reactions of Chlorine Oxide Radicals. 4. Rate Constants for the Reactions of Chlorine Atoms, Oxygen Atoms, Hydrogen Atoms, and Nitric Oxide with Chlorine Dioxide and of Oxygen Atoms with Chlorine Oxide Radicals. J. Chem. Soc. Faraday Trans., vol. 69, pt. 8, 1973, pp. 1356-1374.

D-13. Leu, Ming-Taun; and De More, W. B.: Rate Constants at 295 K for the Reactions of Atomic Chlorine With Hydrogen Peroxide, Hydroperoxoxo, Ozone, Methane, and Nitric Acid. Chem. Phys. Letters, vol. 41, no. 1, 1976, pp. 121-124.

D-14. Davis, D. D.; Fischer, S.; and Schiff, R.: Flash Photolysis-Resonance Fluorescence Kinetics Study: Temperature Dependence of the Reactions $OH + CO \rightarrow CO_2 + H$ and $OH + CH \rightarrow H_2O + CH_3$. J. Chem. Phys., vol. 61, no. 6, 1974, pp. 2213-2219.

D-15. Hampson, R. F.; and Garvin, D., eds.: Chemical Kinetic and Photochemical Data for Modelling Atmospheric Chemistry. NBS Tech. Note 866, June 1975.

D-16. Anderson, J. G.; and Kaufman, F.: Kinetics of the Reaction $OH(v=o) + O_3 \rightarrow HO_2 + O_2$. Chem. Phys. Letters, vol. 19, no.4, 1973, pp. 483-486.

D-17. Baulch, D. L.; Drysdale, D. D.; Horne, D. G; and Lloyd, A. C.: Evaluated Kinetic Data for High Temperature Reactions, vol. 1. CRC Press, 1972.

D-18. Kurylo, M. J.: Absolute Rate Constants for the Reaction $H + O_2 + M \rightarrow HO_2 + M$ Over the Temperature Range 203 — 404 K. J. Phys. Chem., vol. 76, no. 24, 1972, pp. 3518-3526.

D-19. Hochanadel, C. J.; and Ghormley, J. A.: Absorption Spectrum and Reaction Kinetics of the HO_2 Radical in the Gas Phase. J. Chem. Phys., vol. 56, no. 9, 1972, pp. 4426-4432.

D-20. Paukert, T. T.; and Johnston, H. S.: Spectra and Kinetics of the Hydroperoxyl Free Radical in the Gas Phase. J. Chem. Phys., vol. 56, no. 6, 1972, p. 2824.

D-21. Holt, R. B.; McLane, C. K.; and Oldenberg, O.: Ultraviolet Absorption Spectrum of Hydrogen Peroxide. J. Chem. Phys., vol. 16, 1948, pp. 225-229.

D-22. McConnell, John C.; and McElroy, Michael B.: Odd Nitrogen in the Atmosphere. J. Atmos. Sci., vol. 30, no. 8, Nov. 1973, pp. 1465-1480.

D-23. Turco, R. P.; and Whitten, R. C.: A Comparison of Several Computational Techniques for Solving Some Common Aeronomic Problems. J. Geophys. Res., vol. 79, no. 22, Aug. 1, 1974, pp. 3179-3185.

D-24. Oort, A. H.; and Rasmussen, E. M.: Atmospheric Circulation Statistics. NOAA Professional Paper 5, 1971.

D-25. Reed, Richard J.; and Geman, Kenneth E.: A Contribution to the Problem of Stratospheric Diffusion by Large-Scale Mixing. Monthly Weather Rev., vol. 93, no. 5, May 1965, pp. 313-321.

D-26. Luther, F. M.: Monthly Mean Values of Eddy Diffusion Coefficients in the Lower Stratosphere. AIAA paper 73-498, June 1973.

D-27. Nastrom, G. D.; and Belmont, A. D.: Diurnal Stratospheric Tide in the Meridional Wind 30 to 60 km, by Season and Monthly Mean Temperatures 20 to 60 km at 80° N to 0°. NASA CR-137738, 1975.

D-28. Cunnold, D.; Alyea, F.; Phillips, N.; and Prinn, R.: A Three-Dimensional Dynamical-Chemical Model of Atmospheric Ozone. J. Atmos. Sci., vol. 32, no. 1, Jan. 1975, pp. 170-194.

D-29. Alyea, Fred N.; Cunnold, Derek M.; and Prinn, Ronald G.: Stratospheric Ozone Destruction by Aircraft-Induced Nitrogen Oxides. Science, vol. 188, no. 4184, Apr. 11, 1975, pp. 117-121.

D-30. Prinn, R. G.; Alyea, F. N.; and Cunnold, D. M.: Stratospheric Distributions of Odd Nitrogen and Odd Hydrogen in a Two-Dimensional Model. J. Geophys. Res., vol. 80, no. 36, Dec. 20, 1975, pp. 4998-5004.

D-31. Pollack, James B.; Toon, Owen B.; et al.: Estimates of the Climatic Effect of Aerosols Produced by Space Shuttles, SST's, and Other High-Flying Aircraft. J. Appl. Meteorol., vol. 15, no. 3, Mar. 1976, pp. 247-258.

D-32. Anderson, J. G.: The Absolute Concentration of $O(^3P)$ in the Earth's Stratosphere. Geophys. Res. Letters, vol. 2, no. 6, June 1975, pp. 231-234.

D-33. Ackerman, M.; Fontanella, J. C.; et al.: Simultaneous Measurements of NO and NO_2 in the Stratosphere. Planet. Space Sci., vol. 23, no. 4 Apr. 1975, pp. 651-660.

D-34. Loewenstein, Max; Savage, H. F.; and Whitten, R. C.: Seasonal Variations of NO and O_3 at Altitudes of 18.3 and 21.3 km. J. Atmos. Sci., vol. 32, no. 11, Nov. 1975, pp. 2185-2190.

D-35. Ridley, B. A.; Schiff, H. I.; Shaw, A.; and Megill, L. R.: In-situ Measurements of NO in the Stratosphere Using Chemiluminescence. Proceedings of the Third Conference on the Climatic Impact Assessment Program, Anthony G. Broderick and Thomas M. Hard, eds., DOT-TSC-OST-74-15, Nov. 1974, pp. 193-196.

D-36. Patel, C. K. N.; Burkhardt, E. G.; and Lambert, C. A.: Spectroscopic Measurements of Stratospheric Nitric Oxide and Water Vapor. Science, vol. 184, no. 4142, June 14, 1974, pp. 1173-1176.

D-37. Meira, Luiz Gylvan, Jr.: Rocket Measurements of Upper Atmospheric Nitric Oxide and Their Consequences to the Lower Ionosphere. J. Geophys. Res., vol. 76, no. 1, Jan. 1, 1971, pp. 202-212.

D-38. Tisone, G. C.: Measurements of NO Densities During Sunrise at Kauai. J. Geophys. Res., vol. 78, no. 4, Feb. 1, 1973, pp. 746-750.

D-39. Ehhalt, D. H.: Sampling of Stratospheric Trace Constituents. Canadian J. Chem., vol. 52, no. 8, 1974, pp. 1510-1518.

D-40. Ehhalt, D. H.; Heidt, L. E.; and Martell, E. A.: The Concentration of Atmospheric Methane Between 44 and 62 Kilometers Altitude. J. Geophys. Res., vol. 77, no. 12, Apr. 20, 1972, pp. 2193-2196.

D-41. Ehhalt, D. H.; and Heidt, L. E.: Vertical Profiles of CH_4 in the Troposphere and Stratosphere. J. Geophys. Res., vol. 178, no. 24, Aug. 20, 1973, pp. 5265-5271.

D-42. Ehhalt, D. H.; Heidt, L. E.; Lueb, R. H.; and Roper, N.: Vertical Profiles of CH_4, H_2, CO, N_2O, and CO_2 in the Stratosphere. Proceedings of the Third Conference on the Climatic Impact Assessment Program, Anthony J. Broderick and Thomas M. Hard, eds., DOT-TSC-OST-74-15, Nov. 1974, pp. 153-160.

D-43. Ackerman, M.; Frimout, D.; et al.: Stratospheric HCl From Infrared Spectra. Geophys. Res. Letters, vol. 3, no. 2, Feb. 1976, pp. 81-83.

D-44. Farmer, C. B.; Raper, O. F.; and Norton, R. H.: Spectroscopic Detection and Vertical Distribution of HCl in the Troposphere and Stratosphere. Geophys. Res. Letters, vol. 3, no. 1, Jan. 1976, pp. 13-16.

D-45. Lazrus, A. L.; Gandrud, B. W.; Woodard, R. N.; and Sedlacek, W. A.: Measurements of Stratospheric Halogens and HNO_3. Proceedings of the Fourth Conference on the Climatic Impact Assessment Program, Aug. 1976, pp. 465-469.

D-46. Lazrus, A. L. Gandrud, B. W.; Woodard, R. N.; and Sedlacek, W. A.: Stratospheric Halogen Measurements. Geophys. Res. Letters, vol. 2, no. 10, Oct. 1975, pp. 439-441.

D-47. Anderson, James G.: Rocket Measurement of OH in the Mesosphere. J. Geophys. Res., vol. 76, no. 31, Nov. 1, 1971, pp. 7820-7824.

D-48. Ackerman, M.; Frimout, D.; et al.: Stratospheric Nitric Oxide From Infrared Spectra. Nature, vol. 245, no. 5422, Sept. 28, 1973, pp. 205-206.

D-49. Newell, R. E.: Radioactive Contamination of the Upper Atmosphere. Progress in Nuclear Energy, A. M. Francis Duhamel, ed., Series XII, Health Physics, vol. 2, Pergamon Press (Oxford), 1969, pp. 535-550.

D-50. Dütsch, H. U.: Photochemistry of Atmospheric Ozone. Adv. Geophys., vol. 15, 1971, pp. 219-232.

D-51. Whitten, R. C.; Borucki, W. J.; Poppoff, I. G.; and Turco, R. P.: Preliminary Assessment of the Potential Impact of Solid-Fueled Rocket Engines in the Stratosphere. J. Atmos. Sci., vol. 32, no. 3, Mar. 1975, pp. 613-619.

D-52. Pollack, James B.; Toon, Owen B.; et al.: Volcanic Aerosols and Climatic Change: A Theoretical Assessment. J. Geophys. Res., vol. 81, no. 6, Feb. 20, 1976, pp. 1071-1083.

D-53. Hofmann, D. J.; Carroll, D. E.; and Rosen, J. M.: Estimate of the Contribution of the Space Shuttle Effluent to the Natural Stratospheric Aerosol. Geophys. Res. Letters, vol. 2, no. 3, Mar. 1975, pp. 113-116.

TABLE D-1.- REACTION RATE COEFFICIENTS[6]

Number	Reaction	Rate coefficient[a]	Uncertainty	References
R1	$OH + HCl \rightarrow Cl + H_2O$	$2.8\times10^{-12}\ \exp^{-400/T}$	±20 percent	D-10, D-11
R2	$Cl + O_3 \rightarrow ClO + O_3$	$3.4\times10^{-11}\ \exp^{-301/T}$	±15 percent	(b)
R3	$ClO + O \rightarrow Cl + O_2$	5.3×10^{-11}	±20 percent	D-12
R4	$Cl + CH_4 \rightarrow HCl + CH_3$	$5.4\times10^{-12}\ \exp^{-1125/T}$	±20 percent	(c)
R5	$Cl + HO_2 \rightarrow HCl + O_2$	1×10^{-11}	± factor of 10	(d,e)
R6	$ClO + NO \rightarrow Cl + NO_2$	$6.3\times10^{-12}\ \exp^{354/T}$	±50 percent	(f)
R8	$OH + CH_4 \rightarrow H_2O + CH_3$	$2.4\times10^{-12}\ \exp^{-1720/T}$	—	D-14
R9	$O(^1D) + H_2O \rightarrow 2OH$	3.5×10^{-10}	±30 percent	D-15
R10	$OH + HO_2 \rightarrow H_2O + O_2$	6×10^{-11}	± factor of 3	(e)
R11	$O + HO_2 \rightarrow OH + O_2$	1×10^{-11}	± factor of 3	(g)
R12	$O_3 + OH \rightarrow HO_2 + O_2$	$1.3\times10^{-12}\ \exp^{-950/T}$	±50 percent	D-16
R13	$O + OH \rightarrow H + O_2$	3.8×10^{-11}	±50 percent	D-17
R16	$H + O_2 + M \rightarrow HO_2 + M$	$1.9\times10^{-32}\ \exp^{236/T}$	--	D-18
R17	$HO_2 + HO_2 \rightarrow H_2O_2 + O_2$	$1.7\times10^{-11}\ \exp^{-500/T}$	--	D-15
J14	$HO_2 + h\nu \rightarrow OH + O$	1.0×10^{-3}	(e)	D-19, D-20
J15	$HO_2 + h\nu \rightarrow H + O_2$			
J18	$H_2O_2 + h\nu \rightarrow 2\ OH$	1.4×10^{-4}	—	D-21

[a]In units per second for unimolecular processes, cubic centimeters per second for bimolecular reactions, and hexadic centimeters per second for termolecular reactions. The symbol T represents ambient temperature.

[b]This value is based on a least squares best fit to recent measurements by Davis and Watson; Zahniser, Kaufman, and Anderson; and Nip and Cline (1975).

[c]Data from R. T. Watson, to be published.

[d]Leu and De More (ref. D-13) have very recently reported the rate constant for number R5 to be $3\ (^{+4.5}_{-1.8}) \times 10^{-11}\ cm^3\ sec^{-1}$. Use of the mean value rather than that listed will lead to a decrease in predicted values of O_3 reduction of approximately 20 percent.

[e]Estimate (W. B. De More, private communication).

[f]Data from M. S. Zahniser and F. Kaufman, to be published.

[g]F. Kaufman: Neutral Reactions. DASA Reaction Rate Handbook, M. H. Bortner, ed.

---

[6]R. C. Whitten, I. G. Poppoff, and R. P. Turco: Comments on an Assessment of the Potential Impact on the Stratosphere of Solid-Fueled Rocket Engines. To be published.

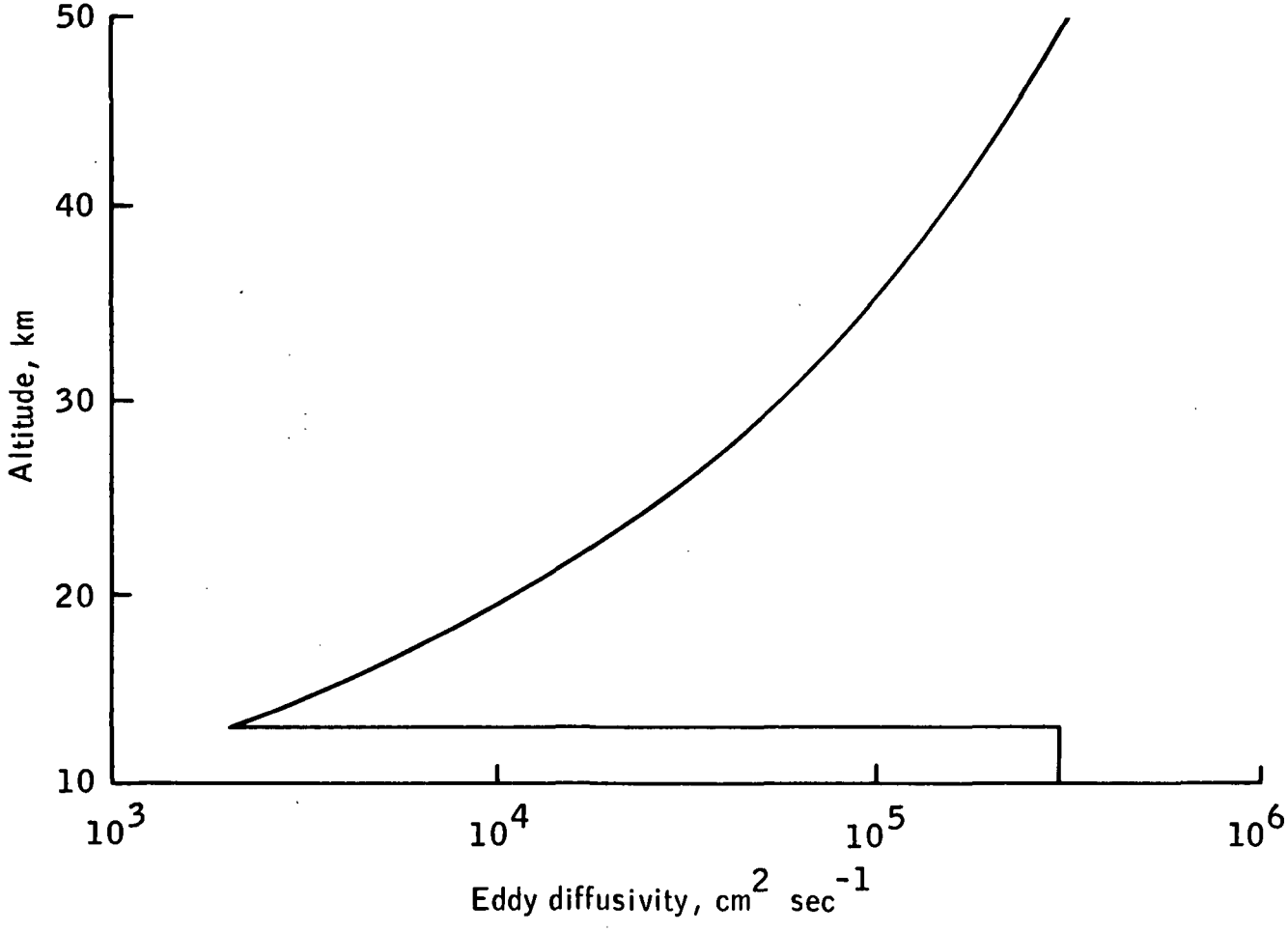

Figure D-1.- Eddy diffusivity profile (ref. D-22) (adapted from ref. D-23).

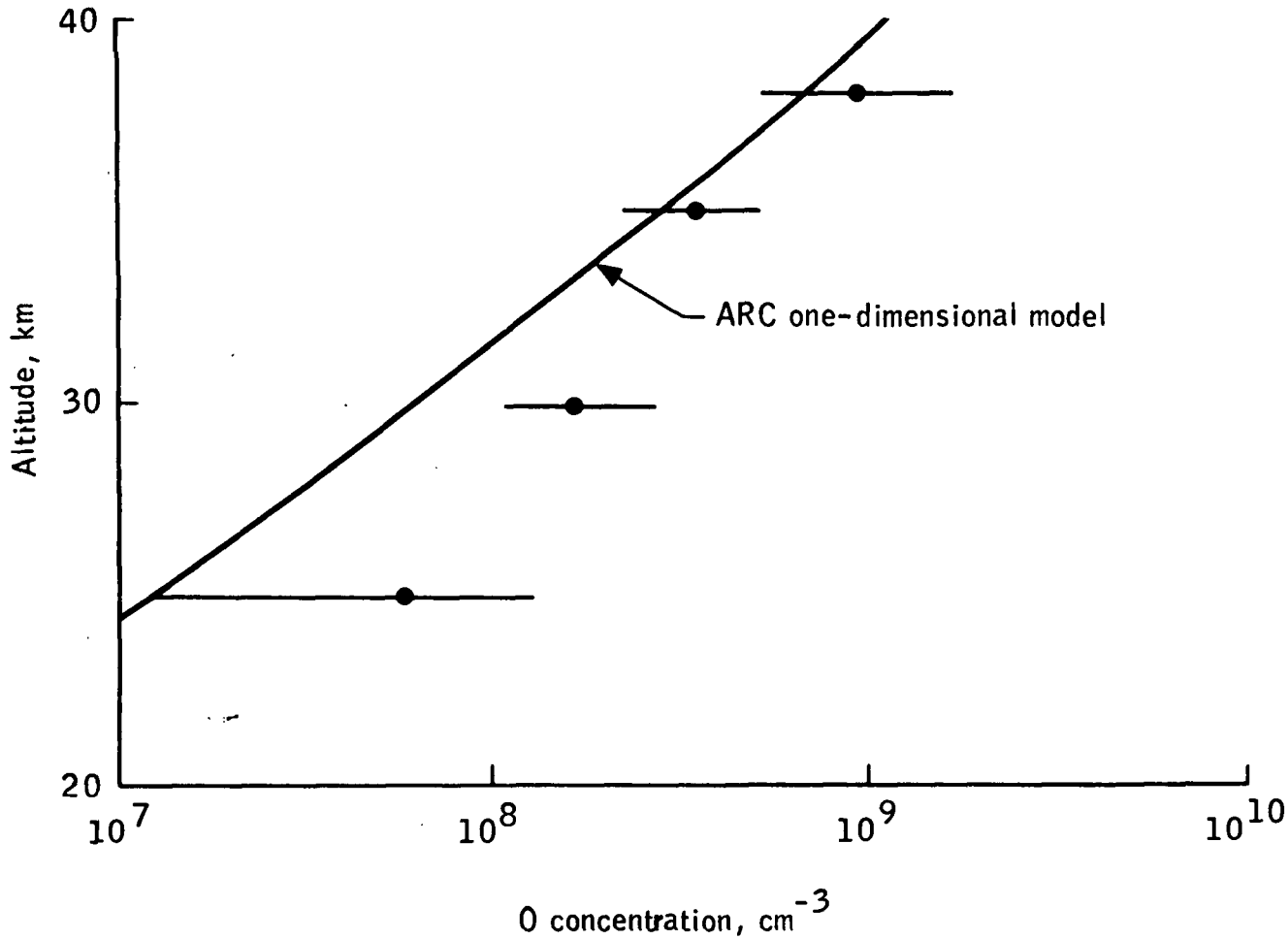

Figure D-2.- Atomic oxygen concentrations (experimental points from ref. D-32).

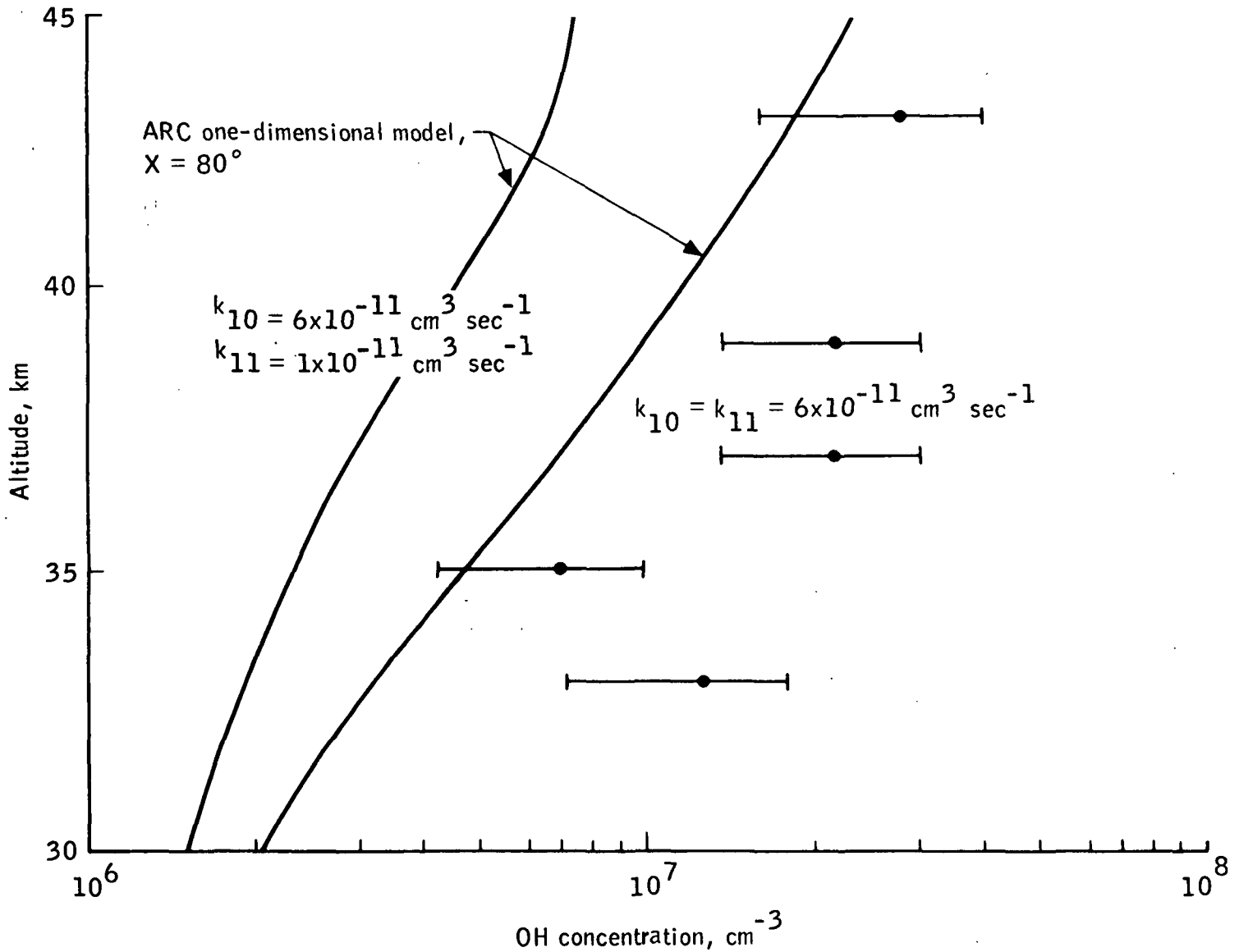

Figure D-3.- Hydroxyl concentrations for a solar zenith angle of 80° (experimental points from ref. D-9).

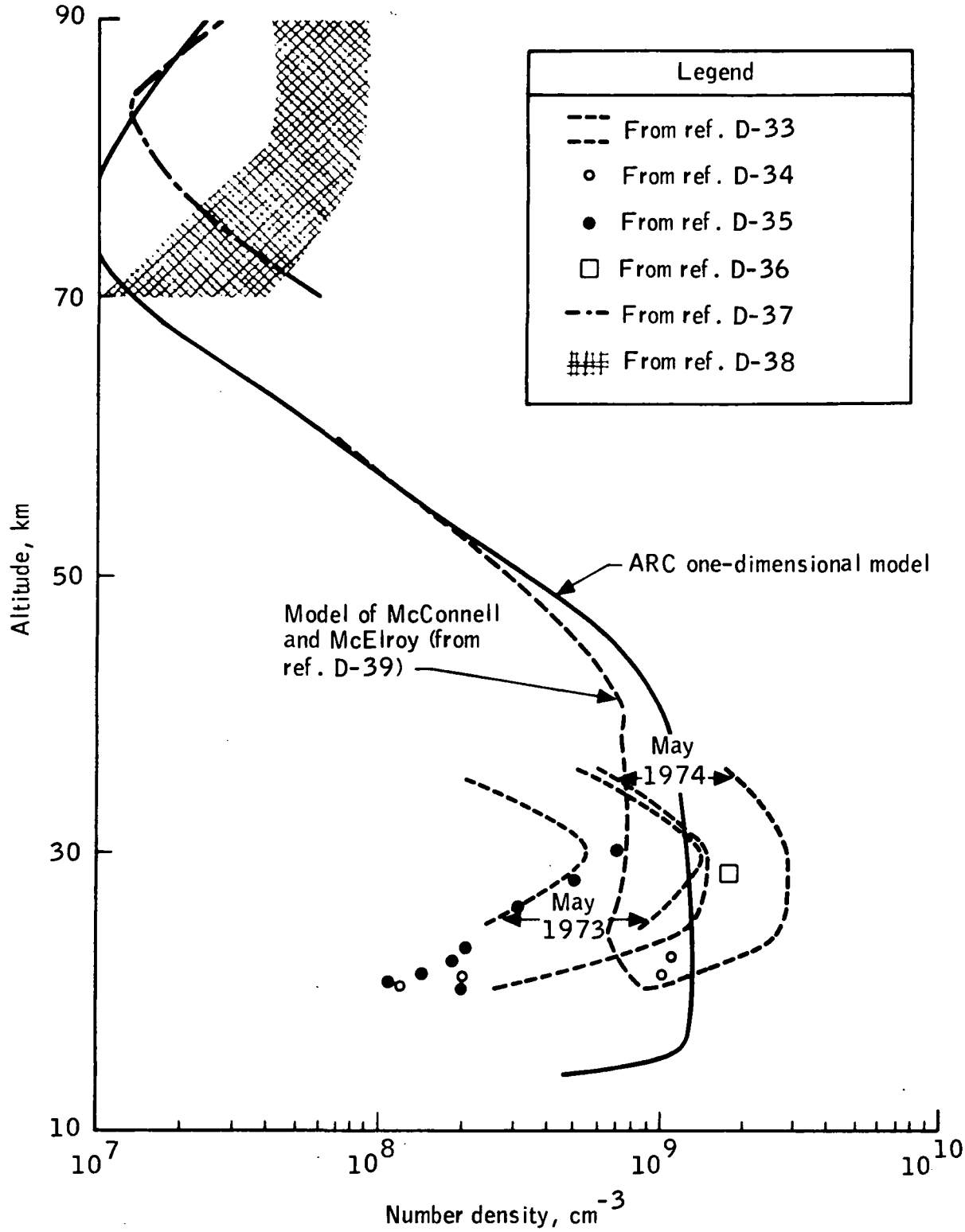

Figure D-4.- Nitric oxide concentrations.

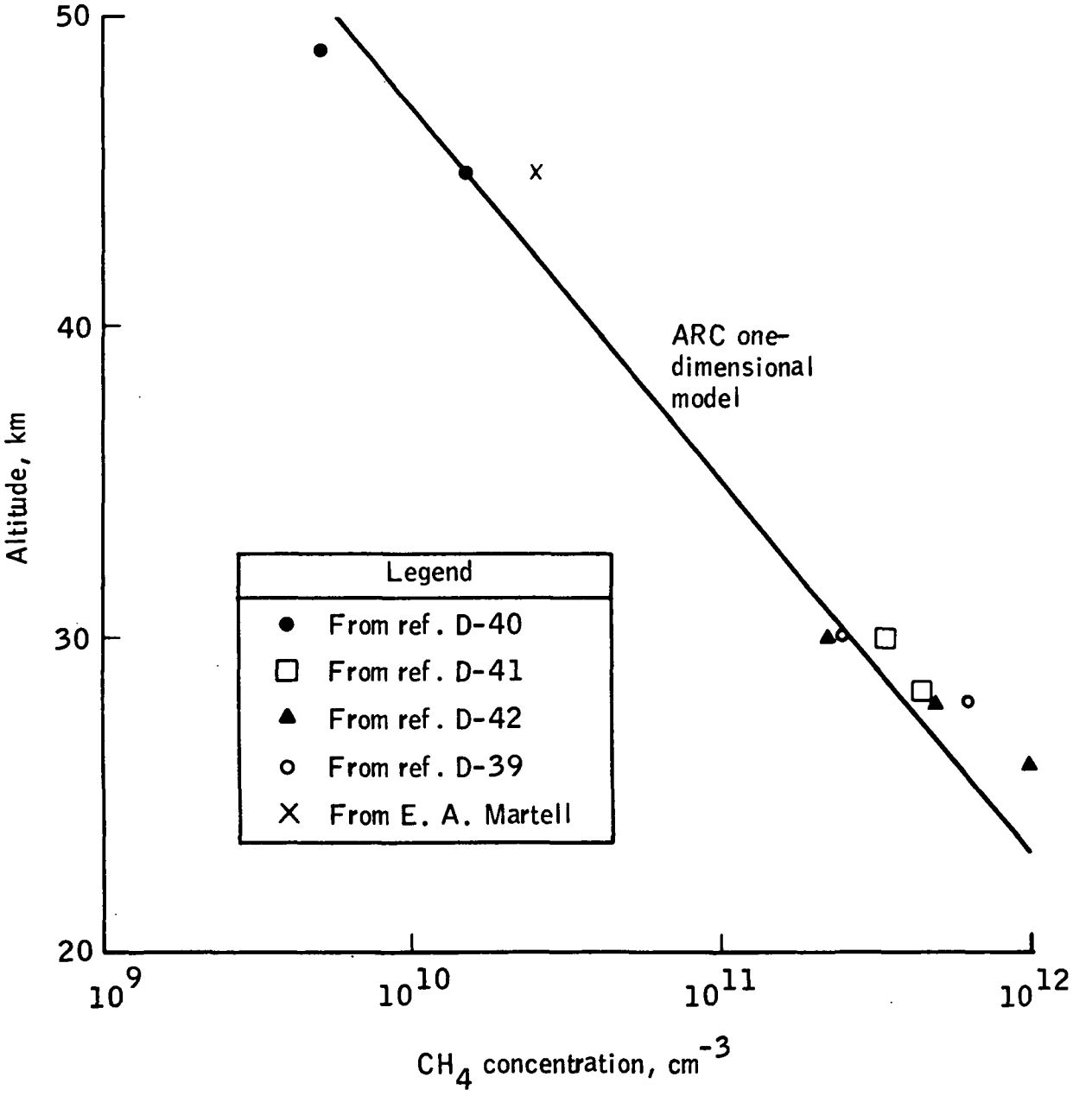

Figure D-5.- Methane concentrations.

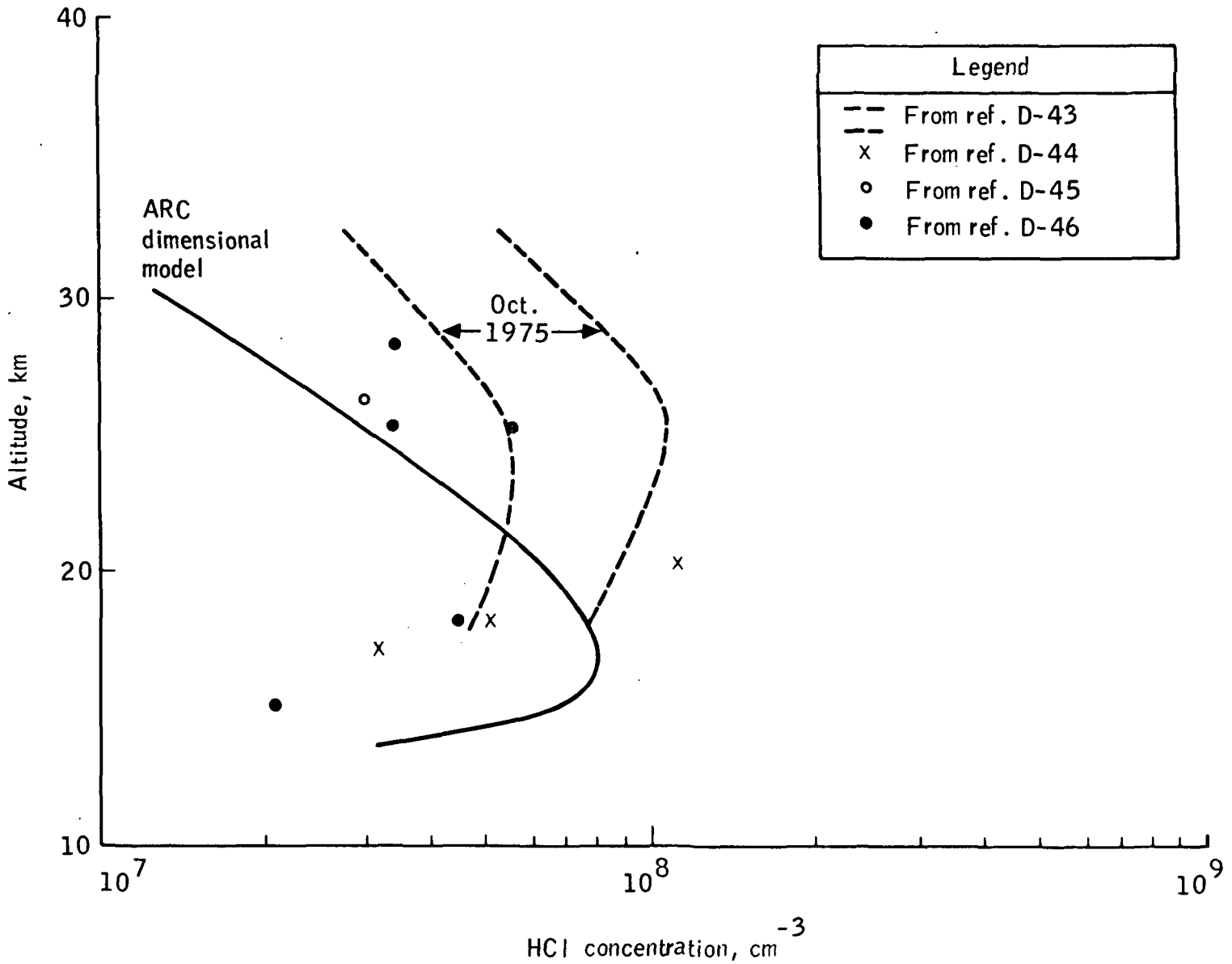

Figure D-6.- Hydrogen chloride concentrations.

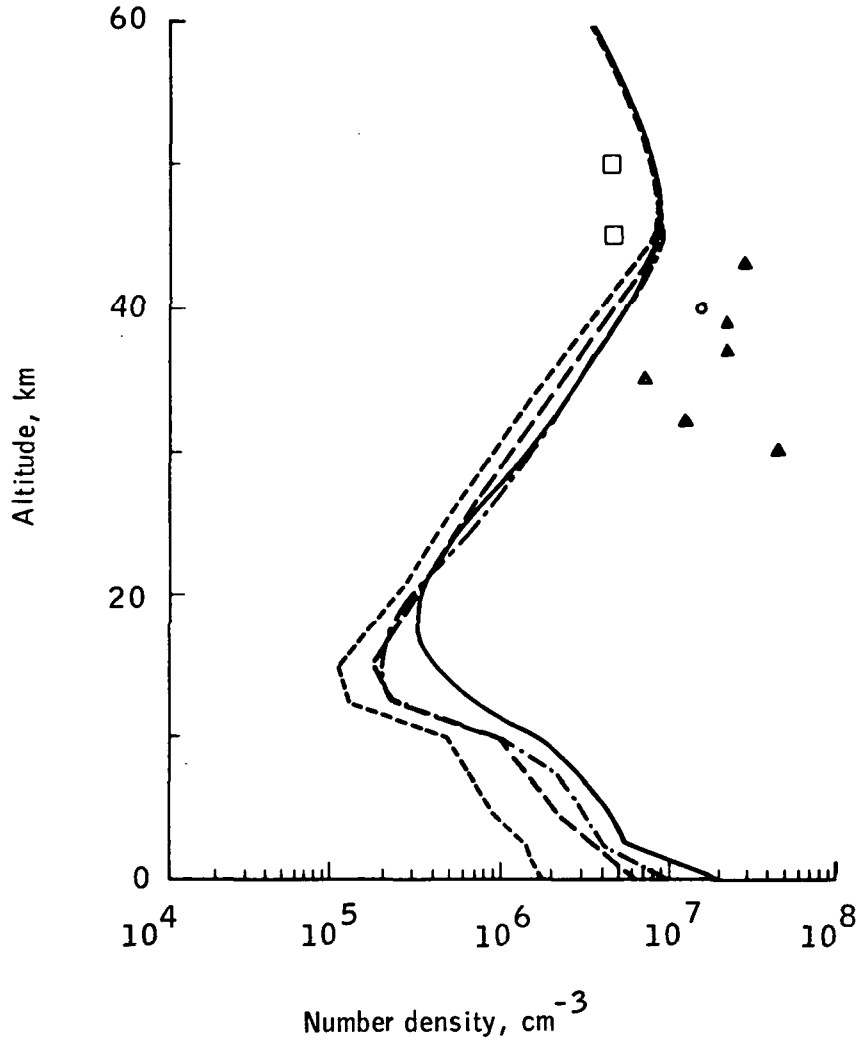

Legend
— 0° lat.
-·- -20° lat.
-·· -40° lat.
--- -60° lat.
□ DH, Anderson, JGR 76,7820, Apr. 1971, TWI, lat. 33° N (from ref. D-47)
○ OH, Anderson, July 1975, PSI = 80 (from ref. D-9)
▲ OH, Anderson, Jan. 1976, PSI = 80 (from ref. D-9)

Figure D-7.- Hydroxyl concentration profiles obtained using the ARC two-dimensional model (day 7823).

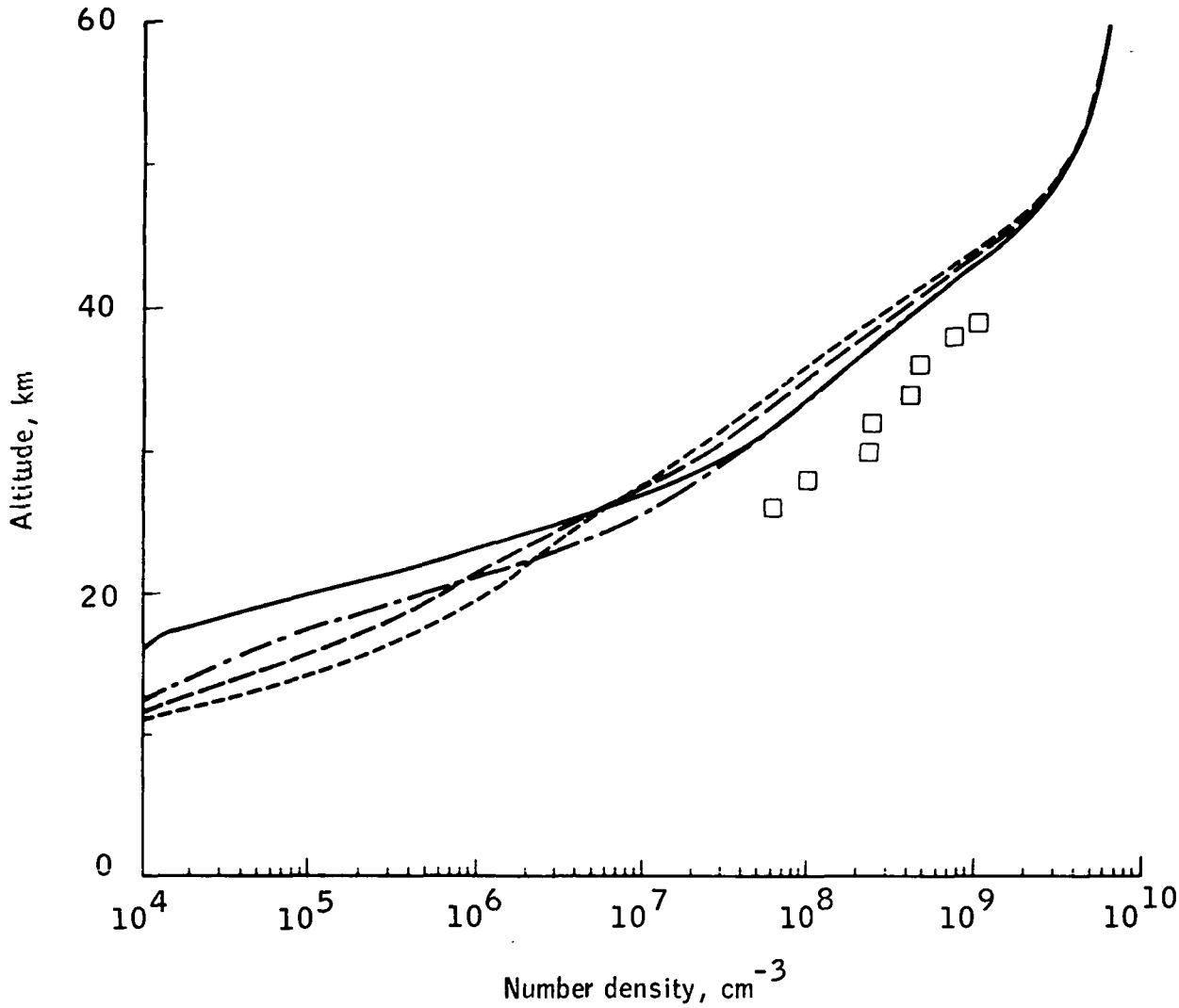

Legend
—— 0° lat.
-·- -20° lat.
— — -40° lat.
- - - -60° lat.
□ 0 (3P), Anderson, Nov. 1975, lat. 32° N, PSI = 56 (from ref. D-32)

Figure D-8.- Atomic oxygen concentration profiles obtained using the ARC two-dimensional model (day 7823).

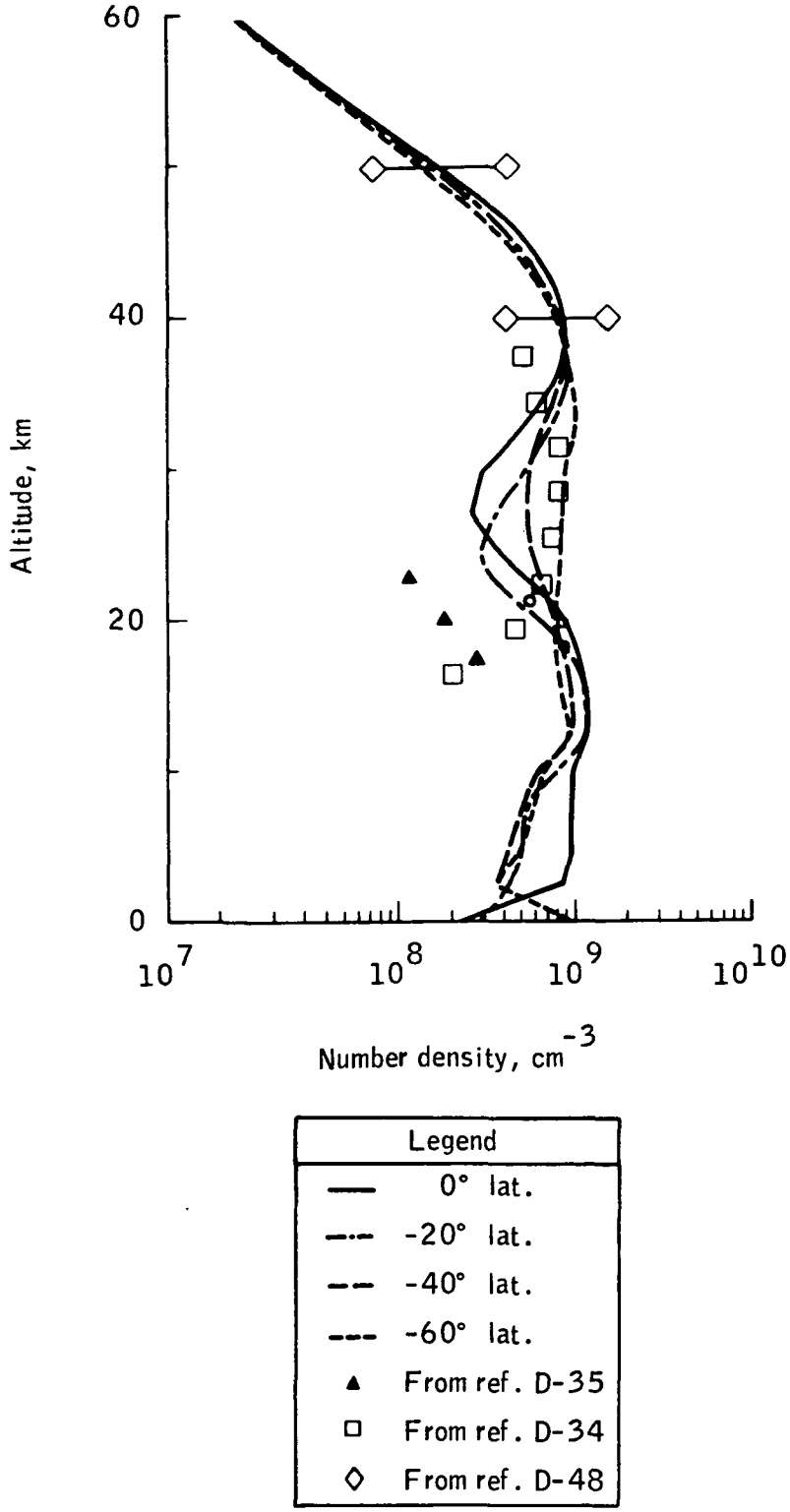

Figure D-9.- Nitric oxide concentration profiles obtained using the ARC two-dimensional model.

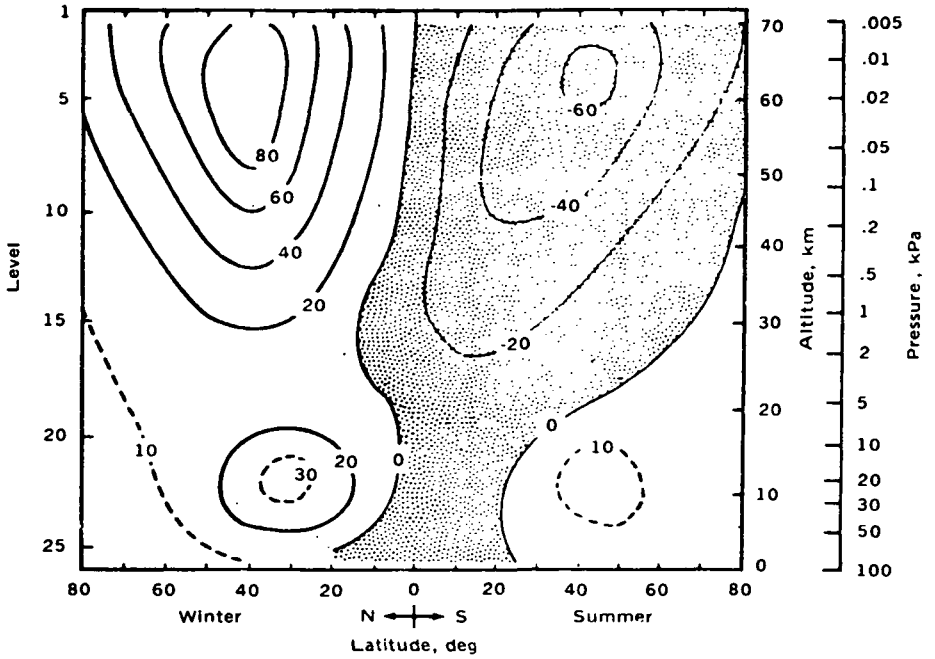

(a) Observed (ref. D-49).

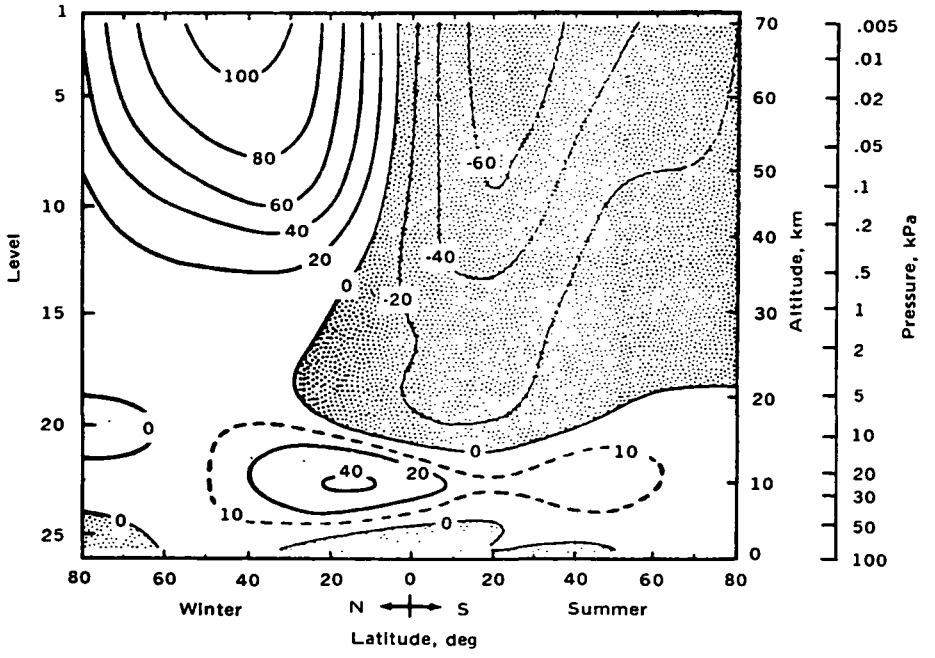

(b) Modeled (MIT three-dimensional model for season 10).

Figure D-10.- Vertical cross section of mean zonal windspeeds. Contour interval is 20 m/sec.

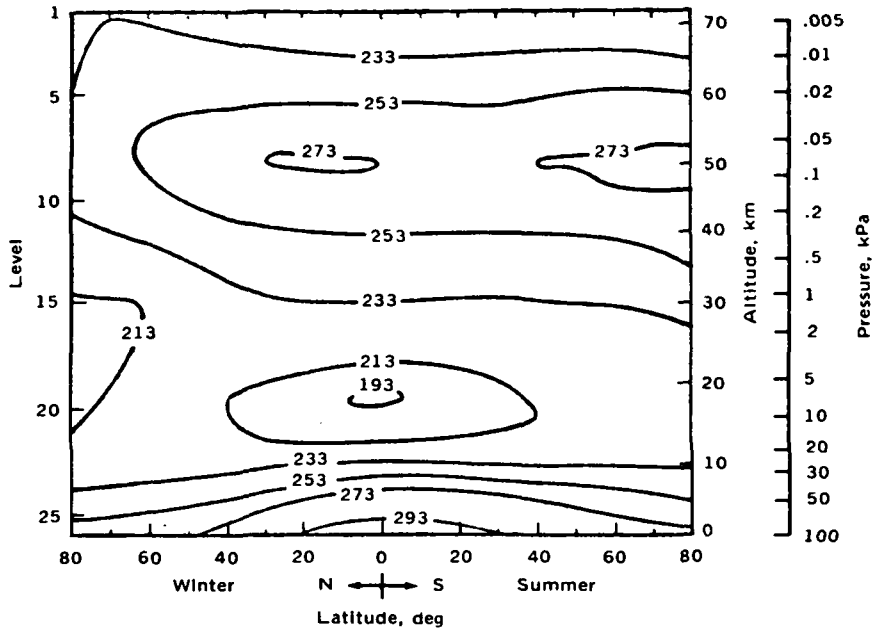

(a) Observed (ref. D-49).

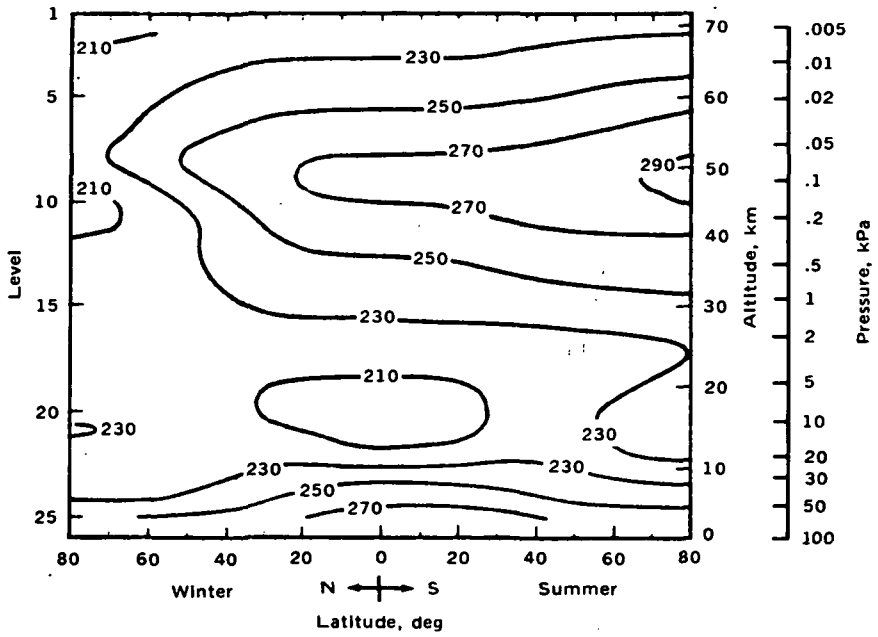

(b) Modeled (MIT three-dimensional model for season 10).

Figure D-11.- Vertical cross section of mean zonal temperature distributions. Contour interval is 20 K.

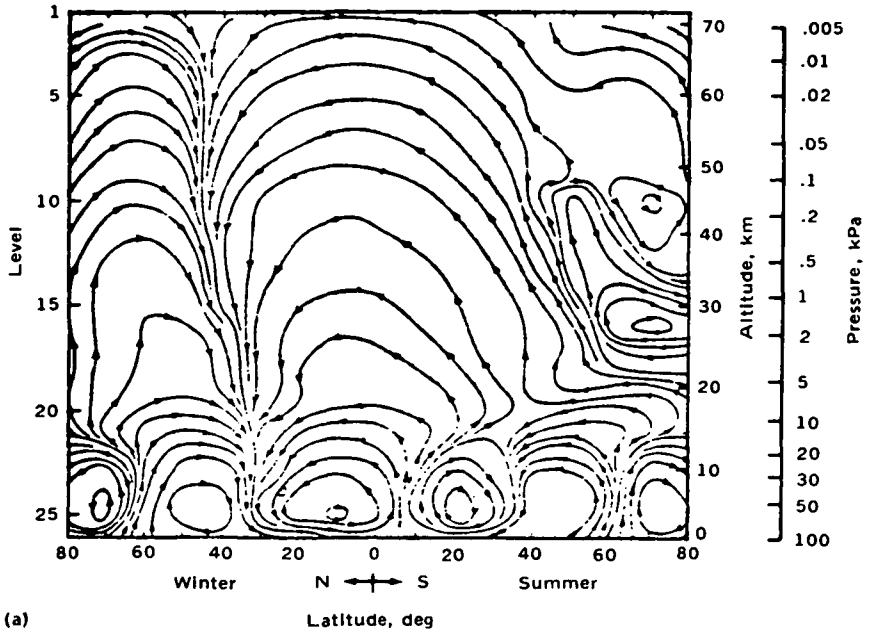

(a) Season 10 (solstice).

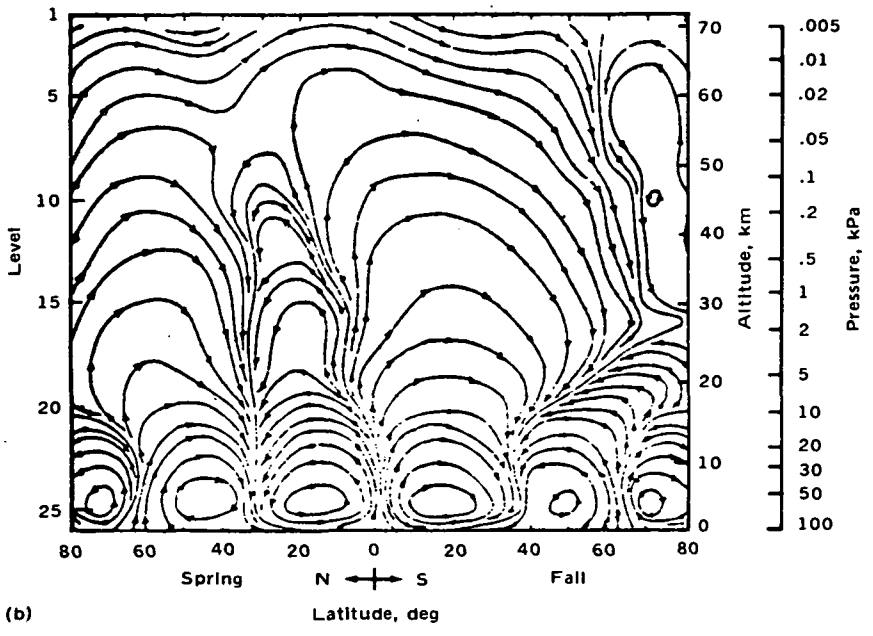

(b) Season 11 (equinox).

Figure D-12.- MIT three-dimensional model mean meridional circulation patterns.

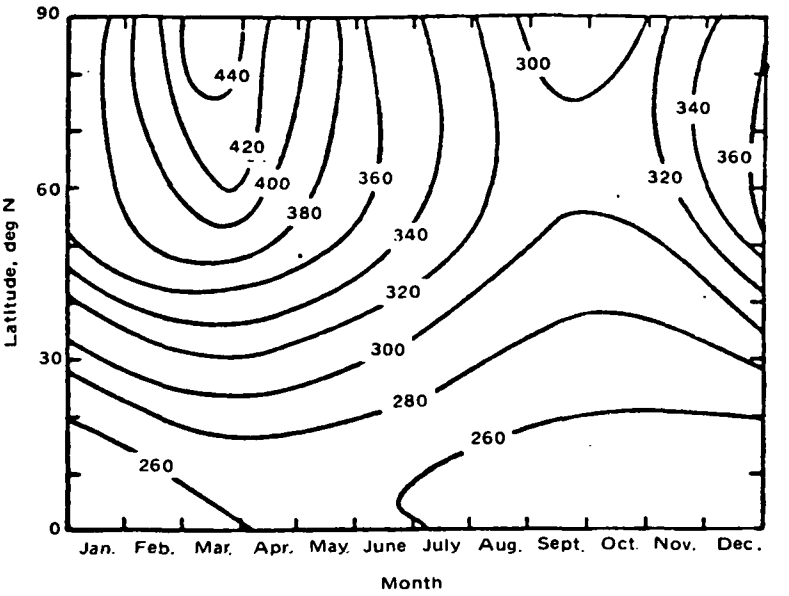

(a) Determined by Dütsch (ref. D-50) from observations.

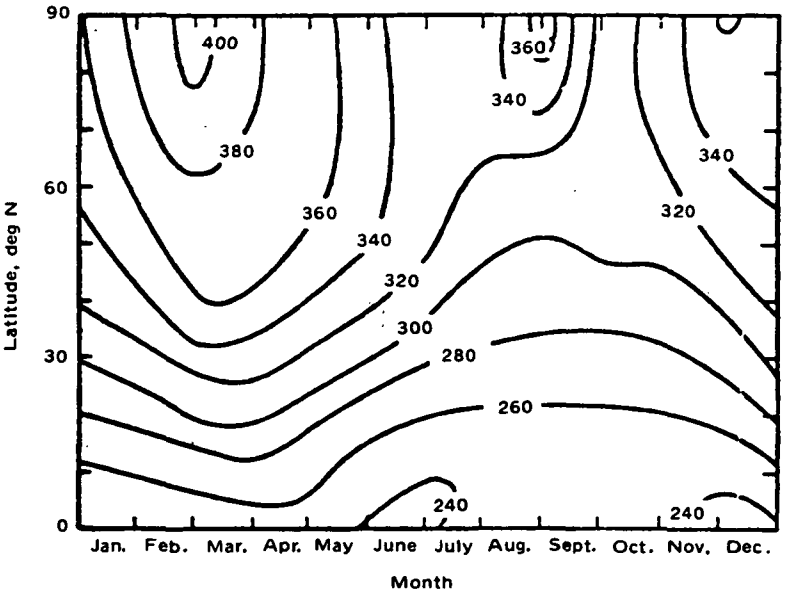

(b) Predicted during year 3 in the unperturbed model run.

Figure D-13.- MIT three-dimensional model columnar O_3 density in the Northern Hemisphere as a function of season and latitude. Contour interval is 20 cm^{-3}.

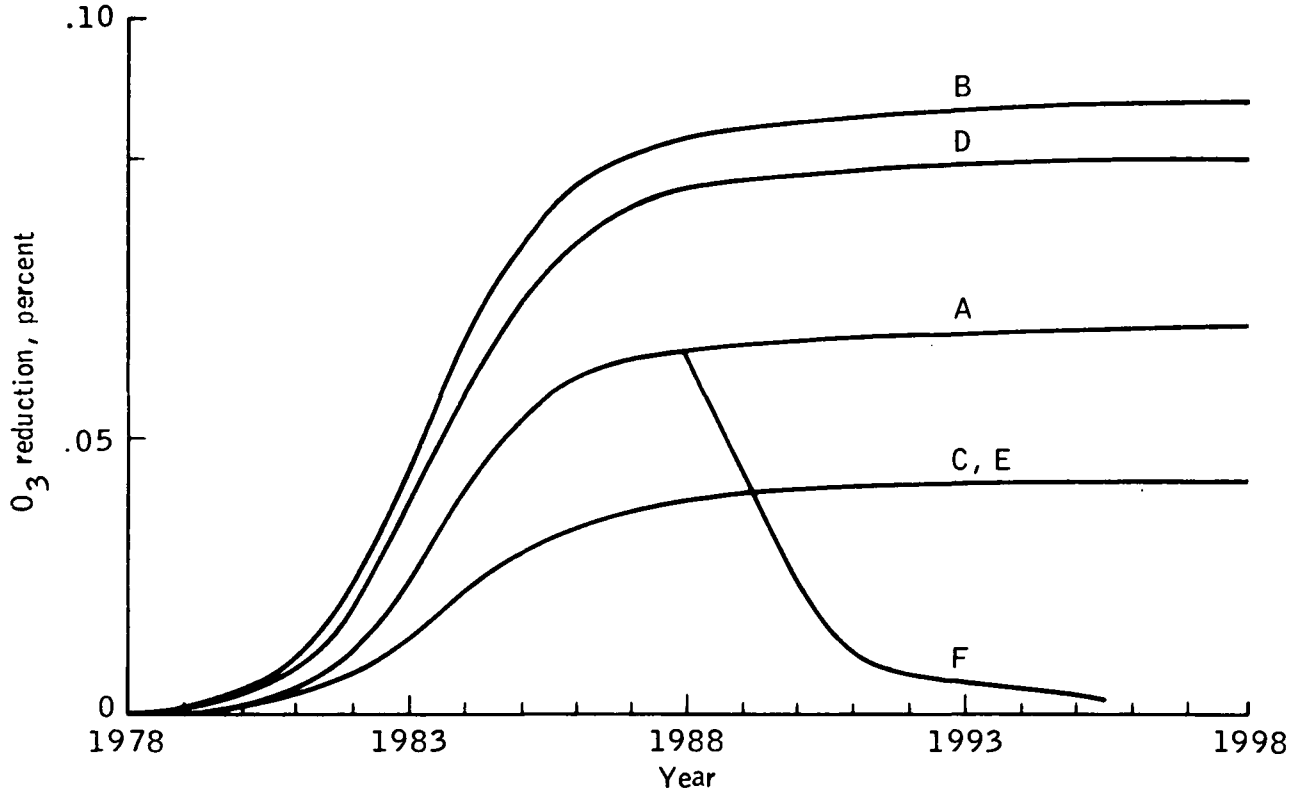

Figure D-14.- Computed (ARC one-dimensional model) O_3 reductions for the HCL deposition rate shown in figure 4-3. Solar photolysis rates recomputed whenever the vertical ozone column above 30 or 10 kilometers changed by more than 0.01 percent. Curve A represents the reduction if Space Shuttle launches are continued indefinitely, and the rate coefficients listed in table D-I are used. For curve B, the rate coefficient of reaction (D-7) was changed from $6.3 \times 10^{-12} \exp^{354/T}$ to 1.7×10^{-11} cm^3 sec^{-1}. For curve C, the rate coefficient of reaction (D-11) was changed from 6×10^{-11} cm^3 sec^{-1} to 2×10^{-10} cm^3 sec^{-1}. For curve D, the curve A parameters were used, but $k_{11} = k_{10} = 6 \times 10^{-11}$ cm^3 sec^{-1} was set. For curve E, the rate coefficient for reaction (D-6) was increased to 10^{-10} cm^3 sec^{-1}. For curve F, the curve A parameters were used, but launch operations were considered to be terminated after 10 years.

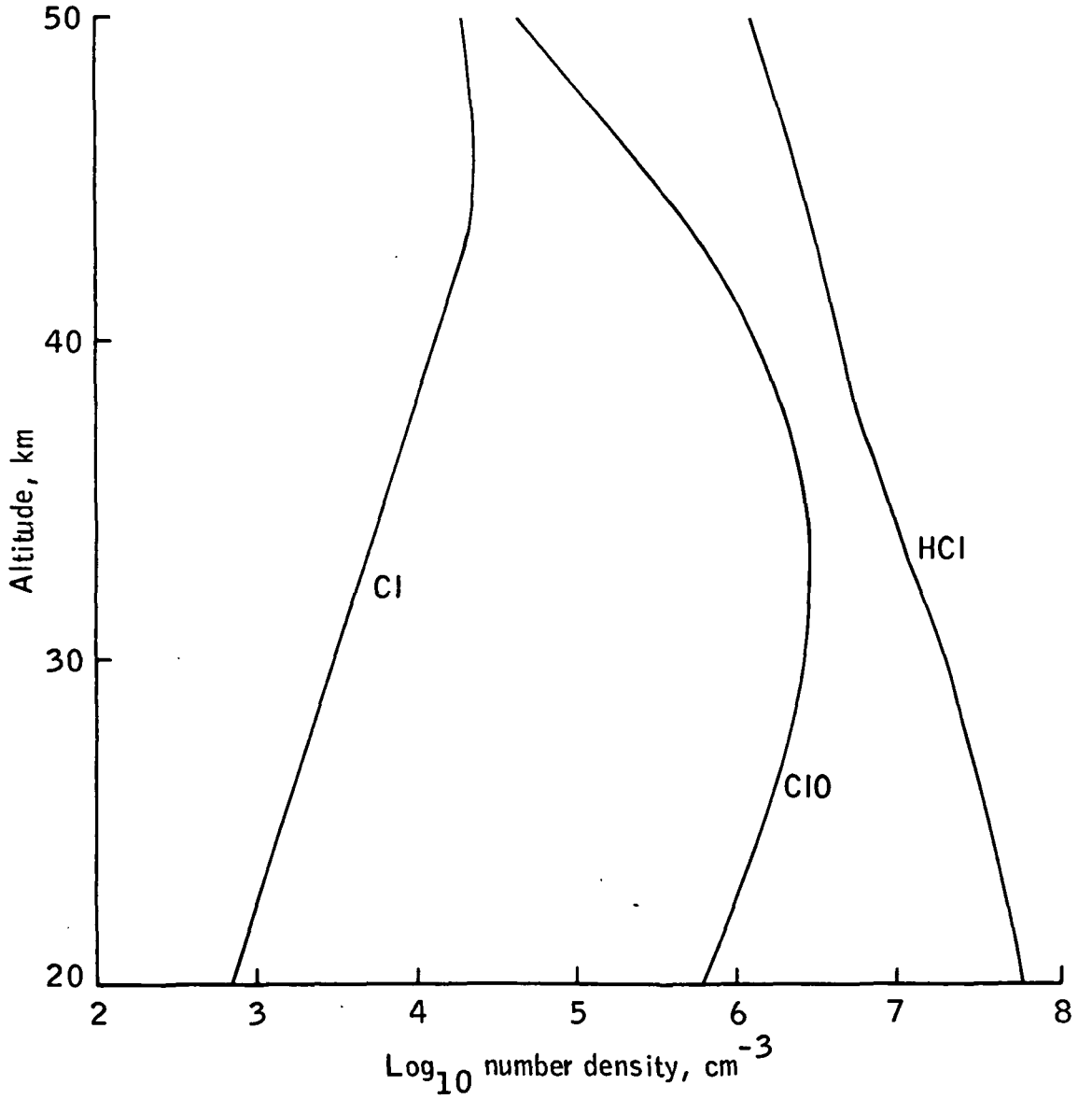

Figure D-15.- Incremental steady-state vertical distributions of Cl, ClO, and HCl resulting from Space Shuttle operations.

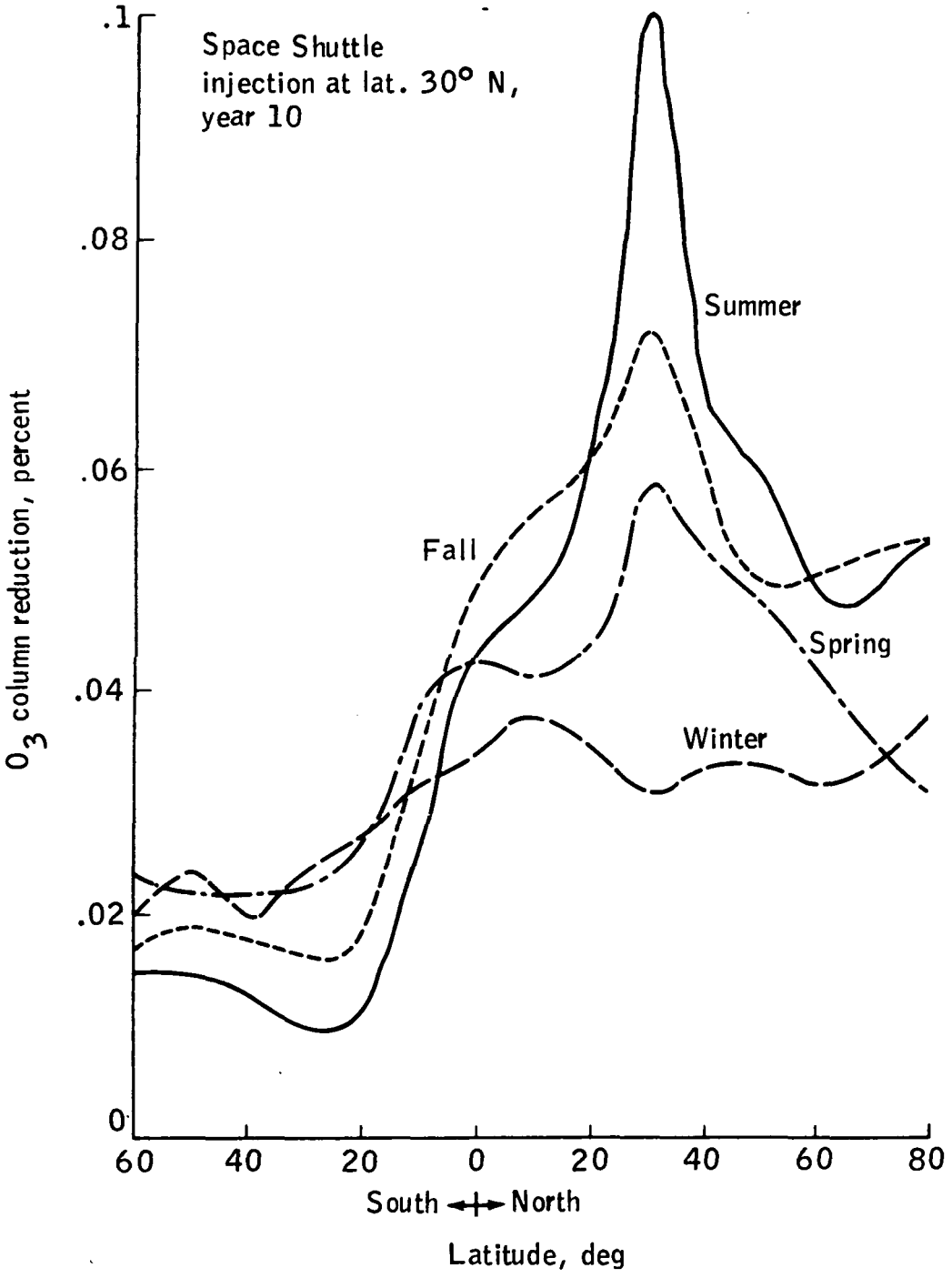

Figure D-16.- Computed O_3 column reduction as a function of latitude after 10 years of Space Shuttle operations, using the ARC two-dimensional model.

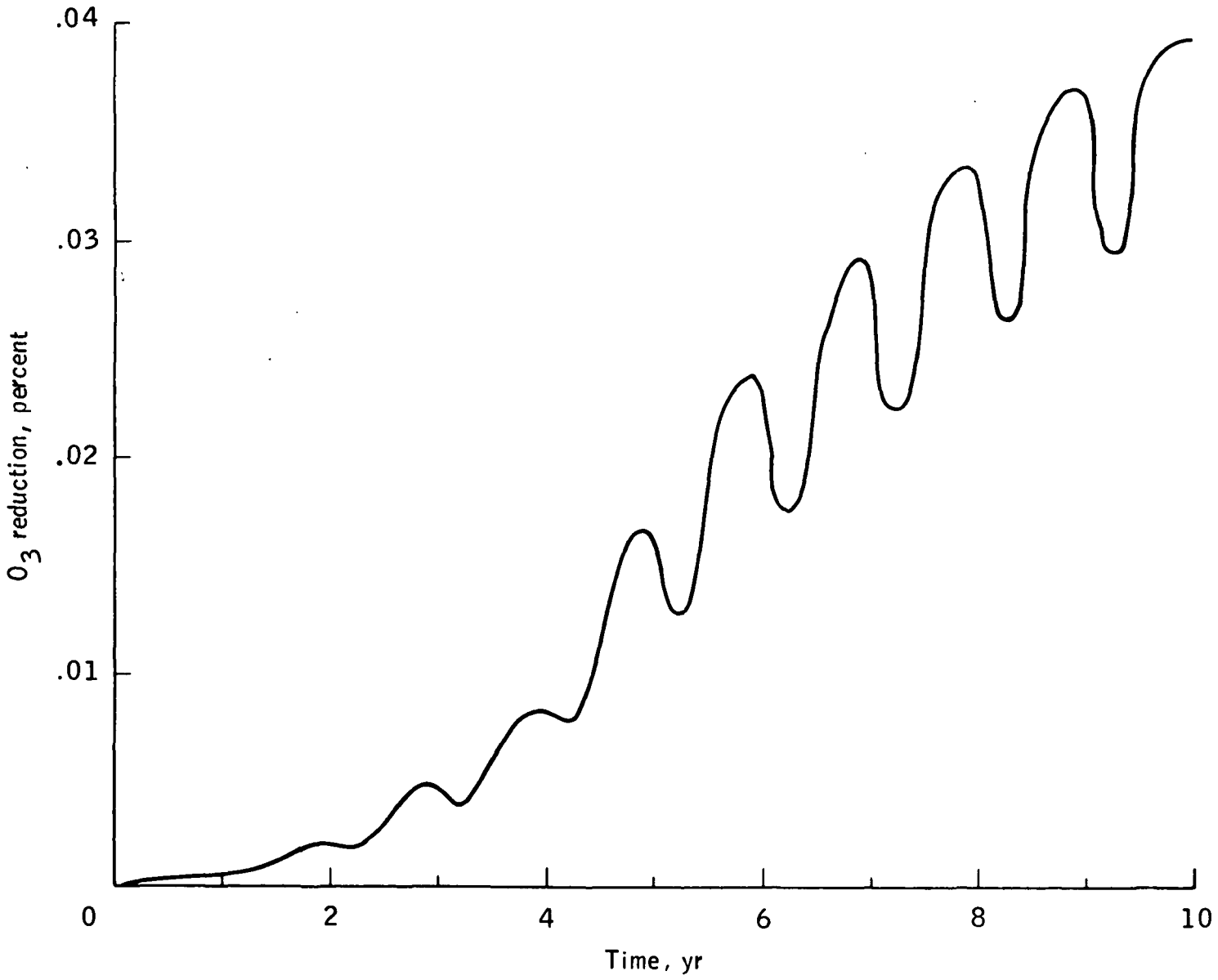

Figure D-17.- Time dependence of the globally averaged O_3 reduction using the ARC two-dimensional model.

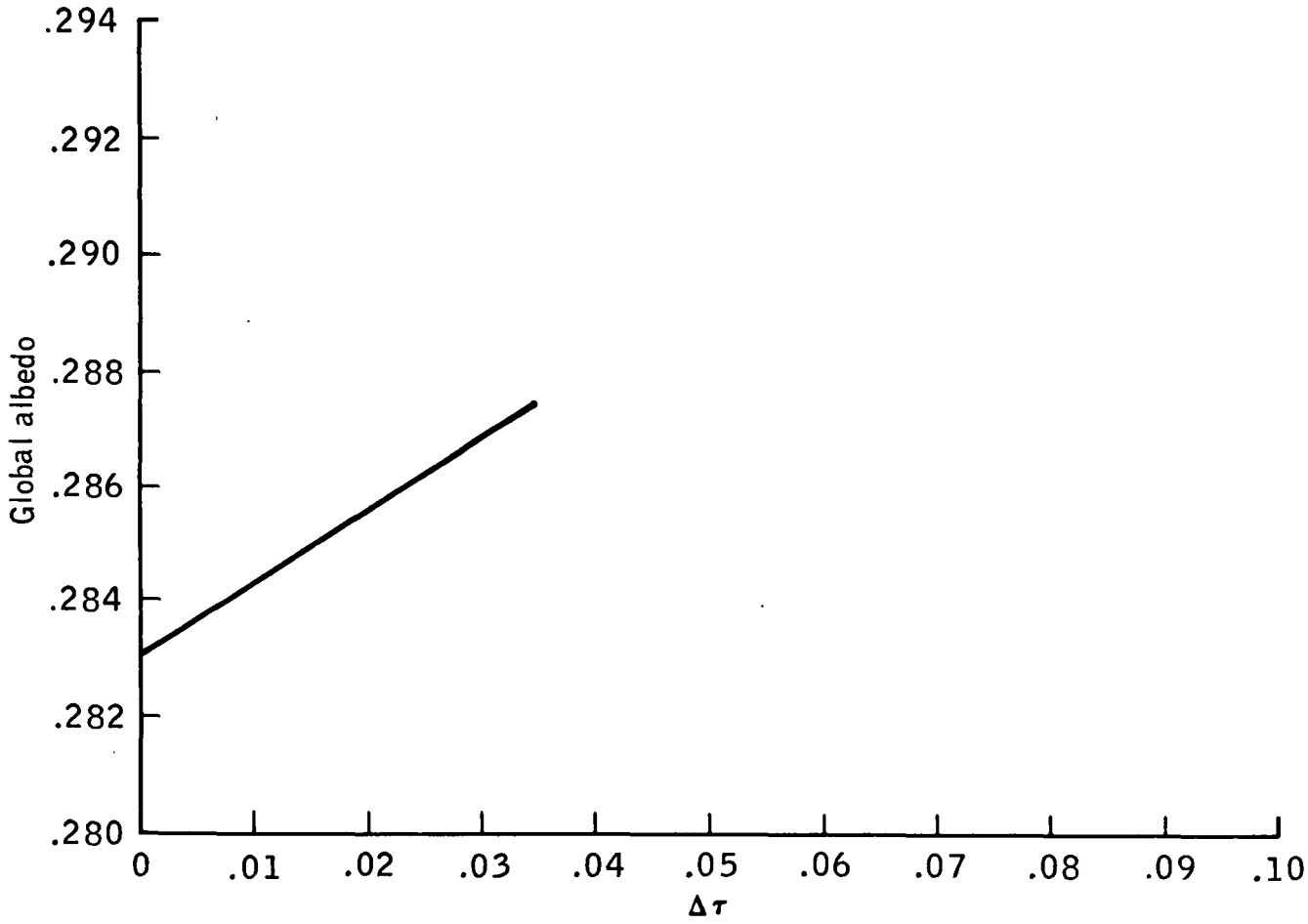

Figure D-18.- Dependence of the global albedo on the optical depth perturbation $\Delta\tau$ at 0.55 micrometer of Space Shuttle Al_2O_3 aerosols.

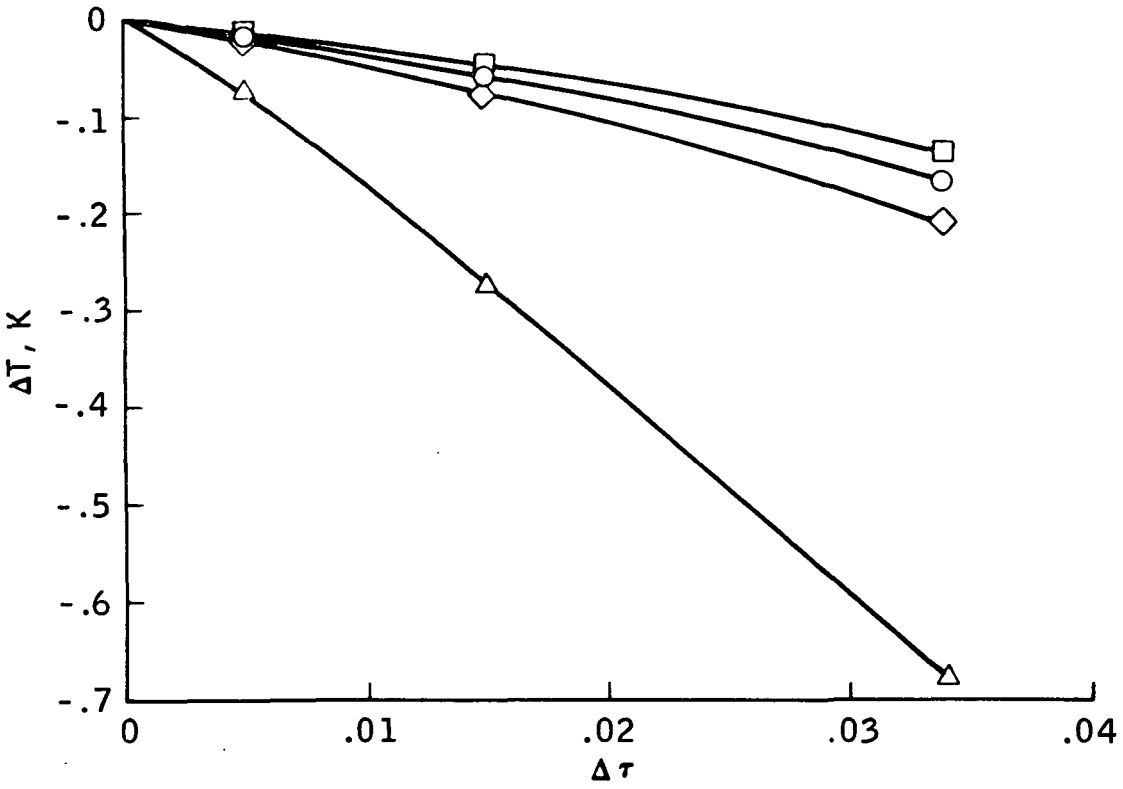

Legend
○ Curve A = constant relative humidity
□ Curve B = constant absolute humidity
◇ Curve C = constant relative humidity and stratosphere temperature
△ Curve D = constant relative humidity and infrared aerosol opacity

Figure D-19.- Change in the mean surface temperature ΔT as a function of the optical depth perturbation $\Delta\tau$ of Al_2O_3 aerosols.

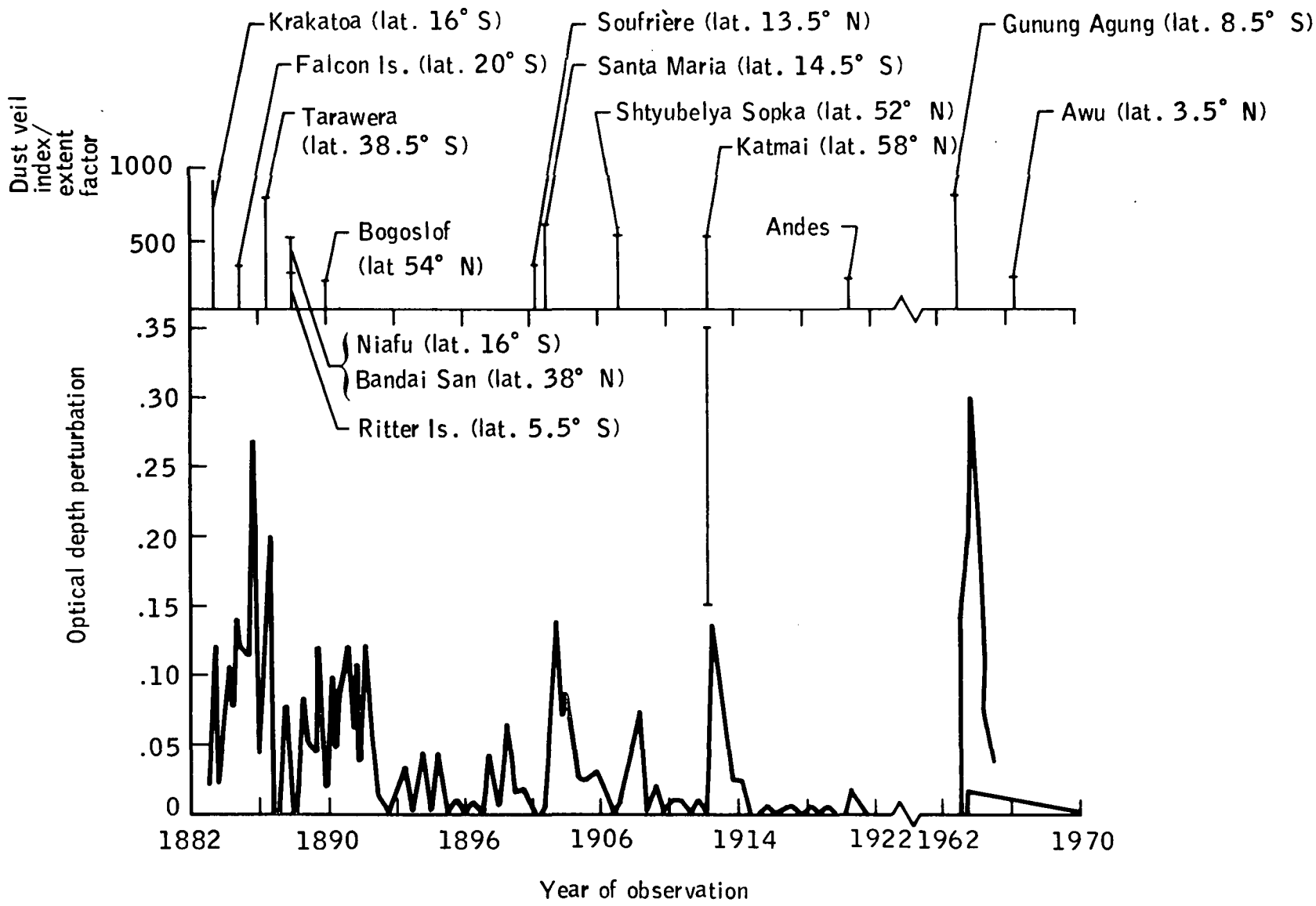

Figure D-20.- Perturbations of optical depth caused by volcanic explosions during the last century.

APPENDIX E

PARTICULATE MEASUREMENTS

By G. Varsi[a]

INTRODUCTION

After the publication of the July 1972 environmental statement for the Space Shuttle Program, questions arose on some of the characteristics of the particles emitted by the solid rocket boosters.[9] An experimental program was started to resolve some uncertainties and to provide better characterization of the particles. Because existing data were obtained mostly from firings of motors considerably smaller than the Space Shuttle booster when large particles were of principal concern, because two-phase aerodynamic losses occurred, and because scaling laws are not established, it was decided that new measurements were necessary on the largest solid rocket motor possible and that an effort should be made to detect the small particles. Current launches of Titan III C/D vehicles appeared the best of available choices. A comparison of Space Shuttle and Titan boosters is given in table E-I.

SCOPE OF WORK

In the Space Shuttle Program, interest was focused on particles emitted by the boosters; no consideration was given to particles formed by atmospheric reactions of gaseous or liquid compounds of such elements as nitrogen (N), hydrogen (H), and chlorine (Cl) (e.g., $NH_3 + HCl \rightarrow NH_4Cl$). Futhermore, because of program constraints (funds and time), no instrument development was thought possible.

PROGRAM PARTICIPANTS

The following organizations and individuals participated directly in the flight measurements: NASA Ames Research Center (ARC) — N. H. Farlow, G. V. Ferry, and W. A. Page; NASA Jet Propulsion Laboratory (JPL) — R. E. Gauldin, E. G. Laue, L. Strand, and G. Varsi; and Los Alamos Scientific Laboratory (LASL) — W. A. Sedlacek. The following organizations and individuals

---

[a]NASA Jet Propulsion Laboratory.

[9]Letter from Sheldon Meyer, Director of the Office of Federal Activities, Environmental Protection Agency, to Ralph E. Cushman, Special Assistant, Office of the Administrator, NASA, June 26, 1972.

participated in the analysis of the data: the University of Southern California — E. Hall; EMS Laboratories; and the University of California (Lawrence Berkeley Laboratory) — W. Siekhaus.

AIRCRAFT AND INSTRUMENTS

The following additional instrumentation was supplied: (1) the tape impactor supplied to JPL by EG&G, Santa Barbara (L. Franks and D. Seaver), (2) the photographic equipment supplied to ARC by Lockheed Palo Alto Laboratories, and (3) the photographic equipment supplied to JPL by Edwards Air Force Base (Hiroshi Hoshizaki). The experimental platforms used and some of the principal characteristics of the instrumentation are shown in table E-II.

HISTORY AND STATUS OF MEASUREMENTS

The following Titan launches have been monitored at the Western Test Range (WTR) in California and at the Eastern Test Range (ETR) in Florida:

Date	Location	Measurement group
Apr. 1974	WTR	ARC, JPL, LASL
Oct. 1974	WTR	ARC, JPL
May 1975	ETR	JPL
June 1975	WTR	JPL

The participants believe that useful preliminary data have been obtained which significantly correct previous existing knowledge. The abrupt interruption of the activities in August 1975 prevented the performing of final measurements. All flight experiments have been suspended. Reporting of past activities is in progress.

RESULTS

Most of the available data pertain to the size of the particles; limited information exists on the composition.

Particle Size

Data obtained in April 1974 from the coated-wire impactor and from the tape impactor by ARC and JPL, respectively, are shown in figure E-1. The agreement is quite satisfactory, especially when one considers the difference in technique and the fact that the ARC data represent the sum of nearly six transits

through the plume in the hour following launch of a Titan III-D from WTR, whereas the JPL data were obtained during a single transit approximately 10 minutes after launch.

From the observation of the filters exposed during the same Titan launch, it is quite apparent that the majority of the particles are smaller than a micrometer. The mean diameters computed from both distributions are similar and have the following values.

$$\bar{D}_1 \approx 0.1 \text{ micrometer (number average)} \qquad \text{(E-1)}$$

$$\bar{D}_3 \approx 0.2 \text{ micrometer (volume average)} \qquad \text{(E-2)}$$

Furthermore, the distribution can be well approximated by a power law in the range of 0.07 to approximately 10 micrometers. Using an intermediate value from the two distributions, one obtains

$$dN = N_o D^{-4.5}\, dD; \quad 0.07 \text{ micrometer} \leq D \leq 10 \text{ micrometers} \qquad \text{(E-3)}$$

where N is the number of particles. More recent data obtained by JPL with an electrical mobility analyzer are reported in figures E-2 and E-3. Again, satisfactory agreement is observed, but the extension of the distribution to smaller sizes by means of this more sensitive instrument seems to show a peak in the distribution around 0.07 to 0.08 micrometer, just at the lower limit of the impactor data.

In conclusion, although the experimenters consider these data good preliminary measurements (rather than definitive determinations), the substantial agreement between them suggests that equations (E-1), (E-2), and (E-3) and the information presented in figures E-1, E-2, and E-3 can be reasonably used to represent the particles found in the plume shortly after launch.

Particle Concentration

Less satisfactory information is available on absolute particle concentrations; it is difficult to estimate the effective volume swept by the wire impactor because the boundary of the plume is poorly defined. The tape impactor is immune to this problem, but it requires absolute calibration of its collection efficiency. Because of the program interruption, such a calibration has not yet been obtained. Filters have the same difficulty as the wire impactors. Under certain flight conditions, the electrical mobility analyzer can measure absolute concentrations (when the sampling time is shorter than the transit time); however, it was not clear whether such conditions existed during the preliminary flight measurements performed before the interruption of the program.

The closure condition, based on calculated booster emission at an altitude of approximately 20 kilometers (63 000 feet) of 930 grams of aluminum oxide (Al_2O_3) per meter altitude, a density for Al_2O_3 of approximately 4 g/cm^3, a plume diameter of 2.0 kilometers (6563 feet), and a volume-averaged particle diameter of 0.2 micrometer, yields an average concentration C.

$$C = \frac{930\ g\ m^{-1}}{\pi\ 10^6\ m^3\ m^{-1} \times \frac{4}{3}\pi\ (10^{-5})^3\ cm^3 \times 4\ g\ cm^{-3}}$$

$$\approx 1.76 \times 10^{10}\ particles/m^3 \qquad (E\text{-}4)$$

As shown, estimates obtained for the wire impactors and the electrical mobility analyzer are in the $10^9\ m^{-3}$ and $10^{10}\ m^{-3}$ range, respectively.

The Aitken nuclei counter measured at least 3×10^{10} particles/m^3. Overall, there is agreement within a factor of 2. Of course, a 50-percent increase in the diameter of the particles or in the size of the plume can each accommodate about half an order of magnitude. The particle diameter has been discussed in the section entitled "Particle Size," whereas the estimate of 2 kilometers (6300 feet) for the plume diameter was obtained from a common pilot report that approximately 10 seconds are required to cross the plume at a speed of 206 m/sec (400 knots) approximately 15 minutes after launch and at a 20-kilometer (63 000 foot) altitude. It appears that a reasonable assumption for calculations is approximately 10^{10} particles/m^3 in the early plume.

Particle Density

Very preliminary measurements were performed at JPL using a gravimetric technique to determine the density of the particles collected. Several authors reported that many of the Al_2O_3 spheres collected from rocket firings have hollow interiors and therefore an apparent or aerodynamical density inferior to the theoretical density of approximately 3.97 g/cm^3. The preliminary measurements have yielded a wide range of densities from 1.5 to 3.5 g/cm^3; no indication of relative abundances was given.

Particle Appearance

Spherical objects were mostly reported, with occasional agglomeration producing a covering of, for example, a 10-micrometer sphere with perhaps fifty 0.1-micrometer particles. Various textures have been observed. Some particles are smooth to a resolution of 20 nanometers; others are finely grained and deeply grooved, an indication of a polycrystalline structure (fig. E-4).

Particle Structure and Composition

The crystalline structure of ARC-collected Al_2O_3 particles was examined by EMS Laboratories, Pasadena, California. The structures were found to be mostly hexagonal (α) phase for particles in the 0.1-micrometer size range. Both transmission and reflection electron diffraction were used. Significant amounts of iron oxide were also found; these concentrations presumably were caused by a propellant additive for controlling the burn rate. However, earlier transmission diffraction measurements on a few 0.1-micrometer particles collected by JPL using an impactor showed cubic (γ) structure for the Al_2O_3. Other measurements on material collected by JPL from small motors fired in a closed tank also indicated a cubic structure. At present, it would appear that the evidence is in favor of hexagonal (α) structure for the material injected in the stratosphere.

Elemental composition of the particles was obtained by ARC, JPL, and LASL, mostly by X-ray fluorescence. Besides aluminum and occasionally potassium, sodium, and titanium, significant quantities of iron and silicon were found. Very rarely has chlorine (Cl) been observed by X-ray fluorescence. However, a series of samples collected by JPL on Nuclepore filters and analyzed by electron spectroscopy (ESCA) at the Lawrence Berkeley Laboratory revealed a significant, often large signal from Cl in varying degrees of oxidation ranging from a tight bond (as in a chloride) to a free atom (as for surface absorption). It was reported in the literature that such a variability in the bond energy of Cl deposited on metal surfaces is normal and dependent on the Cl surface concentration. From the ESCA shift of the aluminum peak, it is presumed that various compounds of aluminum, chlorine, and oxygen may be formed.

The apparently contradictory evidence for Cl obtained by electron spectroscopy and X-ray fluorescence can probably be best explained by the different penetration capabilities of the two techniques. The typical signal for X-ray fluorescence originates from a layer a fraction of a micrometer thick, whereas the ESCA signal is produced in only a few nanometers. If it is hypothesized that Cl is not uniformly distributed in the molten Al_2O_3 but is deposited on the surface after the particle has frozen to form an almost complete monolayer, one has a situation in which ESCA may detect 10 to 20 percent Cl in the first few layers but the X-ray yield of this small quantity of Cl would be undetectable. Whether the less tightly bound portions of such a layer can be released to the surrounding stratosphere under some conditions is not known.

CONCLUSIONS

The unanimous agreement of the various experimenters is that most of the particles are smaller than a micrometer and are typically 10^{-5} centimeters in diameter, whether a number, surface, or volume average is used. This new finding contrasts with widely quoted previous estimates that the mean diameter is of the order of 10^{-3} centimeters. The immediate and obvious consequence is that the typical residence times in the atmosphere are much longer (about two orders of magnitude).

Number concentrations in the early plume of the order of 10^{10} particles/m^3 are probably correct. Other properties of the particles are less certain, and the results should be viewed as preliminary.

TABLE E-I.- COMPARISON OF TITAN AND SPACE SHUTTLE BOOSTERS

Parameter	Titan III C/D	Space Shuttle
Total mass of propellant (2 boosters), kg	384×10^3	922×10^3
Nozzle throat diameter, cm	95.76	136.14
Propellant formulation		
Total solids, percent	84	84
Aluminum, percent	16	16
Binder	PBAN[a]	PBAN[a]
Combustion chamber pressure, MPa (bar)	3 to 4.5 (30 to 45)	3.5 to 5.5 (35 to 55)

[a]Polybutadieneacrylonitrile.

TABLE E-II.- EXPERIMENTAL PLATFORMS AND INSTRUMENTATION

Organization	Aircraft	Instruments
ARC	NASA U-2	Wire impactors (coated and uncoated); collection efficiency estimated unity for particles greater than 0.07 μm
	Lear jet	Photographic cameras
JPL	USAF[a] U-2	Continuous tape impactor (supplied by EG&G; particle size collection range estimated at 0.1 μm to more than 50 μm
		Nonfibrous membrane multiple filter; useful collection range estimated at 0.005 to 10 μm with varying efficiency
		Electrical mobility analyzer; useful particle size range from 0.02 to 1 μm with automatic size classification
		Panoramic camera (supplied by USAF)
LASL	WB-57F	Stratospheric Aitken nuclei detector systems; sensitivity from 0.005 to 0.1 μm; no classification capability
		Fibrous filters; sensitivity of 0.1 μm and larger

[a]USAF = U.S. Air Force.

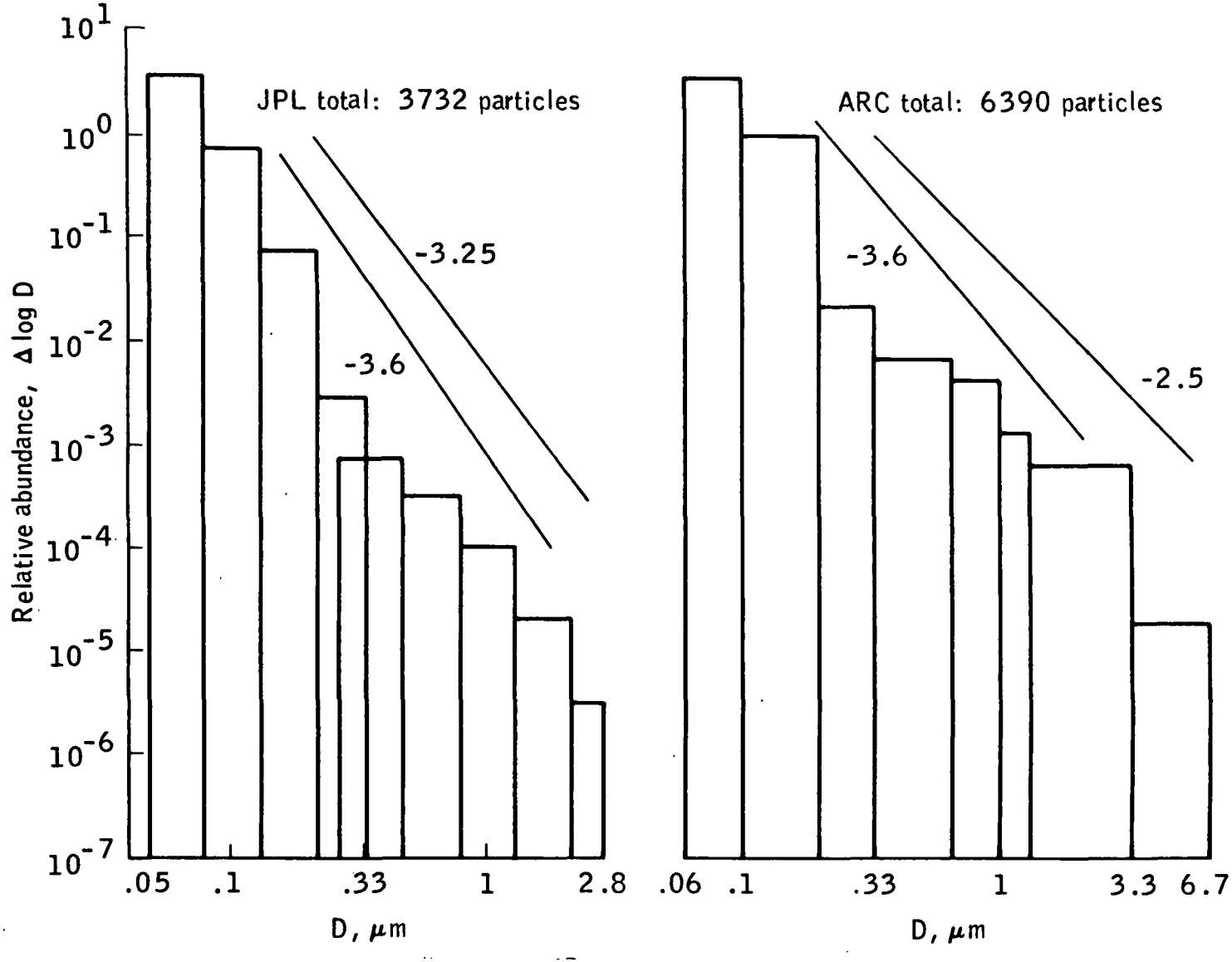

Figure E-1.- Impactor data for April 1974, at an altitude of 20 kilometers (65 000 feet), for particle diameter D.

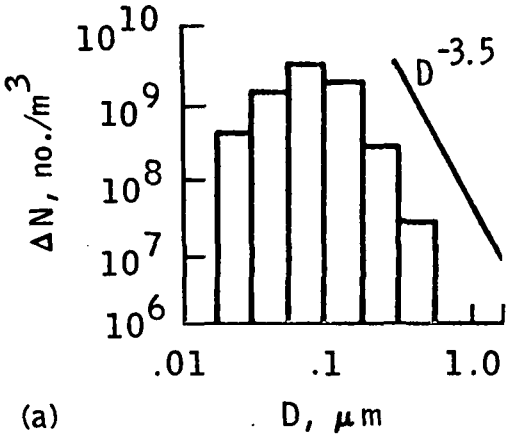

ETR, May 20, 1975, 7 hours after lift-off,
$\Sigma N = 7.41 \times 10^{9}/m^3$.

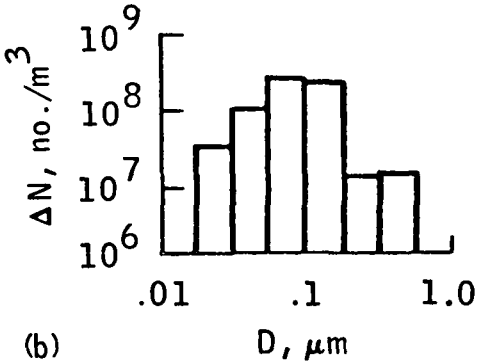

ETR, May 20, 1975, 13 hours after lift-off,
$\Sigma N = 6.07 \times 10^{8}/m^3$.

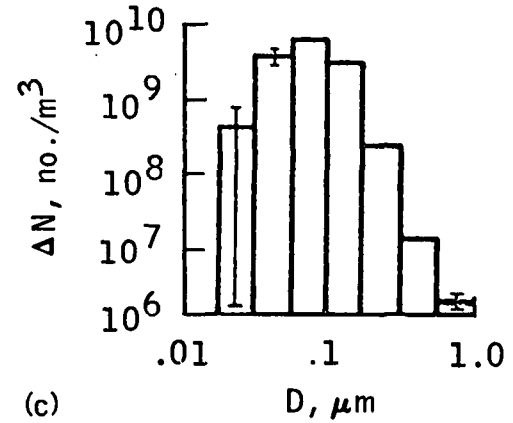

WTR, June 8, 1975, 6.5 hours after lift-off,
$\Sigma N = 1.47 \times 10^{10}/m^3$.

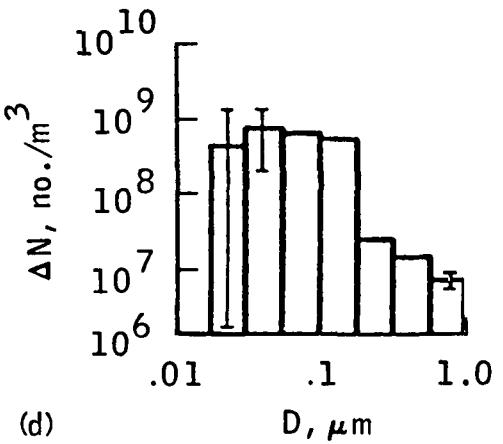

WTR, June 8, 1975, 13.5 hours after lift-off,
$\Sigma N = 2.33 \times 10^{9}/m^3$.

Figure E-2.- Electrical mobility analyzer data at an altitude of 19 kilometers, where N is the number of particles.

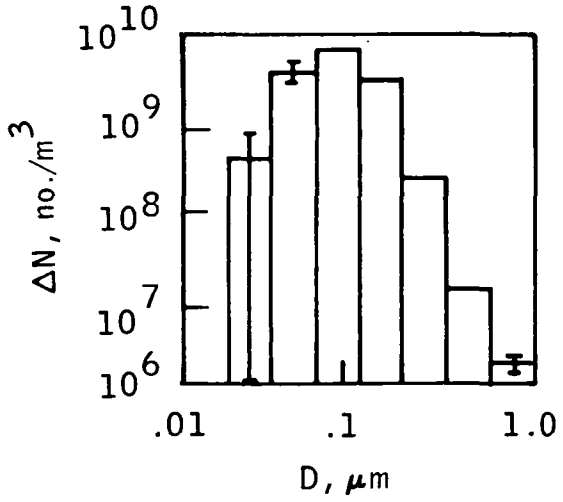

(a) Number, $\Sigma N = 1.47 \times 10^{10}/m^3$.

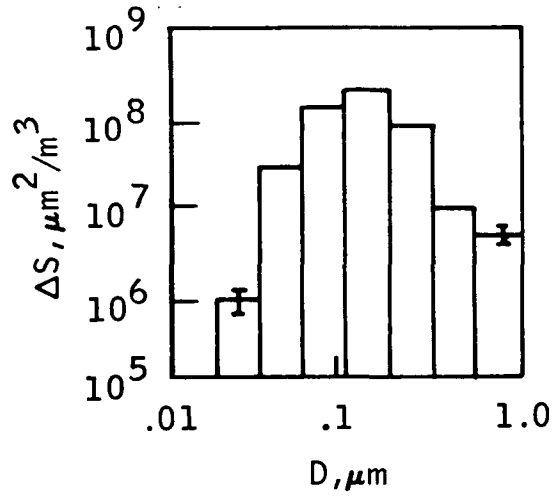

(b) Surface, $\Sigma S = 3.78 \times 10^{8}$ $\mu m^2/m^3$.

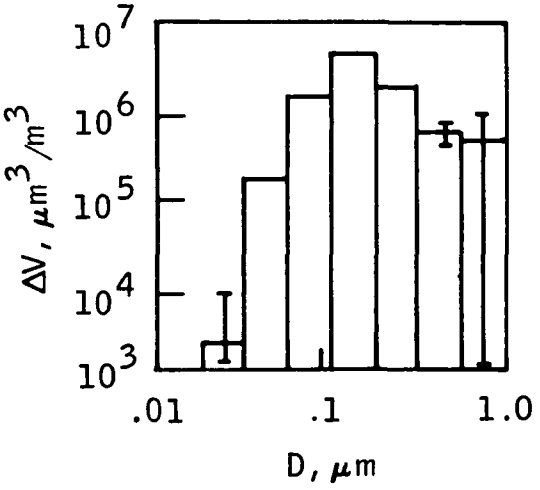

(c) Volume, $\Sigma V = 8.34 \times 10^{6}$ $\mu m^3/m^3$.

Figure E-3.- Electrical mobility analyzer data at an altitude of 19 kilometers for WTR, June 8, 1975, 6.5 hours after lift-off, where S is surface and V is volume.

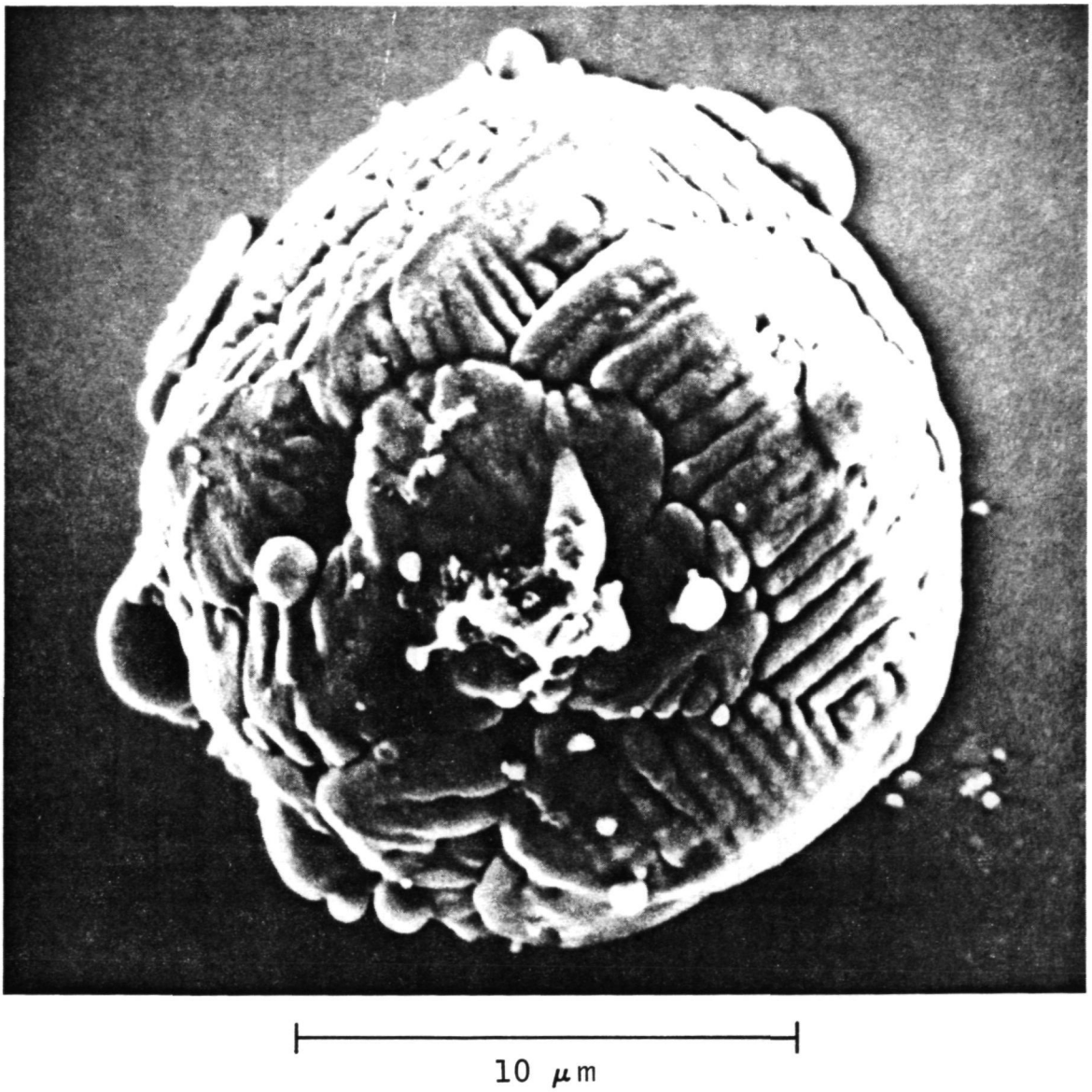

Figure E-4.- Scanning electron microscope photograph of Titan III-D exhaust particle.

APPENDIX F

ESTIMATES OF THE CLIMATIC IMPACT OF AEROSOLS PRODUCED BY SPACE SHUTTLES, SST's, AND OTHER HIGH-FLYING AIRCRAFT*

By James B. Pollack,[a] Owen B. Toon,[ab]
Audrey Summers,[a] Warren Van Camp,[a] and Betty Baldwin[a]

ABSTRACT

Aircraft and Space Shuttle vehicles flying in the next several decades will add hydrogen sulfate and aluminum oxide particles, respectively, to the stratosphere. To evaluate the effect of these additional aerosols on the global heat balance, solar and terrestrial radiative transfer calculations have been performed. The solar calculations employed an accurate numerical method for solving the multiple scattering problem for unpolarized light to determine the dependence of the global (spherical) albedo on the optical depth perturbation $\Delta\tau$. Correct allowance was made for absorption by gases. With these results and those obtained from calculations of the terrestrial, thermal flux at the top of the atmosphere, the resulting change in the mean surface temperature ΔT was determined as a function of $\Delta\tau$. In both calculations, the measured optical constants of the aerosol species of interest were used.

To apply these results to the problem of interest, engine exhaust properties for the various types of vehicles were used to estimate their optical depth perturbation, and the record of past climate changes was examined to set a threshold value, 0.1 K, on the mean surface temperature change, below which no significant impact is to be expected. Use of this information showed that no significant climate change should result from the aerosols produced by Space Shuttle, supersonic transport, and other high-altitude aircraft operating at traffic levels projected for the next several decades. However, the effect of supersonic transports is sufficiently close to the threshold limit to warrant a reevaluation as their characteristics are updated.

---

*This work was supported in part by the Climatic Impact Assessment Program of the U.S. Department of Transportation and by the National Science Foundation (grant NSF-DES 74-20458).

[a]NASA Ames Research Center.

[b]Work initiated while at Cornell University.

INTRODUCTION

In recent years, a growing concern that pollutants produced by this technological civilization may inadvertently change the Earth's climate on a global scale has been evident. Much attention has been directed toward material introduced into the troposphere. It was pointed out that increases in the carbon dioxide (CO_2) and aerosol content of the atmosphere could change the overall heat balance of the Earth and thereby alter the mean surface temperature (refs. F-1 and F-2). Recently, the debate over the desirability of fleets of supersonic transports has engendered a careful scrutiny of the potential effects of their exhaust products. Although considerable emphasis has been placed on evaluating the change in the ozone (O_3) content of the atmosphere and its resultant biological consequences, much effort has also been expended in evaluating the climatic implications of the aerosols that will be added to the stratosphere. Similar questions have been raised on the effects of the exhaust products expected from Space Shuttle vehicles.

Aerosols introduced by vehicles flying through the stratosphere might be climatologically significant for two reasons. First, since the residence time of particles smaller than 1 micrometer in the stratosphere is on the order of years, large steady-state perturbations in the number of particles might be created. By contrast, similarly sized particles in the troposphere have lifetimes only on the order of weeks. Second, since these vehicles can be expected to operate for an indefinitely long period of time, the relatively large thermal inertia of the atmosphere surface system offers no effective barrier to changes in the mean surface temperature. This paper contains estimates of the change in mean surface temperature caused by aerosols introduced into the stratosphere by supersonic transports, other aircraft flying at high altitudes, and Space Shuttle vehicles. Radiative transfer calculations are performed for visible and infrared wavelengths to determine the effect of the aerosols on both the solar and thermal energy budgets. Because many processes affect the climate of the Earth, changes in the radiative energy balance do not completely determine the response of the climate to a perturbing influence. Although this study neglects atmospheric dynamics and many possible climatic feedback loops, it provides a useful estimate of the climatic significance of increased aerosol levels.

Numerous attempts have been made to calculate the radiative effects of aerosols on the Earth's climate in recent years, and the reliability and sophistication of the calculations have increased rapidly. In reference F-2, the effect of an increased particulate burden in the lower troposphere is investigated, and it is found that a cooling of the Earth would result. Plausible values for the optical constants and for the size distribution function of the aerosols were used in performing calculations at one representative wavelength in the visible and one in the infrared. For the visible albedo calculations, the two-stream approximation (ref. F-3) to the multiple-scattering problem was used. The change in surface temperature was found by balancing the amount of sunlight absorbed with the thermal emission at the top of the atmosphere.

A number of the subsequent papers dealing with this problem contained improvements in the numerical method used to determine the visible albedo. Much effort has also gone into investigating the effect of changing various parameters that are used in such calculations. In reference F-4, the principle of invariance (ref. F-5) was used to obtain an accurate solution of the radiative transfer problem at visible wavelengths. It was found that the sign of the albedo change caused by an enhanced turbidity depended sensitively on the value of the imaginary index of refraction of the aerosols. Large values ($\gtrsim 0.05$) of the refractive index led to a lower albedo and therefore to warming of the surface.

Improved estimates of the albedo change by including the effects of gaseous absorption are cited in reference F-6. However, these calculations were inexact in this regard because wavelength-averaged transmission functions, which do not obey Beer's law, were used to describe the opacity properties of the gases. Because the numerical technique provided solutions to the multiple-scattering problem only for small optical depths, tropospheric water clouds could not be included in the model.

In reference F-7, a modified two-flux approximation was used to study the effect of aerosols in both the visible and infrared. It was found that the effect of the aerosols on the thermal radiative fluxes cannot be ignored and that the sign of the aerosol effect on the surface temperature depends on the value of the surface albedo, with net heating occurring when the surface reflectivity exceeded 0.3. In the context of the supersonic transport (SST) problem, the importance of including the effect of the aerosols in the infrared was also emphasized (see ref. F-8). By contributing to the infrared opacity, aerosols cause an enhanced greenhouse effect. This acts in the opposite direction to the typical effect of aerosols at visible wavelengths, where they usually enhance the global albedo.

In an earlier paper (ref. F-9), initial estimates of the effect of aerosols produced by SST emission on the global albedo were presented. This paper includes a more detailed description of these results and the infrared calculations for estimating the magnitude and sign of the surface temperature change. These computations encompass the cumulative effect of all aircraft flying in the stratosphere. The term "SST" is used to refer to this case. The corresponding calculations for the aerosols produced by Space Shuttle flights are also performed.

These calculations represent an improvement over many of the previous investigations because they include more accurate optical properties of the aerosols, allow for the effect of the aerosols in the thermal infrared, treat accurately gaseous absorption in the visible, and include water clouds in the troposphere. The optical properties of the aerosols have been modeled as accurately as is presently feasible using measured optical constants of both current and perturbed aerosol components together with a carefully constructed model of the other aerosol properties.

In previous calculations, the optical constants, especially the imaginary indices of refraction, either were considered to be free parameters or were

set equal to "plausible" values. Since even the sign of the net effect of the aerosols on the mean surface temperature depends critically on the values of the optical constants, employment of measured values represents a significant advance over earlier efforts.

The particle size distribution functions used are also based on a more thorough scrutiny of available empirical data than those used by many earlier investigators. The model of the aerosol properties and the sources for their optical constants are described in reference F-10.

The description of the radiative transfer calculations is followed by a discussion of the results. The dependence of various quantities of interest is plotted as a function of the change in the optical depth of the stratosphere at a reference wavelength of 0.55 micrometer. Then, the perturbation optical depths that will result from the amount of emission expected from SST's and Space Shuttle vehicles over the next several decades are determined. From a comparison of perturbation optical depth values to the results of the calculations, the magnitude and importance of the surface temperature change resulting from the added aerosols are assessed.

COMPUTATIONAL TECHNIQUE

The radiative transfer calculations consisted of two parts. A numerical, multiple-scattering scheme was used to determine the global (spherical) albedo and the variation of net solar flux with altitude in the atmosphere. These results were subsequently used as boundary conditions in a numerical calculation of the infrared thermal radiation that yielded the value of the surface temperature. In both calculations, only the global or hemispherical heat balance was considered. Thus, the calculations did not allow for latitudinal or diurnal variations of the model parameters. In the following paragraphs, the numerical technique used to treat the solar radiation is described, the sources of the parameters used in this calculation are summarized, and a similar presentation for the thermal computations is given.

Multiple-Scattering Calculations

For the visible portion of the spectrum, calculations that considered the scattering and absorption of unpolarized light by both aerosols and gases were performed. The solution was accomplished with a computer program based on the inhomogeneous doubling method described in references F-9 and F-11. According to this method, the atmosphere was divided into a series of layers, each one of which is homogeneous in its properties but which can differ in its properties from any other layer. Thus, allowance was made for the vertical inhomogeneity of the atmosphere. An initial step in this computation was determination of the single-scattering properties of the aerosols for each layer by using a Mie scattering program with allowance being made for the scattering and absorption contribution from gases. With this information, the scattering and transmission properties of individual layers were determined by means of the ordinary

doubling principle (ref. F-12). The surface was modeled as a Lambert reflector with a specified reflectivity. Then, a generalization of the doubling method was used to combine the separate layers, including the surface. The end result of these operations was a specification of the upward, downward, and net fluxes at all layer interfaces, including the top of the atmosphere and the surface. Integration of the net fluxes over solar zenith angle yielded the globally averaged value of the solar energy deposition profile, whereas a comparable integration of the upward component of the flux at the top of the atmosphere resulted in a determination of the global (spherical) albedo. (These integrals are defined in ref. F-4.) The term "global albedo" refers to the total amount of solar energy reflected by the Earth to space divided by the amount of solar energy incident at the top of the atmosphere.

This calculation has several attractive features. It employs an accurate solution to the multiple-scattering problem that allows for cases in which the total optical depth is significantly greater than unity. As a result, optically thick water clouds can be included in the lower atmosphere. Allowance for gaseous absorption is also made accurately. Ordinarily, inclusion of the near-infrared absorption bands of water vapor, CO_2, and oxygen (O_2) presents a problem for multiple-scattering calculations. To limit the number of wavelength points at which calculations are necessary, one must normally consider the absorption that takes place over fairly broad wavelength intervals (~0.1 to 0.3 micrometer). Such transmission averages of the gas absorption destroy its monochromatic nature, and, in particular, Beer's law is no longer obeyed by such averages. Thus, it is not correct to employ directly transmission averages in multiple-scattering calculations. However, in accordance with references F-9 and F-11, the usual equivalent width formulas were analyzed into a sum of monochromatic transmission factors multiplied by a probability coefficient. In essence, this technique is equivalent to transforming integrals over wavelength into integrals over the absorption coefficient (ref. F-13) and allows a small number of monochromatic calculations. Multiple-scattering calculations were performed for each term of the absorption coefficient distribution, and the results were weighted by the probability factors.

A final important characteristic of these calculations was the use of measured optical constants for each chemical component of the aerosols. When a given layer included several kinds of aerosols, separate Mie scattering calculations were performed for each component and the results were added together, weighted by their relative cross sections at the wavelength of interest. The aerosol optical depth of a given layer was found by multiplying the aerosol optical depth at a reference wavelength by the ratio of the total aerosol cross section at the wavelength of interest to that at the reference wavelength (ref. F-10).

Solar Calculation

The sources of the parameters used in the solar calculation and the nature of the model used are described in this section. The solar spectrum from 0.24 to 4.6 micrometers was divided into 26 wavelength intervals. Separate calculations were performed for each wavelength interval; and the results were

combined, weighted by the amount of solar energy in each interval. In some near-infrared intervals that contained gas absorption bands, a number of calculations were performed, each one corresponding to a given gas absorption coefficient. The atmosphere was divided into 15 layers, each 3 kilometers (9800 feet) deep. The ground was included as an additional layer and characterized by a reflectivity of 0.10 (ref. F-2). Water clouds were considered to be present over 50 percent of the planet and were located in the layer that covered the altitude range from 3 to 6 kilometers (9800 to 19 600 feet) above the ground (ref. F-2). Separate calculations were performed for regions with and without water clouds, and the results were combined.

The properties of the aerosols were specified as follows. The results cited in reference F-10 were used to define the aerosol properties in each atmospheric layer for the "base" or unperturbed model. These properties included optical depth at the reference wavelength of 0.55 micrometer, chemical composition, optical constants, and size distribution function. The properties used are summarized in reference F-10. The major component of the aerosols expected to be produced by SST's and by Space Shuttle vehicles are hydrogen sulfate (H_2SO_4) and aluminum oxide (Al_2O_3), respectively (ref. F-14). The particle size distribution function of the stratospheric H_2SO_4 layer under perturbed conditions is not known, but some evidence exists that the "base" sulfate distribution does not change significantly during epochs of large increases in the stratospheric optical depth resulting from volcanic explosions (ref. F-10). Hence, the size distribution of the unperturbed stratosphere was adopted for the perturbed component due to SST's. By coincidence, measurements of the aerosol size distribution made in the exhaust of prototype Space Shuttle engines (refs. F-15 and F-16), when convoluted with a one-dimensional diffusion-sedimentation model (ref. F-17), resulted in a function very similar to the "base" stratospheric function. Hence, the "base" distribution was also used to describe the perturbation caused by Space Shuttle vehicles. In both cases, if differences actually exist between the base stratospheric function and the perturbed function, the differences will be increased numbers of larger particles in the perturbed case. This difference would tend to increase the infrared effects of the aerosols and would most probably reduce the temperature changes that are found. Thus, the use of the base size distribution function is probably a conservative choice in that it may lead to overestimates of the net effects. The total optical depth of the two perturbation sources is taken as a free parameter in the calculations. In the section entitled "Discussion," estimates of this important parameter are provided from studies of the amount of effluent that is expected from SST's and Space Shuttle vehicles during the next several decades. When material was added to the stratosphere, the base optical depth of each layer of this region was multiplied by the same factor. Because the base optical depth of a layer decreases with altitude, aerosols were effectively added mainly to the lower portions of the stratosphere.

Deirmendjian's (ref. F-18) cloud model chlorine (C1) was adopted to describe the size distribution function of the water cloud particles; this function has a mode radius of 4 micrometers. The water cloud optical depth at a 0.55-micrometer wavelength was chosen to be 6 so that the global albedo of the unperturbed model equaled a value of 0.28, which was determined from

satellite measurements (ref. F-19). The optical constants of the water droplets were obtained from reference F-20.

The sources of the parameters for the gaseous components of the model are described next. Allowance was made for gaseous absorption caused by O_3, water vapor, CO_2, and O_2 and for Rayleigh scattering by the air molecules. The vertical profiles of water vapor and the constant mixing ratios of O_2 and CO_2 were obtained from data given in reference F-21, whereas the O_3 profile was obtained from Whitten's results (private communication). The water vapor abundances were converted to relative humidity profiles since, in many of the calculations, the reasonable assumption was made that this variable would remain constant with changing surface temperature. The equivalent width parameters and formulas for the major water vapor and CO_2 bands were adopted from reference F-22, whereas similar data for the major O_2 bands were obtained from reference F-23. These data were analyzed to determine the probability distribution functions of monochromatic absorption coefficients for each major band region of a given gaseous constituent. Lindzen and Will's (ref. F-24) square wave model of the Hartley and Chappuis bands of O_3 and their absorption coefficients were used at four gauss-point, wavelength locations for the Huggins band. Finally, scattering coefficients given in reference F-25 were used to compute the Rayleigh scattering optical depths. The data in reference F-25 include an allowance for slight departures from a λ^{-4} dependence, where λ is wavelength.

The objective of infrared thermal calculations was to obtain an estimate of the change in the mean surface temperature caused by a given stratospheric aerosol perturbation. In general, this task was accomplished by performing an energy balance calculation at the top of the atmosphere. However, in a few cases, this calculation was supplemented by one in which the entire vertical temperature structure was found under conditions of radiative-convective equilibrium. In the first type of calculation, the thermal infrared flux at the top of the atmosphere was determined for a sequence of surface temperatures, and the results were interpolated to find the surface temperature for which the thermal energy radiated to space equaled the solar energy absorbed by the planet. The formulas used to calculate the thermal infrared flux are given in reference F-26. These equations involve a reformulation of the formal solution of the transfer equation in terms of transmission average functions, with the source function set equal to the Planck function. The amount of solar energy absorbed was obtained by interpolation from calculations made with the solar energy program at two values of the surface temperature. Thus, allowance was made for the small, but not insignificant, dependence of the solar component on temperature. This dependence arises from changes in the absolute amount of water vapor in the atmosphere under conditions of constant relative humidity.

A few calculations of the vertical temperature structure were performed under conditions of radiative-convective equilibrium using the flux iterative

method cited in reference F-27. The results of the solar calculations were used to specify the desired net infrared fluxes for this set of calculations. The iteration procedure provided a method to determine the vertical temperature structure for which the net infrared flux at each layer in the atmosphere was balanced by the net solar flux at that location. Such a state is one in which pure radiative equilibrium holds. However, when the local lapse rate exceeded a critical value at which convection commenced, the lapse rate was readjusted to equal this limiting convective lapse rate. Unfortunately, the iteration scheme was not fully convergent, and it led to mean fractional flux residuals of approximately 1 to 2 percent after a number of iterations. Thus, this type of calculation was applied to cases involving large optical depth perturbations to determine the general behavior of the stratospheric temperatures, which may follow quite a different trend from that of the surface and tropospheric temperatures.

Many infrared model parameters, such as aerosol properties, have already been described. The infrared was divided into 44 spectral intervals, which totally covered the spectral region from wave numbers 25 to 3000 cm^{-1} (wavelengths 400 to 3.3 micrometers). The 25- to 50-cm^{-1} interval was divided into a single region, the 50- to 1300-cm^{-1} region into 50-cm^{-1} segments, and the 1300- to 3000-cm^{-1} interval into 100-cm^{-1} partitions. Within each spectral interval, the transmission behavior of the gases was modeled by using an exponential of a broad-band opacity variable, which in turn followed a power law dependence on gas amount, total effective pressure, and temperature (ref. F-26). The value of the power law exponents and the proportionality constant for each gas species and wavelength were obtained by fitting this representation to a combination of laboratory and theoretical estimates of the transmission properties of water vapor, CO_2, and O_3 at conditions relevant for the Earth's troposphere and stratosphere (refs. F-21 and F-28 to F-32).

The infrared aerosol optical depth was found for each layer of the atmosphere and each wavelength interval by multiplying the aerosol optical depth at 0.55 micrometer by the ratio of the aerosol absorption cross section of the wavelength of interest to the total cross section at the reference wavelength (ref. F-10). This ratio was determined by a Mie scattering program. The neglect of scattering by the aerosols at infrared wavelengths was found to be reasonable since the single-scattering albedo was usually quite low. A low, single-scattering albedo was the result of the large imaginary index of refraction and the small ratio of the mean particle size to the wavelength in the infrared part of the spectrum. The optical constants for most materials are not known as far as 400 micrometers. The values were used at the largest wavelength at which they are known to specify the optical constants beyond this point.

The starting point for the temperature/pressure structure of the atmosphere was the U.S. standard atmosphere (ref. F-33) for midlatitude spring and fall conditions. In the energy balance calculations, the temperature structure of the entire vertical column was generally changed in response to a change in surface temperature from the U.S. standard atmosphere values in such

a way that the lapse rates were kept constant. However, in some calculations, the stratospheric temperatures were kept constant, and only the tropospheric temperatures were changed under the constraint of a constant lapse rate. In the flux iterative calculations, the convective lapse rate was set equal to 6.5 K/km, a value characteristic of the present troposphere.

RADIATIVE TRANSFER CALCULATIONS

In this section, the radiative transfer calculations are summarized by showing the manner in which various quantities of interest, such as global albedo and surface temperature, depend on the enhancement of the stratospheric aerosol optical depth $\Delta\tau$ at the reference wavelength of 0.55 micrometer. Separate calculations were performed for Al_2O_3 and H_2SO_4 particles, which are produced by Space Shuttle and SST vehicles, respectively. Because only small values of $\Delta\tau$ are of interest for each case, the cumulative effect of both vehicles is additive to first approximation.

The results of the calculations in the visible portion of the spectrum are as follows. The variation of the global albedo with $\Delta\tau$ for the two sources of added particles is shown in figure F-1. In both cases, the added aerosol burden in the stratosphere leads to an increase in the global albedo, which, alone, will cause a cooling of the Earth. For an equal $\Delta\tau$, the Al_2O_3 particles cause a larger increase in the Earth's albedo than do the H_2SO_4 particles. This difference is a result of the Al_2O_3 aerosols having a larger value for the real part of their refractive index (~1.77 compared to 1.43) and, therefore, backscattering a larger fraction of the incident solar radiation.

Next, the change in the vertical distribution of the absorbed solar energy is examined. The $\Delta\tau$ dependence of the fraction of energy absorbed in the stratosphere is shown in figure F-2. Here, as elsewhere in the discussion, fractional absorption refers to the ratio of the amount of solar energy absorbed to that incident at the top of the atmosphere. In contrast to the trend for the Earth as a whole, an increase in $\Delta\tau$ leads to an increase in the amount of solar energy deposited in the stratosphere.

Part of the reason for this trend in the stratospheric heating is the absorption of solar radiation by the particles. In figure F-3, the fractional absorption by aerosols is plotted as a function of $\Delta\tau$. It can be seen that as the number of H_2SO_4 particles is increased, the amount of energy they absorb is increased. However, almost no variation is shown by the Al_2O_3 particles. In the added Al_2O_3 particles, the total aerosol heating is dominated by the H_2SO_4 particles of the unperturbed stratosphere that are also present. The H_2SO_4 particles absorb solar energy principally in their near-infrared bands. In contrast, the imaginary index of refraction, which

determines the amount of solar energy absorption, remains very small for the Al_2O_3 particles throughout the entire visible and near-infrared spectral region. It can be seen that the increase in the total fractional heating of the stratosphere with an increase in the H_2SO_4 burden is due in part to energy absorption by the aerosols. In addition, as a result of scattering of the incident sunlight by both types of aerosols, an increase occurs in the amount of sunlight absorbed by the O_3 in the stratosphere. The O_3 absorption accounts for almost all of the trend of the total stratospheric absorption shown in figure F-2 for the Al_2O_3 particles and about half of the trend for the H_2SO_4 particles.

In figure F-4, the effect of H_2SO_4 aerosol enhancement on various levels in the stratosphere is examined. The ordinate is the fractional change in the solar heating at a given level and is referenced to the amount of solar heating at that level in the unperturbed model. The two curves shown correspond to two values of the optical depth perturbation $\Delta\tau$. As expected, the greatest changes occur in the lowest portions of the stratosphere, where most of the added particles are located. Analogous results are found for the Al_2O_3 particles, although at the highest pressure levels in the stratosphere, a decreased heating is found compared to that for the unperturbed model.

In figure F-5, the results for the fractional absorption below the tropopause are shown. This quantity refers to the sum of the energy absorbed in the troposphere and at the ground. In accordance with the trend found for the global albedo in figure F-1, it can be seen that the amount of energy absorbed below the tropopause decreases with increasing aerosol burden in the stratosphere. Alone, this result implies a cooling trend for the troposphere and the surface. However, a judgment on this issue must be deferred until the effect of the aerosol opacity in the thermal infrared region is included.

Besides affecting the global energy budget, aerosols added to the stratosphere can also upset the O_3 photochemical cycle by changing the rate at which O_3 molecules are dissociated by incident sunlight. In figure F-6, the fractional change in the O_3 destruction rate for the entire atmospheric column is shown as a function of $\Delta\tau$. The O_3 destruction rate was calculated by summing the number of photons absorbed by O_3 in each of its three major absorption bands. The number of photons absorbed by O_3 at a given wavelength and in a given atmospheric layer was found in a straightforward fashion from the amount of solar energy absorbed by that layer and the fractional contribution of O_3 to the absorption coefficient of the layer. An increase in the aerosol content of the stratosphere causes an increase in the rate at which O_3 is destroyed and, therefore, a decrease in the steady-state abundance of O_3. However, even for rather large values of $\Delta\tau$, the magnitude of the

change is surprisingly small both in absolute value and in comparison with the O_3 depletions expected as the result of the oxides of nitrogen and Cl compounds released by SST's and Space Shuttle vehicles, respectively. The O_3 destruction rate is only slightly affected by the added aerosols because much of the O_3 photodissociation occurs above the levels at which most of the aerosols are found.

The results of the infrared calculations, which provide estimates of the effect of the added aerosols on the mean surface temperature, are described next. Most calculations of this type involved balancing the radiative energy at the top of the atmosphere. First, such a calculation was performed for the base or unperturbed global average model, and a surface temperature of 292.7 K was obtained. This value is approximately 4.5 K higher than the ground temperature given in reference F-33 for spring/fall conditions at middle latitudes. A global average model is not the same as a midlatitude model. This temperature difference arises partly because the ground temperature varies with latitude for the real Earth and partly because the infrared radiation from various latitudes is weighted by a nonlinear, approximate temperature to the fourth power, relationship. Subsequent calculations provided values of the surface temperature for perturbed cases, which were compared with the result for the base case. The basic parameter derived from this comparison is ΔT, which is the difference in the value of the surface temperature between the perturbed and unperturbed cases.

In figure F-7, the variation of $\Delta\tau$ and ΔT is shown for cases involving added H_2SO_4 particles resulting from SST's. Calculations were performed for four sets of conditions, which are represented by the four curves of figure F-7. Curves A and B were determined for conditions of constant relative and constant absolute humidity. For these calculations and for those represented by curve D, the lapse rates were assumed to be invariant throughout the atmosphere. Curve C represents cases in which both the relative humidity profile and the stratospheric temperatures were held constant. Finally, to determine the importance of the aerosols opacity in the thermal infrared region, curve D was computed. Curve D was calculated under the same set of circumstances as curve A, except that the aerosol opacity was held fixed to its value in the base case.

For all four cases shown in figure F-7, an enhanced aerosol burden causes a decrease in the mean surface temperature. This result indicates that the effect of the aeorsols on the global albedo is more important than their effect in the infrared. In turn, the relative importance of the aerosols in these two wavelength regions is a reflection of their very small mean size. As shown in figure F-5 (ref. F-10), the stratospheric aerosols have a much larger optical depth at visible wavelengths than at longer wavelengths. A comparison of curves A and D shows that the magnitude of the ΔT values is decreased by approximately 40 percent when allowance is made for the infrared opacity of the aerosols. Thus, although this effect is not the dominant one, it cannot be neglected.

Because curves A and C are fairly close, the results are not very sensitive to the assumed change in the stratospheric temperature profile. Calculations performed for conditions of radiative-convective equilibrium for a $\Delta\tau$ value of suggest that curve A provides a more realistic estimate than curve C provides. This result indicates that the added aerosols cool the stratosphere to a greater degree by radiating in the thermal infrared than they warm this region by causing a slight enhancement in the amount of absorbed solar radiation. Finally, a comparison of curves A and B shows that larger ΔT values are achieved under conditions of constant relative humidity than under conditions of constant absolute humidity because, for the constant relative humidity case, the amount of water in the atmosphere decreases with decreasing temperature. In turn, less water vapor implies less solar energy absorption in its near-infrared bands and a smaller greenhouse effect in the thermal infrared. The assumption of constant relative humidity is probably the more realistic one.

Analogous curves are shown in figure F-8 for the Al_2O_3 particles produced by Space Shuttle vehicles. Again, a net cooling of the Earth is found for all four cases. However, the infrared opacity cancels a good fraction of the effect of the particles in the visible region. The infrared effect is more powerful for the Al_2O_3 particles than for the H_2SO_4 particles because the imaginary index of refraction is larger for the former than for the latter. An enhanced imaginary index of refraction in the infrared results in an enhanced absorption cross section.

DISCUSSION

In the preceeding section, estimates of the decrease in the mean surface temperature ΔT were obtained as a function of the optical depth perturbation $\Delta\tau$ caused by H_2SO_4 and Al_2O_3 aerosols introduced into the stratosphere. The results of these calculations are summarized in figures F-7 and F-8, in which ΔT is plotted as a function of $\Delta\tau$. Besides applying to the global average situation, these results can also be used for optical depth perturbations occurring in a single hemisphere. (The angular averages over solar zenith angle are identical in these two cases.) In this section, the values of ΔT that have characterized epochs of major climate changes in the past are discussed so as to estimate a lower bound on ΔT, below which no serious climatic impact is expected. Then, estimates of the magnitude of $\Delta\tau$ expected from SST's and Space Shuttle vehicles operating during the next several decades are provided, and the importance of their effect on the climate is determined.

The significance of a given value of ΔT can be assessed by comparing it with values associated with major climatic events of the past. During the past several million years, the climate of the Earth has undergone a number of major fluctuations, in which the climate has alternated between periods of major glaciation and relative thaw. At the present time, of course, the Earth is within one of the relatively warm epochs, although frequent variations with a smaller amplitude have occurred over the current interglacial period.

The difference between the current mean surface temperature and that estimated for the peak of one of the major ice ages is approximately 5 K (ref. F-34). Over the last 1000 years, there have been extended periods of time when the mean surface temperature was approximately 1 K less than its current value (ref. F-34). This apparently small difference had major consequences in some cases. For example, during some of these colder epochs, the agricultural yield was substantially reduced in countries at high geographical latitude, and major famines resulted (ref. F-34).

This discussion indicates that a temperature change as large as 1 K could have serious consequences. However, values that are a factor of 2 or 3 smaller are probably on the borderline of being important. The numerical calculations of ΔT represent determinations of the change in surface temperature that result from radiative effects. Because many feedback mechanisms were not considered, the actual value of ΔT might be somewhat larger. For example, during colder periods, the amount of surface covered by frost and ice increases. This acts as a positive feedback effect by increasing the global albedo. Calculations (refs. F-35 and F-36) suggest that the net effect of a number of feedback mechanisms is to increase the calculated values of ΔT by a factor of approximately 3. For these reasons, 0.1 K was adopted as a threshold value for ΔT and is believed to be a conservative estimate. Smaller calculated values of ΔT are not expected to change the climate seriously.

To obtain estimates of the optical depth perturbation $\Delta\tau$ that can be expected from SST and Space Shuttle vehicles, the mass of material that will be emitted into the stratosphere from these vehicles over the next several decades was first estimated. The steady-state mass of aerosols produced in one hemisphere by the continued operation of a given type of vehicle is related to the emission rate of the vehicle according to

$$m = H \sum_i e_i f_i \frac{M_a}{M_e} t_i c_i n_i \qquad \text{(F-1)}$$

where m is the steady-state mass of aerosols

H is the fraction of the aerosols deposited in a given hemisphere

e_i is the total amount of mass emitted by a single vehicle per unit time

f_i is the fraction of the total mass that contains the aerosol-producing component

M_a is the molecular weight of the aerosol

M_e is the molecular weight of the aerosol-producing component

t_i is the residence time in the stratosphere

c_i is the efficiency of converting the aerosol-producing component into an aerosol

n_i is the number of vehicles operating in both hemispheres

Σ_i refers to the various altitude ranges in the stratosphere

Estimates were obtained of the steady-state mass of H_2SO_4 and Al_2O_3 particles produced by SST and Space Shuttle vehicles, respectively, by using equation (F-1) in combination with the data given in table F-I. These data have been assembled from information given in references F-14 and F-37. The second column in table F-I provides estimates of t_i. The third column gives values for c_i for H_2SO_4 aerosols produced from the sulfur dioxide (SO_2) emitted by SST and other high-altitude aircraft. The next four columns of the table give estimates of the SO_2 emission rates caused by these types of vehicles for several time frames. Both nominal and upper limit values are given. These emission rates are equivalent to the product $(e_i n_i f_i)$ in equation (F-1). These values were derived by using a value of 10^{-3} for f, the fraction of the total mass that is SO_2, and $M_a/M_e = 1.6$ for an H_2SO_4 solution that is 75 percent H_2SO_4 by weight (ref. F-38). The final column of table F-I provides values of the emission rate of Al_2O_3 particles by the Space Shuttle vehicles expected to be operating in 1990. This quantity is equivalent to the product $(e_i n_i f_i)$ in equation (F-1). In this case, $M_a/M_e = 1$ and $c_i = 1$. Finally, although almost all of the emission takes place in the Northern Hemisphere, meridional transport carries approximately 30 percent of the material into the Southern Hemisphere. Hence, $H = 0.7$ for the Northern Hemisphere and $H = 0.3$ for the Southern Hemisphere.

Next, the mass of aerosols m found from equation (F-1) and table F-I was converted into an optical depth perturbation $\Delta\tau$. The relationship between these two quantities is given by

$$\Delta\tau = \frac{m}{A\rho} \frac{\int_0^\infty Q_{ext} \pi a^2 N(a) da}{\int_0^\infty \frac{4\pi}{3} a^3 N(a) da} \qquad \text{(F-2)}$$

where A is the area of a hemisphere

ρ is the density of the aerosol

Q_{ext} is the efficiency factor for scattering and absorbing incident radiation (ref. F-10)

a is particle radius

N(a) is the size distribution function of the aerosols

The integrals appearing in equation (F-2) were evaluated by using the stratospheric size distribution function (ref. F-10) in a Mie scattering computer program.

If the aerosols are distributed over a scale height of 10 kilometers (32 000 feet), the following numerical relationships exist between $\Delta\tau$ and m.

$$\Delta\tau = 0.0503\ \tilde{m},\ SO_2 \qquad \text{(F-3a)}$$

$$\Delta\tau = 0.0310\ \tilde{m},\ H_2SO_4 \qquad \text{(F-3b)}$$

$$\Delta\tau = 0.0228\ \tilde{m},\ Al_2O_3 \qquad \text{(F-3c)}$$

where $\tilde{m}$ is the mass in units of micrograms per cubic meter. The compound to which $\tilde{m}$ refers is indicated to the right of the comma in these equations. For example, in equation (F-3a), $\tilde{m}$ is the mass of SO_2 that is converted into H_2SO_4 particles, and $\Delta\tau$ is the optical depth of these aerosols.

Table F-II is a summary of the values of $\Delta\tau$ at a wavelength of 0.55 micrometer, as determined from equation (F-2). The SST's cause about 70 percent of the steady-state burden of H_2SO_4 particles produced by high-altitude aircraft. Although planes flying lower in the stratosphere generate more emission than SST's, the effect of these other aircraft is minimized by the short residence time of their products. For the Al_2O_3 particles produced by the Space Shuttle vehicle, the amount of mass found from table F-I was doubled to allow for particles emitted at altitudes above 21 kilometers (68 000 feet); then, the $\Delta\tau$ so found was halved to allow for the rapid loss of the larger particles. About half the mass of the Al_2O_3 produced by the Space Shuttle exhaust is contained in particles larger than a micrometer; these particles are quickly removed from the stratosphere by gravitational sedimentation. In all cases, the optical depth perturbations are quite small; in fact, none of them is as large as the perturbation produced throughout the mid-1960's by small-scale volcanic activity (as discussed in ref. F-10).

The impact of the aerosols produced by SST and Space Shuttle vehicles, is as follows. According to figures F-7 and F-8, optical depth perturbations of approximately 0.01 and 0.015 are required for SST and Space Shuttle, respectively, to cause a decrease in the mean surface temperature equal to 0.1 K. This value for ΔT is the threshold figure discussed previously. All the optical depth perturbations given in table F-II are less than these critical values. From this comparison, it can be concluded that SST and

Space Shuttle vehicles operating at the levels estimated for the next several decades will not cause a serious change in the climate as a result of the aerosols they add to the stratosphere.

This conclusion on the impact of SST and Space Shuttle vehicles can be put into some perspective by estimating the number of vehicles operating on a regular basis required to produce the critical value of ΔT. Since the nominal 1990 case treated in table F-II was based on 250 SST's flying every day for 4.5 hours in the stratosphere and since these vehicles contributed approximately 70 percent of the $\Delta\tau$ attributable to high-altitude aircraft, approximately 7500 SST's are required to generate the critical value of ΔT. The Space Shuttle case treated in table F-II involved about one launch per week. To raise ΔT to its critical figure would require approximately 70 launches per day. The critical number for the Space Shuttle is far in excess of the number of vehicles that are likely to be operating in the near future. Thus, the climatic effect of these vehicles is unlikely to be changed by reasonable modifications to the parameters used in these calculations. However, for high-altitude aircraft, the projections for the number of SST's and other aircraft operating in the year 2000 are sufficiently near the critical numbers that estimates of ΔT for such aircraft should be updated as new projections become available.

CONCLUSIONS

Calculations of the effect on the global heat budget of adding aerosols to the stratosphere have been presented. The global albedo increases and the mean surface temperature decreases as a result of increases in the number of H_2SO_4 and Al_2O_3 particles that are produced by SST and Space Shuttle vehicles, respectively. The effect of the aerosols on thermal radiation was important; furthermore, the thermal radiation effect partly counteracted the cooling of the surface caused by the effect of the aerosols at visible wavelengths. The results of these calculations on the decrease in surface temperature as a function of optical depth perturbation are summarized in figures F-7 and F-8.

These results were used to assess the significance of the climatic impact of aerosols produced by SST's, other high-altitude aircraft, and Space Shuttle vehicles operating during the next several decades. For this task, the ΔT values associated with past major changes in the climate were used to infer that ΔT values below 0.1 K would not have major consequences. Next, the emission rates estimated for the vehicles of interest over the next several decades were used to determine the $\Delta\tau$ values summarized in table F-II. After the data were combined, it was concluded that the aerosols produced by SST's, other high-altitude aircraft, and Space Shuttle vehicles operating during the next several decades would not seriously alter the climate. Very large numbers of these vehicles are required before threshold conditions are reached: approximately 7500 SST's and approximately 70 Space Shuttle launches per day. It seems highly unlikely that the conclusions about the impact of Space Shuttle vehicles will be altered by changes in their projected number or by changes in their exhaust characteristics. However, the same statement cannot

be made for SST's and other high-altitude aircraft. As new projections of their numbers and other characteristics become available, the estimates of $\Delta\tau$ attributable to such aircraft should be revised and their impact reevaluated.

REFERENCES

F-1. Manabe, Syakuro; and Wetherald, Richard T.: Thermal Equilibrium of the Atmosphere With a Given Distribution of Relative Humidity. J. Atmos. Sci., vol. 24, no. 3, May 1967, pp. 241-259.

F-2. Rasool, S. I.; and Schneider, S. H.: Atmospheric Carbon Dioxide and Aerosols: Effects of Large Increases on Global Climate. Science, vol. 173, no. 3992, July 9, 1971, pp. 138-141.

F-3. Sagan, Carl; and Pollack, James B.: Anisotropic Nonconservative Scattering and the Clouds of Venus. J. Geophys. Res., vol. 72, no. 2, Jan. 15, 1967, pp. 469-477.

F-4. Yamamoto, Giichi; and Tanaka, Masayuki: Increase of Global Albedo Due to Air Pollution. J. Atmos. Sci., vol. 29, no. 8, Nov. 1972, pp. 1405-1412.

F-5. Chandrasekhar, Subrahmanyan: Radiative Transfer. Dover Publications (New York), 1960, pp. 89-104.

F-6. Braslau, Norman; and Dave, J. V.: Effect of Aerosols on the Transfer of Solar Energy Through Realistic Model Atmosphere, Parts I and II. J. Appl. Meteorol., vol. 12, no. 4, June 1973, pp. 601-619.

F-7. Wang, Wei-Chyung; and Domoto, Gerald A.: The Radiative Effect of Aerosols in the Earth's Atmosphere. J. Appl. Meteorol., vol. 13, no. 5, Aug. 1974, pp. 521-534.

F-8. Luther, F. M.: Relative Influence of Stratospheric Aerosols on Solar and Longwave Radiative Fluxes for a Tropical Atmosphere. J. Appl. Meteorol., vol. 15, Sept. 1976, pp. 951-955.

F-9. Pollack, James B.; and Toon, Owen B.: A Study of the Effect of Stratospheric Aerosols Produced by SST Emissions on the Albedo and Climate of the Earth. Proceedings of the Third Conference on the Climatic Impact Assessment Program, Anthony J. Broderick and Thomas M. Hard, eds., DOT-TSC-OST-74-15, 1974, pp. 457-460.

F-10. Toon, O. B.; and Pollack, J. B.: A Global Average Model of Atmospheric Aerosols for Radiative Transfer Calculations. J. Appl. Meteorol., vol. 15, Mar. 1976, pp. 225-246.

F-11. Lacis, Andrew A.; and Hansen, James E.: A Parameterization for the Absorption of Solar Radiation in the Earth's Atmosphere. J. Atmos. Sci., vol. 31, no. 1, Jan. 1974, pp. 118-133.

F-12. Hansen, James E.: Radiative Transfer by Doubling Very Thin Layers. Astrophys. J., vol. 155, Feb. 1969, pp. 565-573.

F-13. Domoto, G. A.: Frequency Integration for Radiative Transfer Problems Involving Homogeneous Non-Gray Gases: The Inverse Transmission Function. J. Quant. Spectrosc. Radiat. Transfer, vol. 14, 1974, pp. 935-942.

F-14. The Stratosphere Perturbed by Propulsion Effluents. Climatic Impact Assessment Program Monograph 3, DOT-TST-75-53, Sept. 1975.

F-15. Ferry, Guy V.; and Lem, Homer Y.: Aerosols at 20 Kilometers Altitude. Paper presented at the Second International Conference on Environmental Impact of Aerospace Operations in the High Atmosphere (San Diego, Calif.), July 8-10, 1974.

F-16. Strand, L. D.; and Varsi, G.: Airborne Measurements of Particulates From Solid Rocket Boosters. Proceedings JANNAF 8th Plume Technology Meeting, 1974, pp. 141-163.

F-17. Hofmann, D. J.; Carroll, D. E.; and Rosen, J. M.: Estimate of the Contribution of the Space Shuttle Effluent to the Natural Stratospheric Aerosol. Geophys. Res. Letters, vol. 2, 1975, pp. 113-116.

F-18. Diermendjian, D.: Electromagnetic Scattering on Spherical Polydispersions. American Elsevier Publishing Co., 1969, p. 78.

F-19. Raschke, Ehrhard; Vonder Haar, Thomas H.; Bandeen, William R.; and Pasternak, Musa: The Annual Radiation Balance of the Earth-Atmosphere System During 1969-70 From Nimbus 3 Measurements. J. Atmos. Sci., vol. 30, no. 3, Apr. 1973, pp. 341-364.

F-20. Irvine, William M.; and Pollack, James B.: Infrared Optical Properties of Water and Ice Spheres. Icarus, vol. 8, no. 2, Mar. 1968, pp. 324-360.

F-21. McClatchey, R. A.; Fenn, R. W.; et al.: Optical Properties of the Atmosphere. AFCRL Rep. 71-0279, May 1971.

F-22. Pollack, James B.: A Nongrey CO_2-H_2O Greenhouse Model of Venus. Icarus, vol. 10, no. 2, Mar. 1969, pp. 314-341.

F-23. Houghton, James T.: The Absorption of Solar Infra-Red Radiation by the Lower Stratosphere. Quart. J. Roy. Meteorol. Soc., vol. 89, no. 381, July 1963, pp. 319-331.

F-24. Lindzen, Richard S.; and Will, Douglas I.: An Analytic Formula for Heating Due to Ozone Absorption. J. Atmos. Sci., vol. 30, no. 3, Apr. 1973, pp. 513-515.

F-25. Van de Hulst, H. C.: Scattering in the Atmosphere of the Earth and the Planets. The Atmospheres of the Earth and Planets, Gerard P. Kuiper, ed., Univ. of Chicago Press, 1952, pp. 49-111.

F-26. Pollack, James B.: Temperature Structure of Nongrey Planetary Atmospheres. Icarus, vol. 10, no. 2, Mar. 1969, pp. 301-313.

F-27. Pollack, James B.; and Ohring, George: A Numerical Method for Determining the Temperature Structure of Planetary Atmospheres. Icarus, vol. 19, no. 1, May 1973, pp. 34-42.

F-28. Davis, Paul A.; and Viezee, William: A Model for Computing Infrared Transmission Through Atmospheric Water Vapor and Carbon Dioxide. J. Geophys. Res., vol. 69, no. 18, Sept. 15, 1964, pp. 3785-3794.

F-29. Palmer, C. Harvey, Jr.: Experimental Transmission Functions for the Pure Rotation Band of Water Vapor. J. Opt. Soc. America, vol. 50, no. 12, Dec. 1960, pp. 1232-1242.

F-30. Stauffer, Frederic R.; and Walsh, T. E.: Transmittance of Water Vapor — 14 to 20 Microns. J. Opt. Soc. America, vol. 56, no. 3, Mar. 1966, pp. 401-405.

F-31. Stull, V. R.; Wyatt, P. J.; and Plass, G. N.: Infrared Transmission Studies. Volume III: The Infrared Absorption of Carbon Dioxide. Aeronutronic Rep. SSD-TDR-62-127, Jan. 1963.

F-32. Wyatt, P. J.; Stull, V. R.; and Plass, G. N.: Infrared Transmission Studies. Volume II: Infrared Absorption of Water Vapor. Aeronutronic Rep. SSD-TDR-62-127, Sept. 1962.

F-33. U.S. Standard Atmosphere Supplements, 1966. Government Printing Office, 1966.

F-34. Bryson, R. A.: A Perspective on Climatic Change. Science, vol. 184, no. 4138, May 17, 1974, pp. 753-760.

F-35. Budyko, M. I.: Climatic Change. Soviet Geog.: Rev. Transl., vol. 10, 1969, pp. 429-457.

F-36. Sellers, William D.: A New Global Climatic Model. J. Appl. Meteorol., vol. 12, no. 2, Mar. 1973, pp. 241-254.

F-37. Panel on Propulsion Effluents, J. M. English, General Chairman: Propulsion Effluents in the Stratosphere. Climatic Impact Assessment Program Monograph 2, DOT-TST-75-52, Sept. 1975.

F-38. Toon, Owen B.; and Pollack, James B.: Physical Properties of the Stratospheric Aerosols. J. Geophys. Res., vol. 78, no. 30, Oct. 20, 1973, pp. 7051-7056.

TABLE F-I.- FACTORS USED TO CALCULATE THE STEADY-STATE MASS OF AEROSOLS INTRODUCED INTO THE STRATOSPHERE BY VARIOUS VEHICLES

Factor		SST and other high-altitude aircraft					Space Shuttle 1990 nominal Al_2O_3 emission rate, kg/yr
Altitude range, km (ft)	Residence time, yr	Conversion efficiency	SO_2 emission rate, kg/yr, in -				
			1990 nominal	1990 max.	2000 nominal	2000 max.	
9 to 12 (26 000 to 36 000)	0.160	0.810	4.37×10^{7}	8.16×10^{7}	7.50×10^{7}	1.939×10^{8}	- -
12 to 15 (36 000 to 47 000)	.454	.806	1.53×10^{7}	2.85×10^{7}	2.98×10^{7}	7.61×10^{7}	1.4×10^{6}
15 to 18 (47 000 to 58 000)	.978	.869	7.0×10^{5}	1.4×10^{6}	1.8×10^{6}	5.6×10^{6}	1.2×10^{6}
18 to 21 (58 000 to 68 000)	1.715	.945	1.46×10^{7}	3.74×10^{7}	1.10×10^{8}	1.10×10^{8}	1.1×10^{6}

TABLE F-II.- ESTIMATES OF THE STRATOSPHERIC OPTICAL DEPTH PERTURBATION CAUSED BY VARIOUS VEHICLES

[Northern Hemisphere][a]

Vehicle	Time frame	$\Delta\tau$
SST's and other high-altitude aircraft	1990 nominal	4.9×10^{-4}
	1990 max.	8.9×10^{-4}
	2000 nominal	1.1×10^{-3}
	2000 max.	3.3×10^{-3}
Space Shuttle	1990	[b] 3.3×10^{-5}

[a] Values for the Southern Hemisphere can be obtained by multiplying the tabulated numbers by three-sevenths.

[b] Adjusted as described in text.

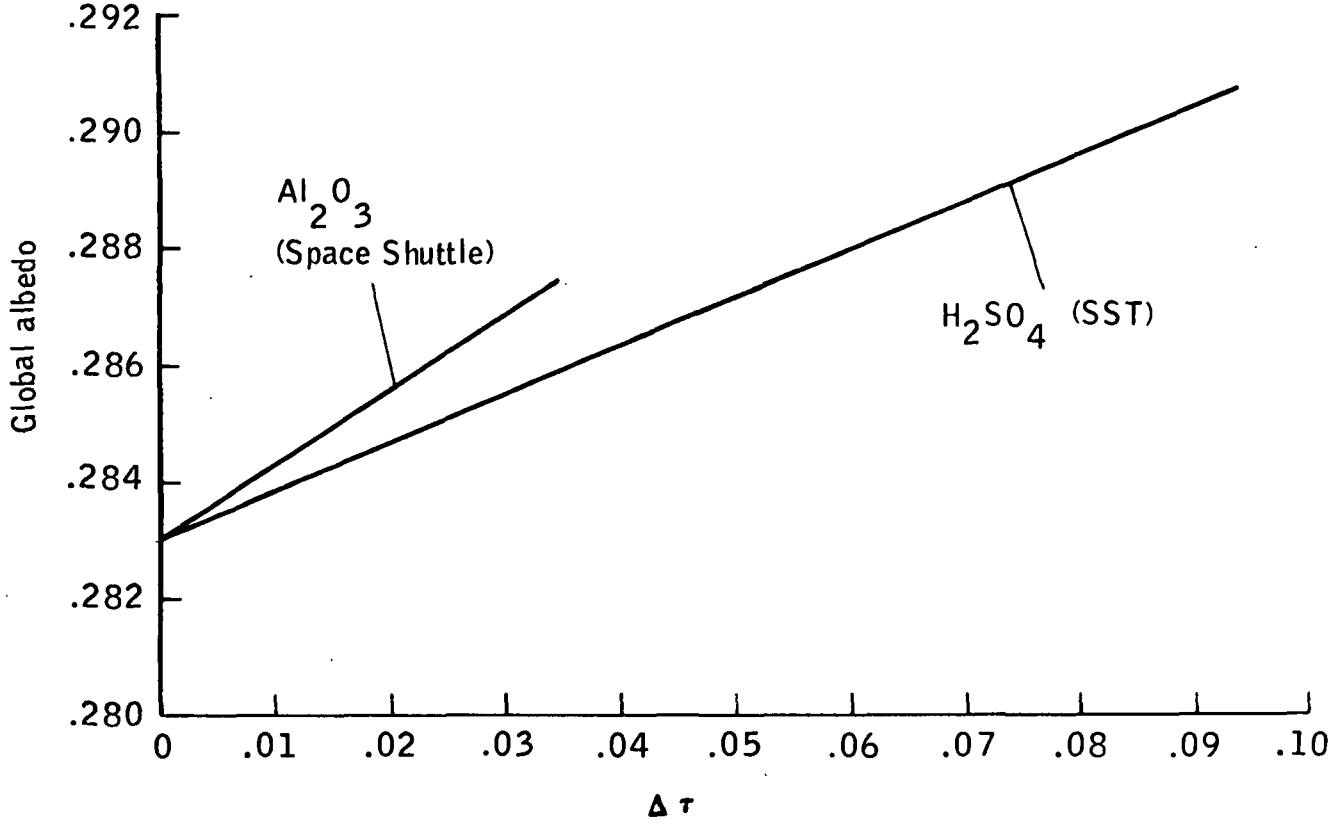

Figure F-1.- Dependence of global albedo on optical depth perturbation $\Delta\tau$ of H_2SO_4 and Al_2O_3 aerosols.

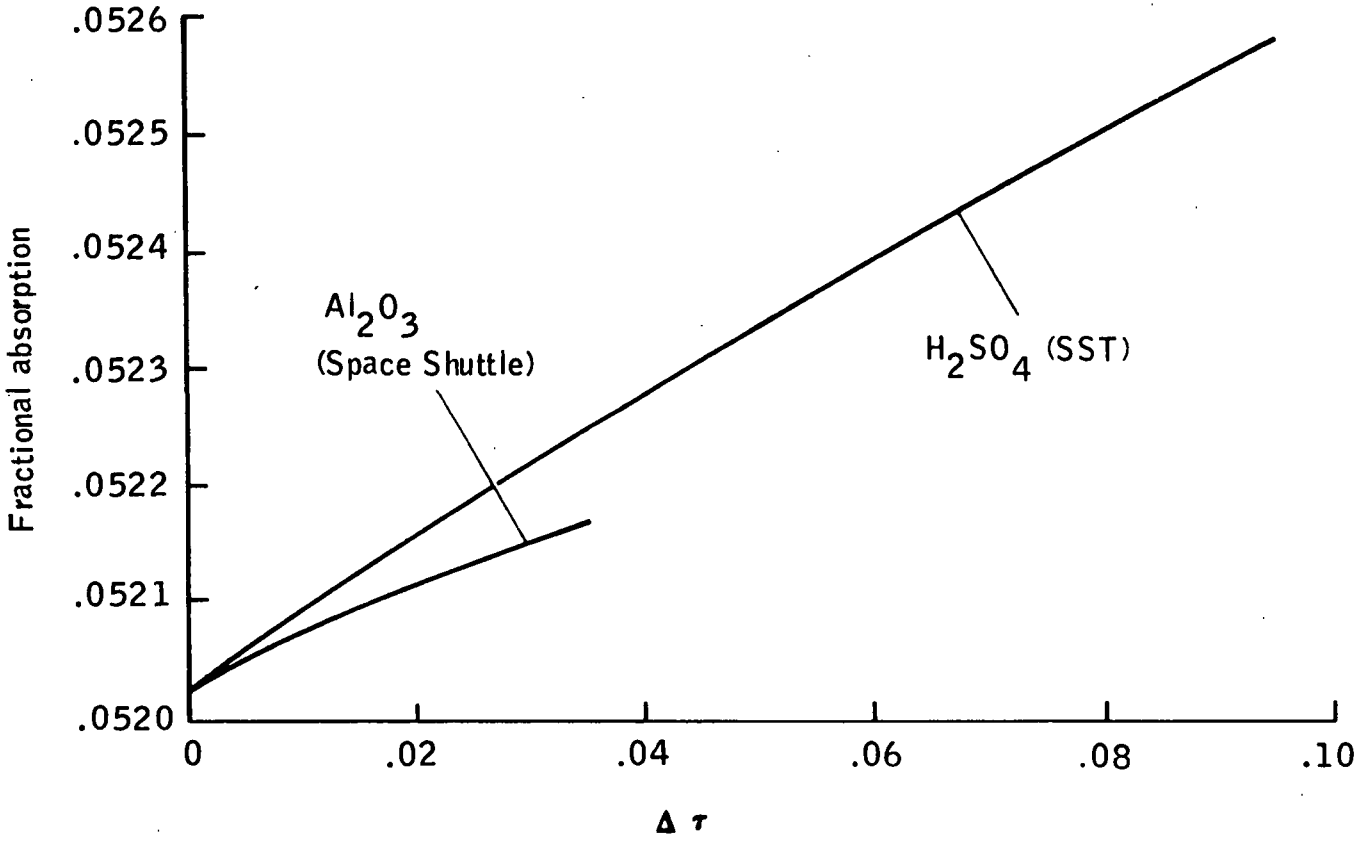

Figure F-2.- Dependence of fractional absorption in the stratosphere on optical depth perturbation of H_2SO_4 and Al_2O_3 aerosols.

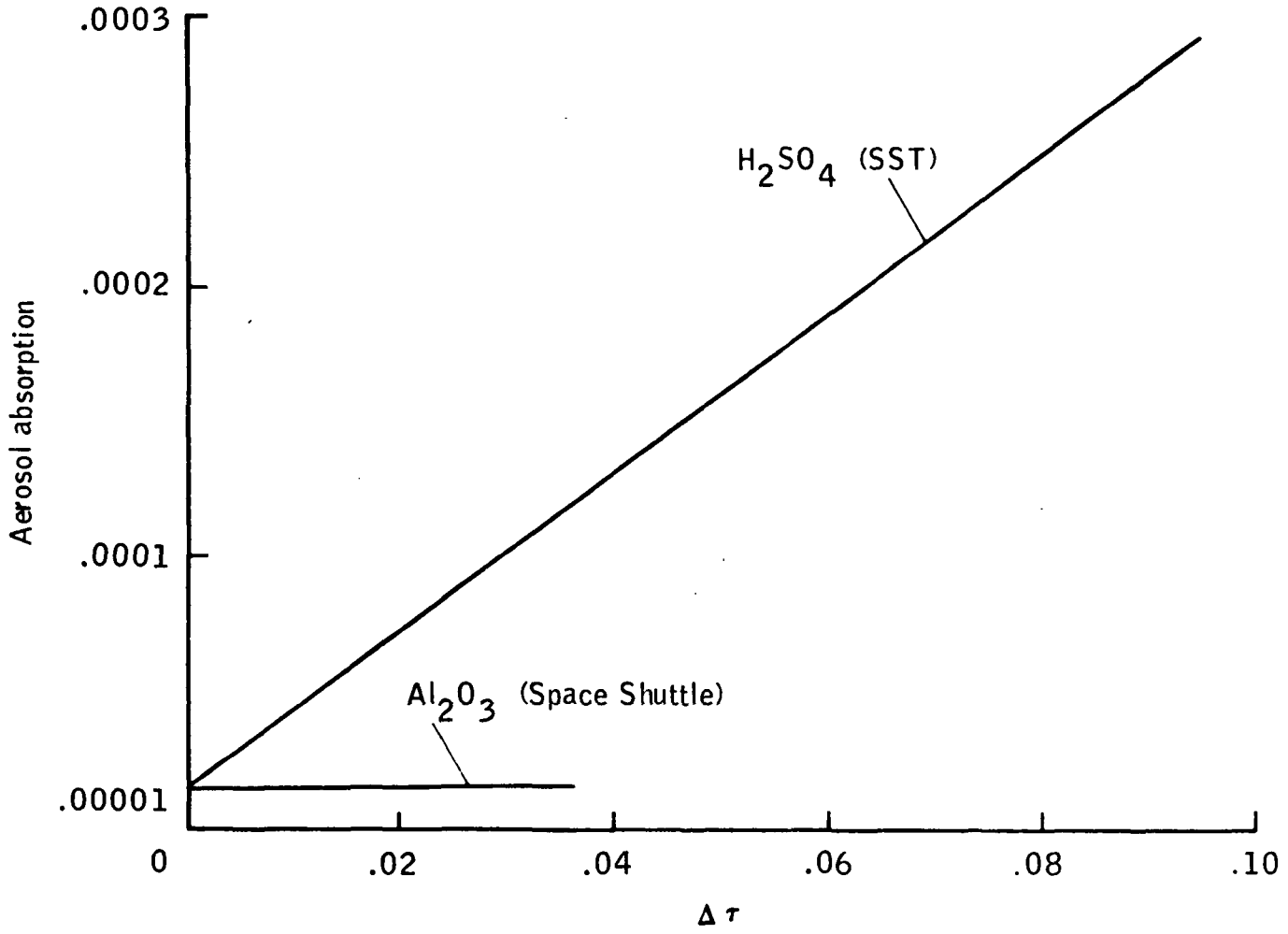

Figure F-3.- Dependence of fractional aerosol absorption in the stratosphere on optical depth perturbation of H_2SO_4 and Al_2O_3 aerosols.

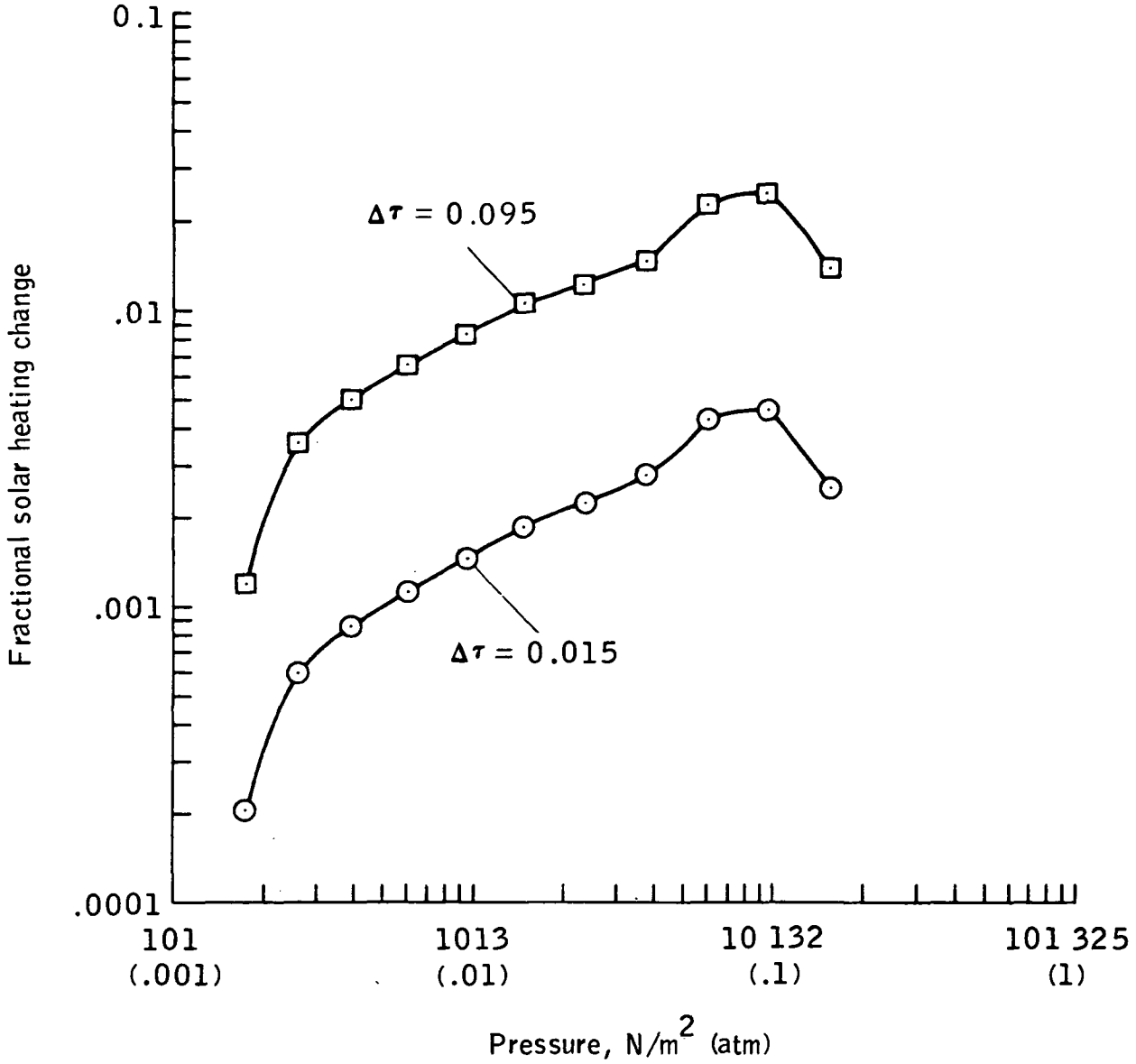

Figure F-4.- Fractional change in solar heating as a function of pressure in the stratosphere for SST-produced H_2SO_4.

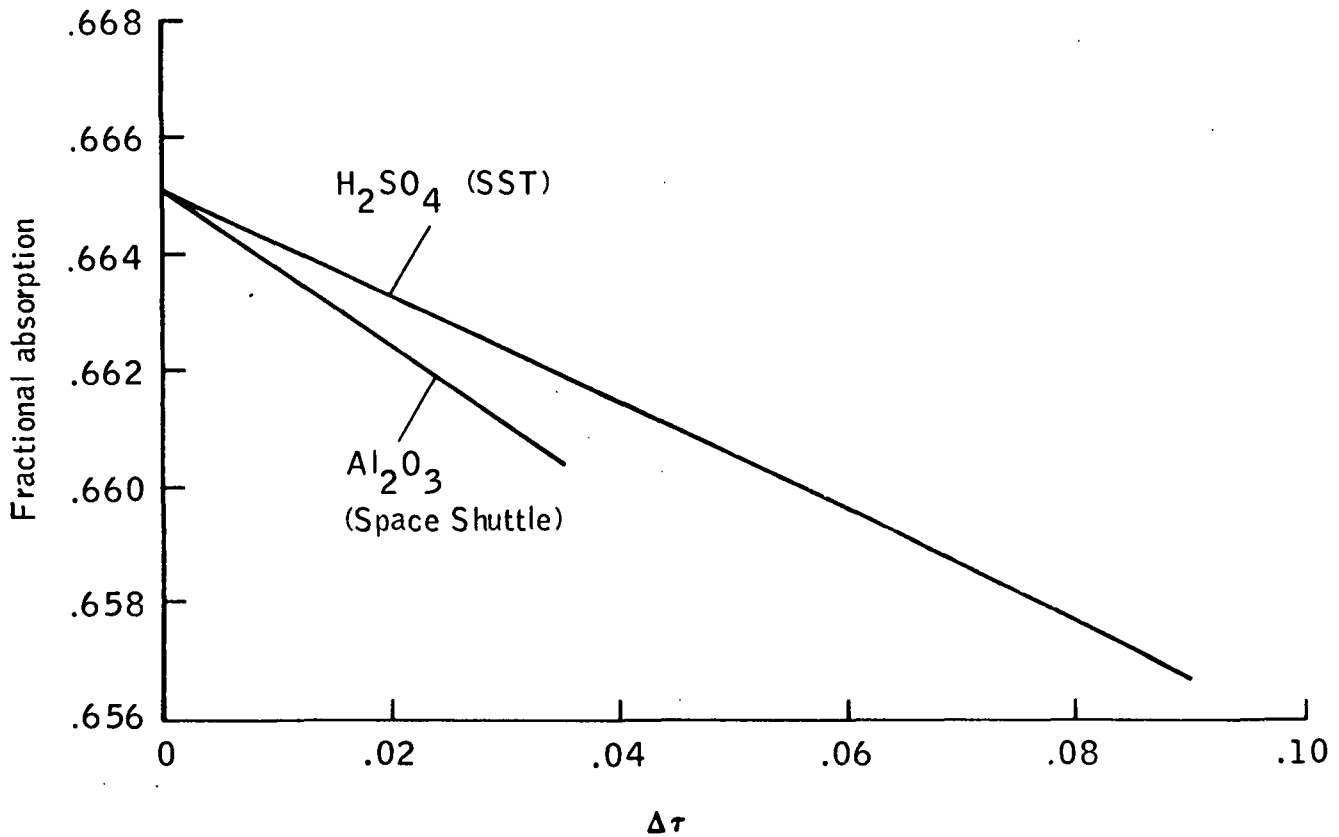

Figure F-5.- Fractional absorption below the tropopause as a function of aerosol optical depth perturbation of H_2SO_4 and Al_2O_3 aerosols.

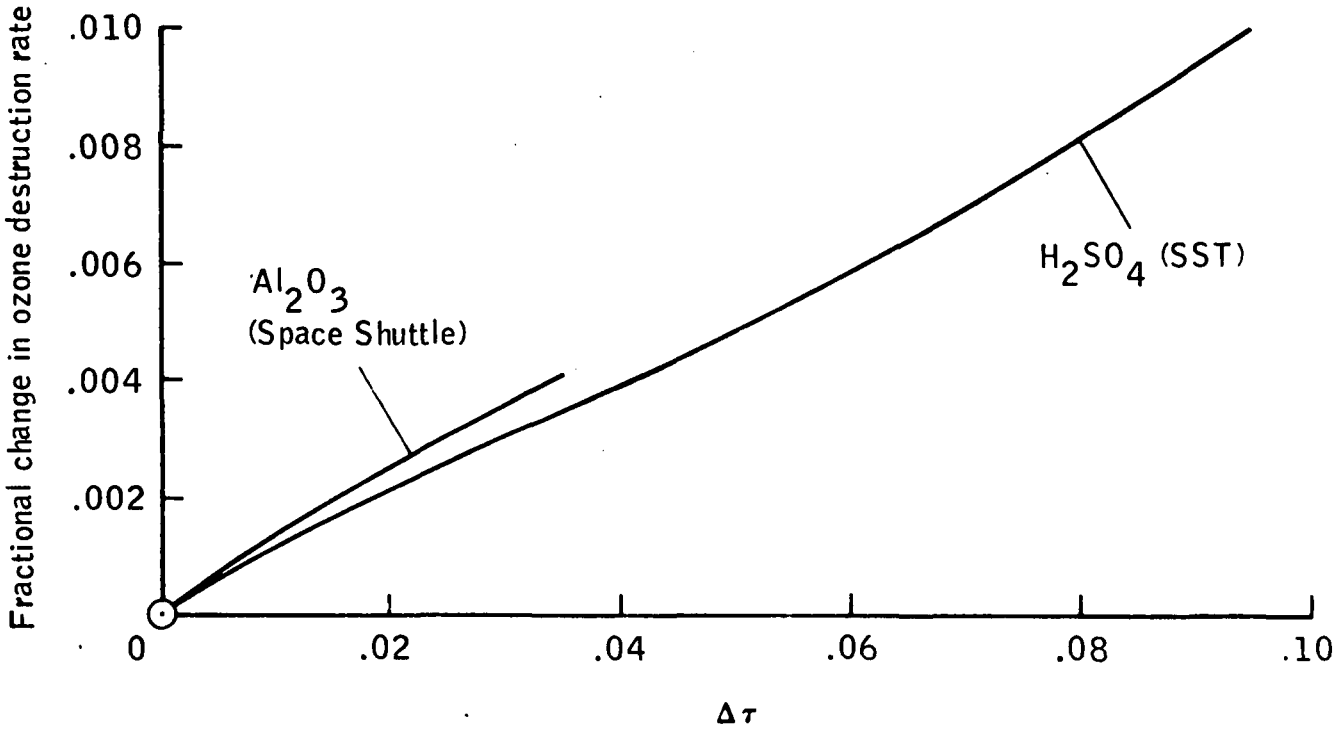

Figure F-6.- Fractional change in O_3 destruction rate for whole atmospheric column as a function of optical depth perturbation of H_2SO_4 and Al_2O_3 aerosols. Changes are referenced to values for unperturbed atmosphere.

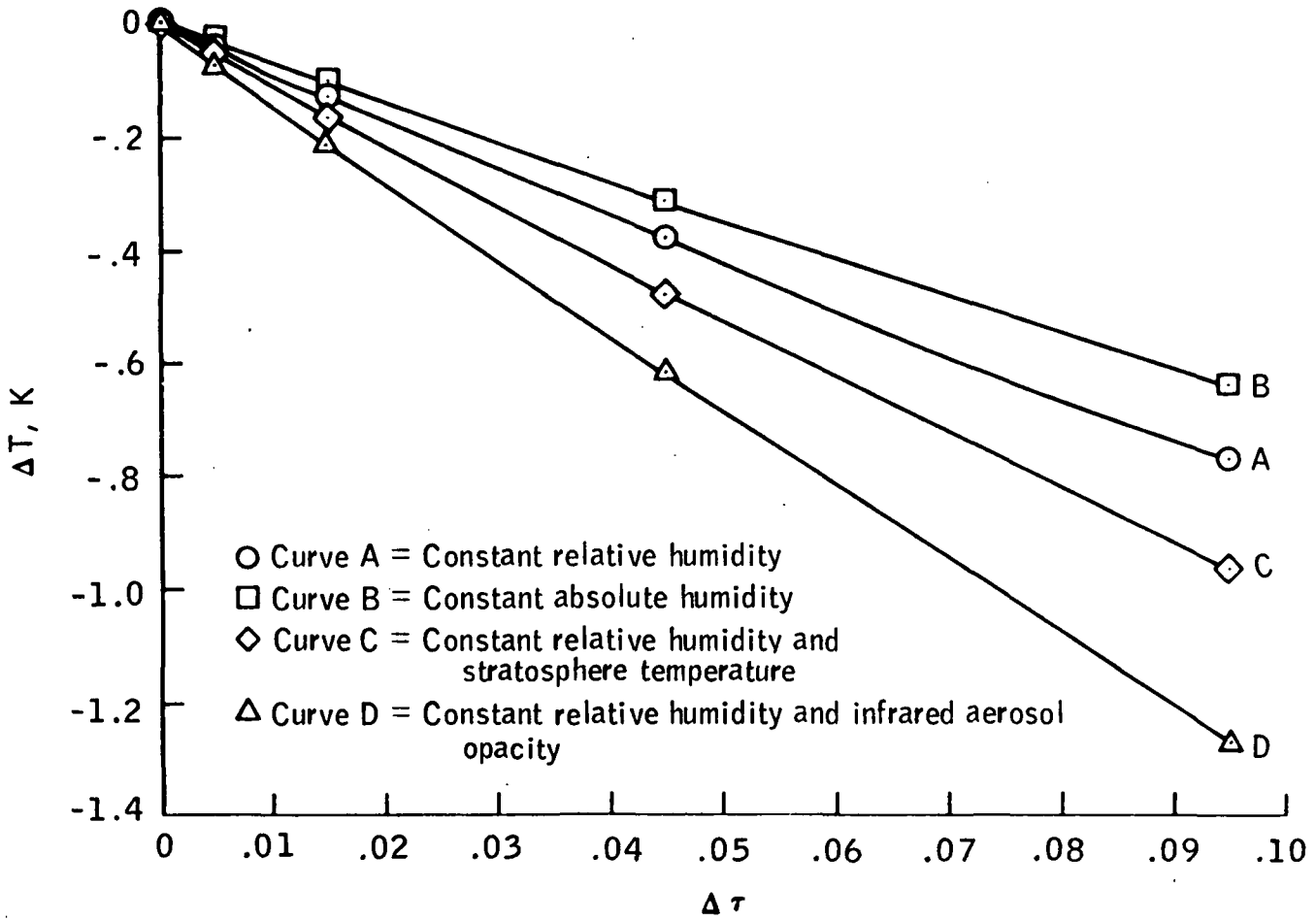

Figure F-7.- Change in mean surface temperature ΔT as a function of optical depth perturbation of SST-produced H_2SO_4 aerosols.

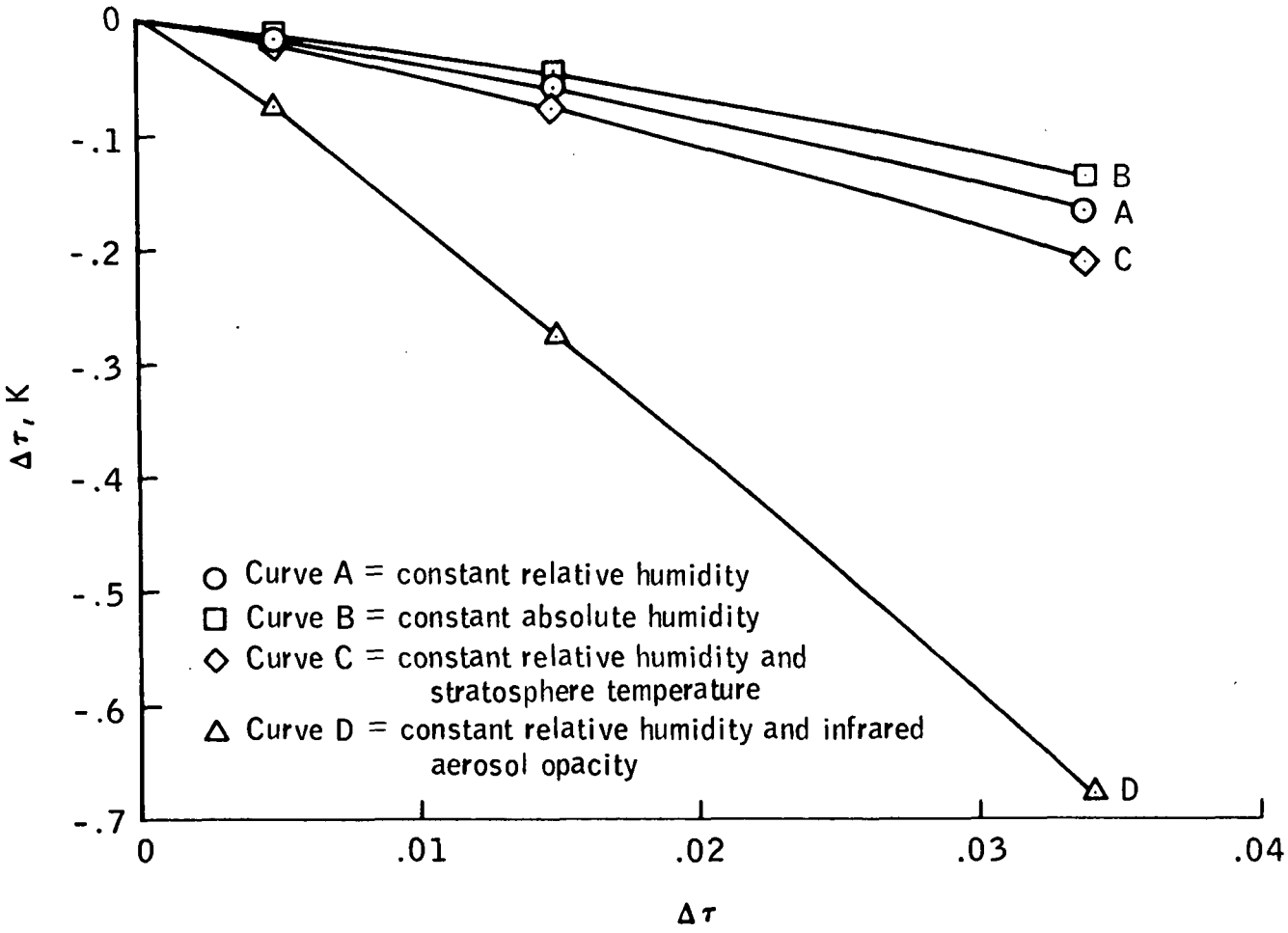

Figure F-8.- Change in mean surface temperature as a function of optical depth perturbation of Space Shuttle Al_2O_3 aerosols.

APPENDIX G

NO_x DEPOSITION IN THE STRATOSPHERE FROM THE SPACE SHUTTLE ROCKET MOTORS

By H. S. Pergament,[a] R. I. Gomberg,[b] and I. G. Poppoff[c]

APPROACH

The determination of the amount of oxides of nitrogen (NO_x) deposited in the stratosphere by the Space Shuttle solid rocket motors has been based primarily on an extensive series of calculations using state-of-the-art computer codes to determine both the mass flow of NO_x leaving the nozzle and the mass of NO_x produced in the Space Shuttle plume as a result of shocks and afterburning. This is the first attempt to predict total NO_x deposition rates in the stratosphere using the new calculation procedures described in references G-1 and G-2 and elsewhere.[2] Results are reported (refs. G-1 and G-2) for the baseline propellant at 30-kilometer (95 000 foot) altitude; calculations were also made at 15-kilometer (47 000 foot) altitude using a similar procedure. Estimates of the NO_x deposition rate at 15 kilometers (47 000 feet) and 30 kilometers (95 000 feet) for the alternate "A" propellant have been made using a more simplified (and conservative) procedure than the one described in references G-1 and G-2 and elsewhere.[2] It should be stressed that, because both NO_x and hydrogen chloride (HCl) participate in the ozone (O_3) destruction cycle (NO_x less efficiently than HCl), the primary interest is in the ratio of NO_x to HCl deposition rates in the stratosphere.

Experimental verification of these calculations is limited; only a single field measurement of nitric oxide (NO) in the exhaust cloud of a Titan III booster has been taken at an 18-kilometer (58 000 foot) altitude. The NO_x measurements have also been made within Titan III ground clouds. The usefulness of these data in verifying the predicted NO_x deposition rates is discussed in the following sections.

---

[a]AeroChem Research Laboratories, Inc.

[b]NASA Langley Research Center.

[c]NASA Ames Research Center.

[2]R. D. Thorpe, H. S. Pergament, and B. Hwang: NO_x Deposition in the Stratosphere by the Space Shuttle Solid Rocket Motors. Proceedings of the 9th JANNAF Plume Technology Meeting, in press.

CALCULATED RESULTS FOR BASELINE PROPELLANT

The total mass flow of NO_x leaving the Space Shuttle plume and deposited in the stratosphere is determined by first calculating the amount of NO_x exiting from the solid rocket motors and by then calculating the enhancement in NO_x caused by plume shocks and afterburning of the hydrogen (H_2) and carbon monoxide (CO) in the exhaust products with ambient air. Because of the relatively slow rate of NO_x depletion in the nozzle, as determined by a nonequilibrium chemistry analysis, the mass fraction of NO_x at the nozzle exit plane is considerably higher than that resulting from standard thermochemical equilibrium calculations. Table 5-I gives the mass flow of NO_x leaving the two nozzles in grams per second and in parts per million by volume; by this means, the NO_x mass flow is related to the total propellant mass flow. The results reported (refs. G-1 to G-3 and elsewhere[2]) show that shocks and afterburning will enhance the mass flow of NO_x by a factor of 1.6 at 30 kilometers (95 000 feet). A similar analysis for 15 kilometers (47 000 feet) shows the enhancement factor to be 4.8. This increase with decreasing altitude is due both to a greater percentage of mass flow passing through the strong plume shock and to the higher temperatures produced in the afterburning region of the plume. The total mass of NO_x deposited per second at 15 kilometers (47 000 feet) and 30 kilometers (95 000 feet) is also shown in table 5-I.

COMPARISON OF NO_x DEPOSITION FROM BASELINE AND ALTERNATE PROPELLANTS

The procedure used to evaluate the NO_x deposition rate from the alternate propellant was to evaluate the manner in which differences between the alternate and baseline propellants could influence both the mass flow of NO_x leaving the nozzle and the plume enhancement. Because of the large amount of ammonium nitrate in the alternate propellant, the possibility that significantly large nonequilibrium levels of NO_x could be produced in the combustion chamber was investigated. Nonequilibrium chemical calculations were made at nominal chamber conditions, assuming (for conservatism) that 25 percent of the N in the propellant was initially converted to NO. (At equilibrium, only 0.1 percent of the N in the propellant is converted to NO.) The results of these nonequilibrium chemical calculations indicate that at the chamber temperature of 2690 K, the decay of NO_x to its equilibrium value occurs in approximately 10

---

[2]R. D. Thorpe, H. S. Pergament, and B. Hwang: NO_x Deposition in the Stratosphere by the Space Shuttle Solid Rocket Motors. Proceedings of the 9th JANNAF Plume Technology Meeting, in press.

milliseconds, which is considerably less than typical combustion chamber residence times. Thus, the alternate propellant NO mass fraction will reach equilibrium value in the chamber at a factor of approximately 50 less than the calculated chamber value for the baseline propellant.

The other major difference between the two propellants is that the alternate propellant contains approximately 15 percent (molar) more fuel (H_2 + CO) in the exhaust products. This increase in fuel will result in more intense afterburning. The effects of shocks in enhancing the NO_x mass flow in the plume should be about the same for each propellant.

Table 5-II gives the results of NO_x deposition calculations for the alternate propellant, compared with the corresponding values for the baseline propellant. The combined effects of shocks and afterburning result in larger plume NO_x production rates (and thus a larger plume enhancement) for the alternate propellant. These results demonstrate that the nozzle exit plane mass flow is not necessarily a good indicator of the total NO_x deposition rate.

INTERPRETATION OF FIELD MEASUREMENTS

Very limited field measurements exist with which to compare the NO_x deposition rates predicted by the model. A single set of flight data was obtained by flying a U-2 aircraft equipped with an NO measurement device through the cloud trailing a Titan III launch vehicle at an altitude of 18 kilometers (58 000 feet). In addition, considerable data are available on the total amount of NO_x contained within ground clouds following Titan III launches.

Stratospheric Measurements

The Titan III is the largest solid rocket using the same fuel as the Space Shuttle solid rocket boosters and, except for the lack of the parallel hydrogen- and oxygen-fueled rocket motor exhaust from the upper stage, can serve as a model for Space Shuttle launches. Titan III thrust is 40 percent of the Space Shuttle solid booster motor thrust. Several attempts have been made to determine stratospheric exhaust trail properties of Titan III-C rockets launched at the Western Test Range. These measurements were made using sampling instruments carried onboard high-altitude aircraft. In April 1974, a successful measurement was made in a Titan III exhaust trail at an altitude of 18 kilometers (58 000 feet) some 13 minutes after launch by Loewenstein and Savage of the NASA Ames Research Center (ARC) using equipment carried onboard the ARC U-2. The instruments measured a reduction of O_3 greater than 40 percent below the background level and an average of 12 parts per billion by volume of NO, approximately 30 times the ambient level. The NO instrument works on the principle of chemiluminescent reaction with an onboard O_3 reactant gas;

the measurement must be treated as an upper limit since it is not known whether other exhaust trail species have residual chemiluminescent reactions.

The duration of the NO signal during exhaust trail penetration by the aircraft suggested that the horizontal dimension was 1600 meters (5200 feet). Ground-based photographs, on the other hand, showed that the exhaust trail had irregular boundaries, moved in different directions in various altitude regions because of winds aloft, and appeared to have a horizontal dimension of approximately 3000 meters (9800 feet) at the altitude and time of aircraft penetration.

A major problem in the interpretation of the data in terms of the NO deposition rate is determining the amount of conversion of NO to nitrogen peroxide during the 13 minutes in which the exhaust cloud mixed with the ambient air before the measurements were made. This problem, in conjunction with the uncertainty of the other chemiluminescent reactions noted, makes interpretation of the measured value in terms of an NO_x deposition rate excessively difficult.

Ground Cloud Measurements

A rough indicator of the adequacy of the chemistry model in the stratospheric calculations can be obtained by a comparison between NO_x data obtained in Titan III ground clouds and calculations with a simplified rocket plume code which used the identical chemistry model. The results of this comparison show that the predicted NO_x deposition is within 30 percent of the measurements, an indication that the overall chemistry model used to predict NO_x production rates in afterburning Space Shuttle plumes is reasonably accurate.

DEPOSITION RATES FOR NO_x and HCl

A comparison between NO_x and HCl deposition rates for both the baseline and alternate propellants is given in table 5-III. The results show that the amount of NO_x deposited in the stratosphere is negligibly small compared to the amount of HCl. In fact, even if the NO_x deposition rate predictions are low by as much as an order of magnitude (an unlikely possibility), the levels would still be negligible for the baseline propellant and the alternate propellant at 30 kilometers (95 000 feet).

REFERENCES

G-1. Pergament, H. S.; and Thorpe, R. D.: NO_x Deposited in the Stratosphere by the Space Shuttle. NASA CR-132715, 1975.

G-2. Pergament, H. S.; Thorpe, R. D.; and Hwang, B.: NO_x Deposited in the Stratosphere by the Space Shuttle Solid Rocket Motors. NASA CR-144928, 1975.

G-3. Stewart, R. B.; and Gomberg, R. I.: The Production of Nitric Oxide in the Troposphere as a Result of Solid Rocket Motor Afterburning. NASA TN D-8137, 1976.

APPENDIX H

MEDICAL/BIOLOGICAL EFFECTS OF INCREASED uv RADIATION RESULTING FROM O_3 REDUCTION

By D. S. Nachtwey[a]

Space Shuttle operations with the baseline solid rocket motor are estimated to reduce the stratospheric ozone (O_3) column thickness by 0.2 percent with an uncertainty of a factor of 3. A percentage reduction in the O_3 column can be converted by a series of assumptions and calculations into a rough estimate of a percentage increase in biologically harmful ultraviolet (BHuv) radiation from the Sun. The rule of thumb that emerges from the assumptions and calculations is that for O_3 reductions of less than 5 percent, a 1-percent decrease in O_3 column thickness represents a 2-percent increase in BHuv (refs. H-1 to H-3). The 1-percent/2-percent rule of thumb (also referred to as an optical amplification factor of 2) is based on calculations involving the increased amount of shorter wavelength uv radiations (the band of 285 to 320 nanometers designated uv-B) penetrating through a reduced O_3 layer and the increased biological effectiveness of those shorter wavelength radiations.

Not all wavelengths of uv are equally effective in producing biological effects; the shorter wavelengths are generally more effective. The relationship of biological effectiveness to wavelength is termed an action spectrum. The calculation of the amount of BHuv involves the summation of all wavelengths weighted by the action spectrum. The optical amplification factor is calculated by dividing the percentage increase in BHuv by the percentage decrease in O_3. The true optical amplification factor for O_3 reduction varies with initial O_3 level, solar zenith angle, and percentage O_3 reduction and on the action spectrum for the particular biological effect. The action spectrum for most plant effects and for human skin cancer induction is unknown; however, many photobiologists believe that the human sunburn action spectrum is an adequate approximation for most purposes. Because of the variation and the unknowns, the optical amplification factor of 2 is widely used. It should be emphasized, however, that near the Equator where the current levels of uv-B are already high, the natural average O_3 level is low, and the solar zenith angle at midday is low (Sun nearly overhead), the true optical amplification factor for a smaller O_3 reduction (e.g., 1 percent) may be closer to 1.2 to 1.3 for sunburning uv than it is to 2.

---

[a]NASA Lyndon B. Johnson Space Center.

Applying the 1-percent/2-percent rule of thumb, 0.2 percent O_3 reduction obviously converts to a 0.4-percent increase in BHuv. It should be emphasized that such an increase in BHuv radiation does not necessarily mean that a 0.4-percent increase in some biological harm will occur. The biological response to BHuv is not necessarily linearly related to dose; in some cases, the dose of BHuv has to be greater than some threshold amount before it causes a perceptible effect (e.g., sunburn).

The impact on the biosphere of a 0.4-percent increase in BHuv radiation can be assessed from extrapolations of the relatively limited experimental data obtained with high doses of simulated solar BHuv (ref. H-4). In addition, a more intuitively convincing assessment of the effects of such an increase in BHuv can be based on observations made during "nature's experiment": the effects or lack of effects on organisms and ecosystems of exposures to the natural, wide variations in solar BHuv irradiances. The highlights of such an assessment follow.

First, some organisms can be eliminated from concern. Not all organisms in the biosphere are vulnerable to an increase in BHuv. Most animals, including invertebrates, avoid the Sun by living underground or in the shade during at least the heat of the day. The important vulnerable components of the biosphere are human beings, unshaded agricultural plants and penned livestock, and natural terrestrial vegetation.

The effects of a 0.4-percent increase in BHuv on the vulnerable components will not be detectable. In the first place, the current natural levels of BHuv fluctuate widely because of fluctuations in O_3 levels[10] and because of clouds and suspended aerosols. Second, even in controlled experiments, the responses or organisms to BHuv are highly variable; biological systems are "noisy detectors." Coefficients of variation of 15 to 20 percent are common. Third, superimposed on the effects of BHuv are the effects of other factors to which plants are exposed such as temperature, moisture, nutrition, competition, and predation (e.g., refs. H-5 and H-6). However, the fact that a cause-and-effect relationship for an increase in BHuv cannot be established

---

[10] Measurements from the BHuv instrument on the Nimbus 4 satellite show that the average O_3 over the entire globe fluctuated during a period from April 20 to July 20 with a standard deviation of ±2.4 percent. The range of values from the mean (31 kilopascal-centimeters (306 milliatmosphere-centimeters)) was ±6.2 percent. On one particular day in April 1969, there was a 300-percent difference between the maximum O_3 level (61 kilopascal-centimeters (600 milliatmosphere-centimeters) in northern Russia) and the minimum O_3 level (20 kilopascal-centimeters (200 milliatmosphere-centimeters) near New Guinea). Measurements from ground stations show that variations of approximately ±10 percent can occur in a single day with the movement of a weather front. The monthly averages at individual stations (e.g., Arosa, Switzerland) vary by ±30 percent throughout a year. The year-to-year range for a particular month can be approximately ±5 percent.

does not mean that an increase in BHuv can be ruled out as a contributor to some deleterious event; lack of detectability of an effect is not equatable with a lack of effect.

Even an undetectable effect can be estimated by extrapolation from experiments at high dosages, although such estimates have a great uncertainty. Such an analysis of experimental data (refs. H-7 and H-8) indicates that the probability is very low that an average 0.4-percent increase in BHuv would have any effect at all on plants or ecosystems. It can be demonstrated experimentally that unnaturally high levels of BHuv can be tolerated by many organisms with no significant effect. On the other hand, it can be demonstrated experimentally that current levels of solar BHuv can be detrimental to some organisms that thrive in nature. These findings indicate that organisms have evolved strategies for coping with the harmful uv radiation to which they are exposed. Many of the mechanisms involved in the strategies for coping have been documented. Some examples are

1. Behavioral avoidance (e.g., nocturnal behavior or complete avoidance by living underground, deep in the water, or under trees)

2. Screening of critical target molecules by hair, feathers, thick skin, pigment, or nonessential absorbing molecules in cells

3. Enzymatic systems that repair solar-uv-radiation-induced damage in critical molecules or that replace damaged molecules

4. At the population level, replacement of killed organisms by reproduction of survivors (This mechanism implies that some other factor limits the rate of population growth.)

It should be remembered that some organisms need tolerate only certain peak levels of BHuv for given times of the year because they may be dormant, resistant, or reduced in ecosystem importance at other times (e.g., grasses dry out during summer drought in some regions and various plants normally succeed one another in predominance throughout the year). Other organisms (such as trees) may accumulate damage over the entire year and on a year-by-year basis; but, in this regard, many trees, even evergreens, replace their more sensitive elements, their leaves, on a routine basis. In many cases, the buds for new leaves are in protected regions of the plant.

The key question in assessing the potential impact on a species of an increase in BHuv is whether the strategies for coping will be overwhelmed by a given increase or the excessive cost of coping may prevent continued competition. If nature as it exists today is assumed to represent the unperturbed situation, some estimates can be made about whether strategies for coping will be overwhelmed by uv increase from a given percentage reduction in the O_3 column thickness (e.g., by the 0.2 percent reduction at equilibrium from 60 Space Shuttle flights per year using solid rocket boosters with aluminum/ammonium perchlorate).

If an individual organism can tolerate the maximum amount of BHuv currently irradiating its locality at any particular time of year, then by deduction, the organism should be able to tolerate anything less than the maximum irradiance. By the same token, if an organic species can tolerate the BHuv at a low latitude and if all other conditions are equal, other members of the same species at higher latitudes (lower amount of BHuv) should be able to tolerate an increase in BHuv up to the tolerable amount demonstrated for the species. Clearly, all other conditions are never exactly equal, but certainly within the range of a few dozen miles, similar organisms under similar conditions (e.g., plants in similar soil and moisture) qualify for comparison. In this context, it is noteworthy that a 0.2-percent O_3 reduction over a point at latitude 35° N will lead to a maximum daily dose of BHuv (in July) that corresponds to the dosage currently received at a point only 23 kilometers (14 statute miles) south (calculated from a table in ref. H-3).

It should be emphasized that this consideration reflects a maximum calculated dose for cloudless skies; the frequent cloudy conditions in summer months are not considered. Moreover, these maximum daily doses are based on average O_3 column thicknesses; there will be temporary excursions beyond these levels.

These considerations emphasize the great variability of BHuv doses to which organisms are currently exposed without apparent detrimental effects. It seems reasonable that organisms in a given ecological niche are adapted or adaptable to cope with much more BHuv (up to some maximum tolerance level) than they are exposed to on the average. Organisms in nature will only show some response to an increase in BHuv when it exceeds their maximum tolerance level. Likely, the maximum tolerance level might be exceeded only when the increase in BHuv from some anthropogenic O_3 reduction is added on to a natural maximum BHuv irradiance resulting from a normal O_3 minimum occurring fortuitously at the time of maximum insolation and under cloudless skies.

Conversely, it might be argued that organisms respond to average BHuv levels. If so, then an increase in BHuv will add to the average and affect all exposed organisms at all latitudes. However, the similarity of physiological function in members of species living under widely divergent average BHuv irradiances suggests that organisms in general do not respond to average BHuv levels. Even complex ecosystems can be quite similar under very different average BHuv irradiances. Thus, it seems more likely that the maximum value of BHuv irradiance is the important factor.

Solar BHuv is probably not a limiting factor in the distribution of living organisms. (However, examination of high-altitude plants near the Equator may reveal some places where BHuv may be limiting.) Animal life is generally limited by food availability, which basically means vegetation. Total vegetative biomass is limited primarily by water; the new dry weight of aboveground biomass produced each year by plants is 0.001 of the weight of the annual rainfall (ref. H-6). This relationship holds for regions as diverse as the grasslands of southwest Africa, the creosote bush deserts of southern California, the beech forests of Central Europe, and the tropical rain forests of the Ivory Coast of Africa. The relationship generally holds everywhere severe

limitations of temperature or moisture are absent. Thus, biomass and productivity involving natural vegetation and associated animal life are very much more limited by water and temperature (see the following paragraph) than they are likely to be by BHuv.

Of course, the species composition or community structure of the biomass may respond to BHuv as one determining factor. Competition usually determines the community structure. If one organism in a particular niche has a slightly greater competitive edge, it will eventually predominate; but it will not necessarily eliminate other organisms. A change in some environmental factor may favor a different organism and thus lead to a community structure shift. Such shifts already occur normally and repeatedly in response to the numerous changing and interacting factors to which the component organisms of an ecosystem are exposed. Such changes are usually not detrimental, but they can be. For example, nutrient enrichment of lakes may favor algal blooms and microorganism growth that kills game fish. Solar BHuv radiation may be one factor in determining community structure; however, because of the numerous interacting factors, it is not likely that the influence of a small change, such as a 0.4-percent increase, can be estimated. Accordingly, it is probably impossible to establish a cause-and-effect relationship for a BHuv increase in any particular documented community structure shift that may occur. As discussed previously, it is more reasonable to implicate the major essentials, temperature and moisture, than it is to implicate BHuv.

As with natural ecosystems, agroecosystems are currently subjected to a much wider range of BHuv irradiances than would occur with an increase in BHuv from a 0.2-percent O_3 depletion. Extensive studies have shown that given sufficient water by natural means or by irrigation, the factor that limits the northern extent of growing regions for particular crops is usually temperature (including the number of frost-free days). The factor that usually limits the southern extent is also temperature. Yields of some plants decrease at lower latitudes partly because of water shortage and partly because of higher rates of respiration (and, therefore, less storage of photosynthate) at the higher summer temperatures. Some plant species are also limited by excessive amounts of light. In these species, it is primarily the visible and near-uv components that are responsible; the high-intensity visible light causes photo-oxidation of plant constituents. Usually, these plants are adapted to living under canopies of trees.

In addition to nature's experiments, preliminary short-term experiments performed in the field and in the laboratory show that many agricultural plants (15 of 24 tested) exposed to very high doses of simulated solar BHuv, under conditions otherwise approximating nature, showed no significant effect on dry weight productivity (refs. H-7, H-8, and H-9). If they showed no response to conditions simulating more than a 40-percent reduction in O_3 for the particular area, then it is unlikely that a 0.2-percent O_3 reduction will have an effect. In the organisms that did show an effect, there was a varying and sometimes inconsistent response to the high BHuv dose. Even in these cases, the response (percentage decrease in dry weight relative to controls) was not proportional to the increase in BHuv. Extrapolation using the

conservative assumption of linearity of effect with dose indicates that any decrease in productivity by the susceptible plants occurring as a result of a 0.2-percent O_3 reduction and a 0.4-percent increase in BHuv would amount to approximately 0.1 percent. This analysis leads to the conclusion that there is a very low probability that an average 0.4-percent increase in BHuv will have any effect on agricultural plants or natural ecosystems.

A 0.2-percent O_3 reduction and a 0.4-percent increase in BHuv may lead to some increase in the incidence of nonmelanoma skin cancer among susceptible individuals. The following factors support an association between nonmelanoma skin cancer incidence and BHuv.

1. Skin cancers are associated with exposed areas of skin (head, neck, arms, hands).

2. Less skin cancer is found among pigmented races than among Caucasians.

3. Among Caucasians, skin cancer incidence is associated with

   a. Decreased pigmentation

   b. Relative inability to tan

   c. Tendency to sunburn

   d. Increased exposure to the Sun (e.g., outdoor occupation)

   e. Increased light intensity (closer to the Equator)

4. Genetic diseases (albinism, xeroderma pigmentosum) which predispose victims to greater skin sensitivity to solar-uv-radiation damage also predispose them to skin cancer induction.

5. Skin cancer can be produced experimentally in albino and hairless mice and albino rats with uv radiation.

Because of the great variability of BHuv and biological responses mentioned previously, such an increase in skin cancer incidence will not be detectable. Moreover, the long latent period (20 to 60 years) for induction of skin tumors and the many other factors that already may be tending to change skin cancer incidence will also prevent detection. In this latter regard, epidemiological data indicate that certain types of skin cancer are already increasing independently of any known changes in BHuv. Such increases may continue. Factors possibly leading to an increased number of cases in the United States include the increased proportion of older people in the population; increased reporting of skin cancer because of Medicare; changing lifestyles, which currently involves more leisure time activity in the sunshine; and the net southward migration of the population. (Between 1940 and 1970, the center of population in the United States moved westward and approximately 55 kilometers (35 statute miles) south from latitude 39° N; this movement corresponds to approximately a 2-percent increase in annual dose of BHuv. Conversely, future decreases are also conceivable. Factors possibly leading

to a decreased incidence include action based on publicity-induced recognition of dangers of overexposure to the Sun and more accurate identification of susceptible individuals as a result of research generated by the O_3 reduction problem.

Despite the many unknowns involved in the relationship of BHuv and skin cancer incidence, several groups of investigators have made sincere attempts to estimate the possible increase in the number of skin cancer cases that might result from an O_3 reduction. The most widely publicized estimate is the following (from ref. H-10).

"Estimated Increases in Skin Cancer for Reductions in Equilibrium Ozone Concentrations — Although experimental studies on animals have demonstrated the link between UV-B radiation and skin cancer, human epidemiological data provide the best basis for quantitative estimates of cancer incidence in humans. The current understanding of the skin cancer development from an epidemiological standpoint, however, is somewhat limited. Answers to many important questions, including the identification of as yet unidentified parameters contributing to skin cancer, are needed to refine estimates.

"Estimates based upon changes in the observed cancer incidence with variations in latitude for each percent reduction in the equilibrium concentration of ozone range from 2,100 to 15,000 (6,000 median) new cases of non-melanoma skin cancer per year in light-skinned individuals in the U.S. at steady state. This conclusion is based upon the following assumptions (Urbach, personal communication, 1975):

"(1) A 1.4 to 2.5% (2% median) increase in UV-B radiation will occur at the Earth's surface for a 1% reduction in the equilibrium ozone concentration of the stratosphere.

"(2) For each 1% rise in UV-B radiation, a corresponding increase in the incidence of non-melanoma skin cancers can range from 0.5 to 2% (1% median) at steady state (i.e., after the latency period).

"(3) Items (1) and (2) combined lead to a 0.7 to 5% (2% median) increase in non-melanoma skin cancers at mid-latitudes for each 1% reduction in the equilibrium ozone level.

"(4) Based upon recent National Cancer Institute (NCI) estimates, there are approximately 300,000 new cases of non-melanoma skin cancer in the U.S. annually.

"(5) Therefore, a 1% reduction in the equilibrium level of ozone in the stratosphere might lead to from 2,100 to 15,000 (6,000 median) new cases of non-melanoma skin cancer per year among light-skinned individuals in the U.S. at steady state."

This approach has been used to estimate skin cancer effects of various human activities. For example, the U.S. Department of Transportation (DOT), in the addendum (ref. H-11) to its Environmental Impact Statement (EIS) on the Concorde supersonic transport (SST) aircraft, employed the same conceptual approach (but a baseline figure of 250 000 cases per year) in calculating the increased number of skin cancer cases resulting from various activities including Shuttle. The DOT calculations are based on the Climatic Impact Assessment Program (CIAP). The unreasoning application of this approach to Shuttle effects is incorrect, as outlined below.

The number of skin cancer cases resulting from a 0.2-percent O_3 reduction lasting for 10 years is not realistically predictable from the existing models and data. The extant experimental and epidemiological data, although suggesting a relationship between solar radiation exposure and skin cancer incidence, are inadequate for making quantitative predictions with reasonable limits of uncertainty for this case.

The data are inadequate for a variety of reasons. Experimental studies with mice indicate that skin tumor induction is a complex multistep process involving some unresolvable uncertainty (ref. H-12) and having systemic and immunological aspects in addition to simple response to BHuv dose (ref. H-13).[11] These and other data indicate that not all skin cancer is induced solely by BHuv. One-tenth to one-third of the basal cell carcinomas occur on areas of the skin receiving little or no solar radiation (refs. H-14 and H-15). The non-uv-induced fraction must be ascertained and accounted for to enable the relationship of incidence and BHuv dose to be established. The existing epidemiological data are inadequate because they were collected in studies that were not specifically designed to determine the relationship of skin cancer incidence to BHuv dose or to latitude; thus, there are unexplained inconsistencies both within and between studies (ref. H-16). Many important aspects (lifestyles, genetic background, previous history of tumors) were omitted from the questionnaire; inclusion might have allowed the resolution of some of the inconsistencies. The factor on which the expected increased number of cases is based (i.e., the present incidence in the United States) is not accurately known; estimates range from 120 000 cases per year (ref. H-17) to 300 000 cases per year (ref. H-14) to 400 000 (ref. H-18). The value of 300 000 cases per year is considered in reference H-14 to be the most likely figure.

The fact that many of the cases arising in a particular year occur in patients who have had a previous history of skin cancer suggests a susceptibility to skin cancer within the population. This suggestion is borne out by the finding that certain ethnic groups (Celtic peoples from Ireland and Scotland) are highly susceptible. If only a certain fraction of the total

---

[11] M. L. Kripke and M. S. Fisher: Effect of UV Light on the Host Response to UV-Induced Tumors. Abstracts of 4th Annual Meeting, American Society of Photobiologists, to be published.

population is susceptible, the postulated increase in skin cancer cases may primarily occur in the already suffering fraction. This point should be considered in estimating skin cancer incidence increases. Data needed for such an estimate are not yet available. The estimated harm to the total population is thus inflated. Although counting cases, as distinguished from counting people, may inflate the estimated number, factors in the analysis of the epidemiological data also deflate the number. The 300 000-case/yr figure is reputedly based on the factor 165/100 000 cases/yr, a demographically weighted average incidence for the entire United States. This factor times the 1970 white population figure equals a number that, rounded off, equals 300 000 cases/yr. Other factors tending to obscure the true incidence of skin cancer is that skin cancer incidence is frequently underreported because of outpatient treatment by general practitioners. In some studies for which biopsies were not taken for histological confirmation, the incidence was overreported because of inclusion of noncancerous actinic keratoses of self-healing keratoacanthomas in the statistics (refs. H-16 and H-19).

Despite the uncertainty in the data, a variety of mathematical models have been proposed that represent attempts to fit the epidemiological data. From these models, amplification factors (percentage increase in skin cancer incidence per percentage decrease in O_3) have been derived. Variation in amplification factors from 1 to 6 have been reported. These amplification factors are very sensitive to underlying assumptions of the models.

The foregoing considerations lead to the conclusion that current data and models are inadequate to enable accurate estimations, within reasonable limits of uncertainty, of the degree of skin cancer increase that might result from a small, temporary O_3 reduction. Of particular importance is the fact that the Shuttle perturbation lasts about 10 years, which is a fraction of the average induction period for skin cancer. Lack of knowledge therefore precludes an accurate estimate of the number of additional skin cancer patients that might result from a 10-year-duration, 0.2-percent O_3 reduction. Given that the 0.2-percent O_3 value will be reached by 1985 if space transportation systems continue as scheduled, given that the O_3 will rapidly return to previous levels, and given that the induction time for skin cancer is 20 to 60 years, it is concluded that any increase in skin cancer induced by proceeding as scheduled for another decade will be extremely small compared to normal incidence.

REFERENCES

H-1. Green, A. E. S.; and Miller, J. H.: Measures of Biologically Effective Radiation in the 280-340 nm Region. Section 2.2.4, CIAP Monograph 5, Impacts of Climatic Change on the Biosphere, Part 1, Ultraviolet Radiation Effects. DOT-TST-75-55, Sept. 1975, pp. 2-60 to 2-70.

H-2. Green, A. E. S.; and Mo, T.: Calculated Erythemal Radiation Doses. Section 2.2.5, CIAP Monograph 5, Impacts of Climatic Change on the Biosphere, Part 1, Ultraviolet Radiation Effects. DOT-TST-75-55, Sept. 1975, pp. 2-70 to 2-73.

H-3. Mo, T.; and Green, A. E. S.: Systematics of Climatic Variables and Implications — Local Erythema Doses. Section 2.2.6, CIAP Monograph 5, Impacts of Climatic Change on the Biosphere, Part 1, Ultraviolet Radiation Effects. DOT-TST-75-55, Sept. 1975, pp. 2-74 to 2-78.

H-4. Caldwell, M. M.; and Nachtwey, D. S.: Introduction and Overview. Chapter 1, CIAP Monograph 5, Impacts of Climatic Change on the Biosphere, Part 1, Ultraviolet Radiation Effects. DOT-TST-75-55, Sept. 1975, pp. 1-3 to 1-30.

H-5. Caldwell, M. M.; and Nachtwey, D. S.: Involvement of Biological Systems in a Monitoring Program. Section 10.2, CIAP Monograph 5, Impacts of Climatic Change on the Biosphere, Part 1, Ultraviolet Radiation Effects. DOT-TST-75-55, Sept. 1975, pp. 10-8 to 10-19.

H-6. Walter, Heinrich: (Joy Wieser, transl.): Vegetation of the Earth in Relation to Climate and the Eco-physiological Conditions. Springer-Verlag (New York), 1973.

H-7. Caldwell, M. M.; Sisson, W. B.; Fox, F. M.; and Brandle, J. R.: Plant Growth Response to Elevated UV Irradiation Under Field and Greenhouse Conditions. Chapter 4, Appendix M, CIAP Monograph 5, Impacts of Climatic Change on the Biosphere, Part 1, Ultraviolet Radiation Effects. DOT-TST-75-55, Sept. 1975, pp. 4-251 to 4-259.

H-8. Thai, V. K.; and Garrard, L. A.: Effects of UV-B Radiation on the Net Photosynthesis and the Rates of Partial Photosynthetic Reactions of Some Crop Plants. Chapter 4, Appendix F, CIAP Monograph 5, Impacts of Climatic Change on the Biosphere, Part 1, Ultraviolet Radiation Effects. DOT-TST-75-55, Sept. 1975, pp. 4-123 to 4-145.

H-9. Biggs, R. H.; and Basiouny, F. M.: Plant Growth Responses to Elevated UV-B Irradiations Under Growth Chamber, Greenhouse, and Solarium Conditions. Chapter 4, Appendix L, CIAP Monograph 5, Impacts of Climatic Change on the Biosphere, Part 1, Ultraviolet Radiation Effects. DOT-TST-75-55, Sept. 1975, 4-195 to 4-249.

H-10. Fluorocarbons and the Environment. Report of Federal Task Force on Inadvertent Modification of the Stratosphere. Federal Council for Science and Technology, June 1975.

H-11. Concorde Supersonic Transport: Final Environmental Impact Statement. Vol. I, Addendum. U.S. Dept. of Transportation Federal Aviation Administration, Feb. 1976.

H-12. Blum, H. F.: Uncertainty of Growth of Cell Population in Cancer. J. Theor. Biol., vol. 46, 1974, pp. 143-166.

H-13. Blum, Harold F.; McVaugh, Julia; Ward, Margery; and Bush, Harry L., Jr.: Epidermal Hyperplasia Induced by Ultraviolet Radiation; Error and Uncertainty of Measurement. Photochem. Photobiol., vol. 21, 1975, pp. 255-260.

H-14. Scotto, J.; Kopf, A. W.; and Urbach, F.: Non-Melanoma Skin Cancer Among Caucasians in Four Areas of the United States. Cancer, vol. 34, 1974, pp. 1333-1338.

H-15. Urbach, Frederick; Epstein, John H.; and Forbes, P. Donald: Ultraviolet Carcinogenesis: Experimental, Global, and Genetic Aspects. Chapter 18, Sunlight and Man (Thomas B. Fitzpatrick, Madhukar Pathak, et al., eds.), Univ. of Tokyo Press, 1974.

H-16. Climatic Impact Committee, National Academy of Science/National Research Council/National Academy of Engineering: Environmental Impact of Stratospheric Flight. National Academy of Sciences, 1975.

H-17. Cancer Facts and Figures: Estimated New Cancer Cases for All Sites, Plus Major Sites, by State. American Cancer Society, 1973.

H-18. Setlow, Richard B.: Testimony before the United States Subcommittee on the Upper Atmosphere of the Committee on Aeronautical and Space Sciences. Congressional Record, Sept. 17, 1975, pp. 442-462.

H-19. Daniels, Farrington, Jr.: Sunlight. Chapter 6, Cancer Epidemiology and Prevention: Current Concepts (D. Schottenfeld, ed.), C. C. Thomas, 1975, pp. 126-152.